Available online at www.sciencedirect.com
ScienceDirect
Journal of Sound and Vibration 314 (2008) 371–452
JOURNAL OF SOUND AND VIBRATION
www.elsevier.com/locate/jsvi

Review

Recent advances in nonlinear passive vibration isolators

R.A. Ibrahim*

Department of Mechanical Engineering, Wayne State University, Detroit, MI 48098, USA

Received 6 November 2006; received in revised form 18 December 2007; accepted 4 January 2008
Handling Editor: P. Davies
Available online 7 March 2008

Abstract

The theory of nonlinear vibration isolation has witnessed significant developments due to pressing demands for the protection of structural installations, nuclear reactors, mechanical components, and sensitive instruments from earthquake ground motion, shocks, and impact loads. In view of these demands, engineers and physicists have developed different types of nonlinear vibration isolators. This article presents a comprehensive assessment of recent developments of nonlinear isolators in the absence of active control means. It does not deal with other means of linear or nonlinear vibration absorbers. It begins with the basic concept and features of nonlinear isolators and inherent nonlinear phenomena. Specific types of nonlinear isolators are then discussed, including ultra-low-frequency isolators. For vertical vibration isolation, the treatment of the Euler spring isolator is based on the post-buckling dynamic characteristics of the column *elastica* and axial stiffness. Exact and approximate analyses of axial stiffness of the post-buckled Euler beam are outlined. Different techniques of reducing the resonant frequency of the isolator are described. Another group is based on the Gospodnetic–Frisch-Fay beam, which is free to slide on two supports. The restoring force of this beam resembles to a great extent the restoring roll moment of biased ships. The base isolation of buildings, bridges, and liquid storage tanks subjected to earthquake ground motion is then described. Base isolation utilizes friction elements, laminated-rubber bearings, and the friction pendulum. Nonlinear viscoelastic and composite material springs, and smart material elements are described in terms of material mechanical characteristics and the dependence of their transmissibility on temperature and excitation amplitude. The article is closed by conclusions, which highlight resolved and unresolved problems and recommendations for future research directions.

Contents

*Tel.: +1 313 577 3885; fax: +1 313 577 8789.
E-mail address: ibrahim@eng.wayne.edu

0022-460X/$ - see front matter © 2008 Elsevier Ltd. All rights reserved.
doi:10.1016/j.jsv.2008.01.014

1. Introduction

The linear theory of vibration isolation is well documented in the literature [1–4]. A linear isolator attenuates transmitted vibrations above an excitation frequency, Ω, which exceeds the value of $\sqrt{2}\omega_n$, where ω_n is the undamped natural frequency of the isolator. The transmitted force, F_t (or displacement, X_0), reaches a value less than the excitation force, F_0 (or displacement, Y_0), at an excitation frequency $\Omega > \sqrt{2}\omega_n$. The ratio F_t/F_0 (or X_0/Y_0) is known as the transmissibility, TR. While the damping is beneficial at resonance, it is non-beneficial in reducing the transmitted force or displacement for $\Omega/\omega_n > \sqrt{2}$. The effectiveness of any isolator can be improved by lowering its natural frequency and its damping ratio. In most cases, the softer the restoring force, the lower the natural frequency, and the better the isolation. The essential constituents of a linear isolator are the resilient load-supporting means and energy dissipation means. In certain types of isolators the functions of the load-supporting and energy-dissipation means may be performed by a single element such as natural or synthetic rubber. In other types, the resilient load-carrying means may lack sufficient energy dissipation such as metal springs. In this case, a distinct energy dissipation means should be provided.

The basic concept of isolating horizontal and vertical motions is shown in Figs. 1(a) and (b), respectively. The transfer functions of the two isolators, shown in Fig. 2, were estimated in Refs. [5,6]. The dashed and solid

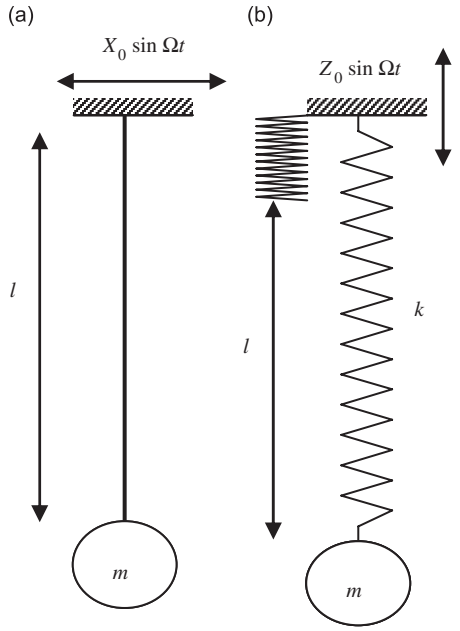

Fig. 1. Typical horizontal and vertical isolation systems: (a) pendulum horizontal isolator and (b) mass–spring vertical isolator $k = (mg/l)$, $\omega = \sqrt{k/m} = \sqrt{g/l}$.

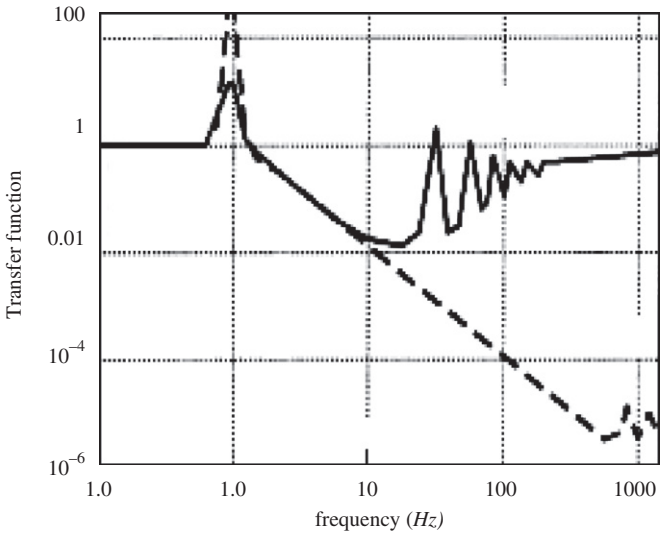

Fig. 2. Typical transfer functions of horizontal and vertical isolators: _____, vertical isolator; ----, horizontal isolator [5].

curves belong to the pendulum and the mass–spring isolators, respectively. Above resonance, the transfer function has a slope of −2 (on the log–log plot).

A different class of linear isolators, known as dynamic anti-resonant vibration isolators, was introduced in Refs. [7–9]. The anti-resonant isolator of Goodwin [7] and Halwes [8] is based on hydraulic leverage, while that of Lanelly [9] relies on a levered mass. Anti-resonant vibration isolators use a levered mass–spring combination to generate an anti-resonant frequency in the system, as shown in Fig. 3 [10]. Anti-resonance occurs when the inertial force generated by the levered mass cancels the spring force. Anti-resonant vibration isolators are implemented on the load path and introduced to a single-degree-of-freedom system in which the

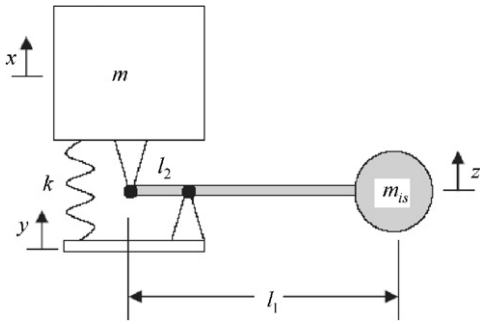

Fig. 3. Lever-type anti-resonant vibration isolator [10].

inertial force generated by the levered mass results in an increase of the system effective mass. Thus, the resonant frequency decreases, and the isolator is capable of operating in a lower-frequency range. This type has been used in helicopter rotor isolation and isolation of floor machines [11–16]. Corcoran and Ticks [17] and Flower [18] replaced the rubber engine mounts by hydraulic engine mounts, which have the so-called "inertia track" and share the same principle with the designs of Goodwin [7] and Halwes [8]. Yilmaz and Kikuchi [10,19] extended the concept of anti-resonant vibration isolators to two- and multi-degree-of-freedom passive isolators having two and multi-anti-resonance frequencies. Their isolators yielded an improvement of the bandwidth in the low-frequency range.

This review article presents an assessment of recent developments in nonlinear vibration isolators utilized in different applications. Section 2 introduces the influence of nonlinearity on the characteristics of different isolators such as shift of resonance frequency, chaotic motion, internal resonance, impact and random loading. The type of an isolator depends on the frequency range in addition to the material of the isolator. Different types of ultra-low-frequency vibration isolation will be discussed in Section 3. Section 4 provides an overview of the Euler spring isolator in the post-buckling state. The exact and approximate analyses of the *elastica* and axial stiffness of Euler column will be presented as essential ingredients of the Euler spring isolator. Methods of reducing the natural frequency, such as anti-spring techniques, are also presented in Section 4. Non-traditional nonlinear isolators based on the Gospodetic–Fresch-Fay beam are then described in Section 5. Essentially, the Gospodetic–Fresch-Fay beam is free to slide on its supports and its dynamics closely resembles the roll dynamics of biased ships. Base isolators such as laminated-rubber bearing with and without lead-core, friction-type sliding, and friction-pendulum isolators are discussed in Section 6. These isolators have been used essentially to isolate buildings, bridges, and liquid storage tanks from ground earthquake motion. Section 7 deals with viscoelastic isolators commonly used in the automotive industry. The basic characteristics of viscoelastic materials are described in terms of their dependence on frequency and temperature. Experimental, analytical, and numerical isolation characteristics of nonlinear viscoelastic mounts are described. Section 8 closes this article with some conclusions and recommendations for further research.

2. Basic characteristics of nonlinear isolators

2.1. Need for nonlinear isolation

Linear vibration isolators are only useful if their natural frequencies are well below the excitation frequency. Thus, they are limited to such applications as moderate environmental disturbances. However, under severe environmental disturbances such as shocks, impact loads, or random ground motion, their spectrum will definitely contain dangerous low-frequency components. The isolator under these conditions experiences excessive deflections that can cause over-stress and even damage to the system. For this reason, it is imperative to consider effective nonlinear isolators, which can serve several applications, such as

1. Reducing line spectra in the radiated acoustical signature of marine vessels.
2. Isolating equipment mounted in ships navigating in extreme sea waves.

3. Reducing the magnitude of the high launch loads across all frequency bands acting on spacecraft.
4. Reducing severe vibrations due to impact loads.
5. Protecting buildings, bridges, liquid storage tanks, oil pipelines, and nuclear reactor plants against the damaging effects of earthquakes.
6. Isolating laser interferometers of gravitational wave detectors.
7. Isolating electronic equipment, automotive vehicle front-end-cooling systems, and passengers from road roughness excitation.
8. Isolating automotive power-train system, engine through proper design of rubber and hydraulic mounting systems.
9. Protecting operators of hand-held machines.

The influence of isolator nonlinearity on transmissibility depends on whether its stiffness is hard or soft [20]. It is known that soft nonlinearity causes a reduction in the resonant frequency and the isolation may be improved. Nonlinearity becomes important in the study of an isolator when large deflections occur due to the effects of equipment weight and sustained acceleration. These effects are encountered in the behavior of suspensions of high-speed vehicles and mounts for sensitive instruments [21].

Many researchers have conducted studies considering various combinations of restoring and damping forces. Earlier activities include the work of Den Hartog [22] who developed an exact solution for the vibratory response of a symmetric system with both coulomb and viscous damping when subjected to a harmonic forcing function. Ruzicka and Derby [23] presented extensive results for isolation systems with linear stiffness and nonlinear pth power damping. The magnitude of stiffness nonlinearity required in the design of nonlinear isolators with reference to resonant amplitudes and force transmissibility was predicted using the analogue computer [24] and finite element method [25]. Hundal and Parnes [26] considered the same system when subjected to base excitation. Metwalli [27] proposed a model to optimize nonlinear suspension systems which were found to outperform their linear counterparts. Nayfeh et al. [28] and Yu et al. [29] considered a passive nonlinear mechanical vibration isolator consisting of discrete mass, stiffness, and damping elements. They showed that by suitably designing the stiffness nonlinearities, localized nonlinear normal modes could be induced in the system. It was found that when the isolator with localized nonlinear normal modes is subjected to a harmonic excitation in certain frequency ranges, the resulting resonances become similarly localized and the level of the transmitted undesirable vibrations is greatly reduced.

The influence of nonlinearity on the performance of these isolators is manifested in shifting the resonance frequency and possibility of chaotic motion. Other factors include the type of excitation and its frequency spectrum, which are addressed in the next sections.

2.2. Shifting of resonance frequency and jump phenomena

Depending on the type of nonlinearity, the resonance frequency may be shifted to the left or right of the linear resonance frequency on the transmissibility plot. Ravindra and Mallik [30] examined the response of nonlinear vibration isolation system subjected to force excitation or base excitation as shown in Fig. 4. These systems were described by the general equation of motion

$$Z'' + 2\zeta Z'|Z'|^{p-1} + Z|Z|^{q-1} = F\cos\nu\tau, \tag{1}$$

where a prime denotes differentiation with respect to the non-dimensional time parameter, $\tau = \omega_n t$, $Z = x/(F_0/k)^{1/q}$, or $Z = (x-y)/Y_0$ refers to the non-dimensional displacement of the system mass or its relative displacement with respect to the base displacement, ζ is the damping factor, $F = 1/$ or $= \nu^2$, and $\nu = \Omega/\omega_n$. Ravindra and Mallik [30] studied different cases of nonlinearity and estimated the corresponding transmissibility for each case using the method of harmonic balance. It was found that an isolator with soft nonlinear characteristics is superior to the one with hard nonlinearity. The effects of damping on resonance transmissibility and the high frequency attenuation rate of the transmissibility were found to be similar to those of isolators with a linear restoring force. An increase of damping power index, p, results in a reduction of the jump width.

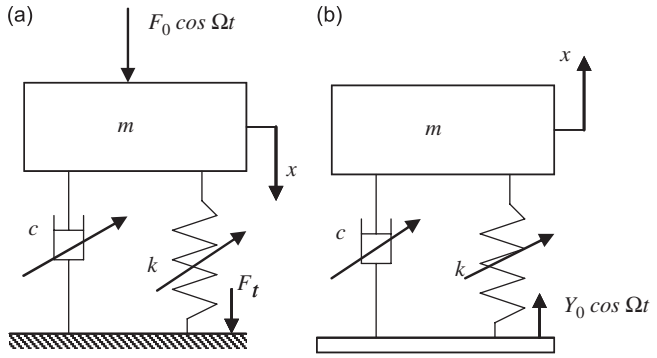

Fig. 4. Force and base motion nonlinear isolators considered in Ref. [30]: (a) force isolation and (b) base motion isolation.

On the one hand, the damping force due to dashpot clearance is normally characterized by a constant damping coefficient and represents linear proportional damping. On the other hand, the damping force due to the orifice is nonlinear with a variable damping coefficient and is a function of internal geometry, frequency of flow oscillation and Reynolds number [31]. The nonlinear damping component usually causes a significant shift of the resonant frequency to a smaller value, compared to the linear damping case. For a two-degree-of-freedom system, the nonlinear damping was found to provide better vibration control in the frequency range between resonance peaks and an increase transmissibility response in the range beyond the second resonance.

Note that in nonlinear isolators the transmitted signal may contain subharmonic, superharmonic, and sometimes chaotic behavior. Thus, the transmissibility defined by the linear theory of vibration isolation should be redefined by using a suitable performance index. Lou et al. [32] proposed the ratio of the rms values of the response to the excitation, i.e.,

$$\mathrm{TR}_n = -\frac{\sqrt{E[x^2]}}{\sqrt{E[y^2]}}. \tag{2}$$

This index provides a measure of the energy transmission relationship.

For a flexible ship excited by ocean waves a vibratory power flow was examined [33] for a nonlinear isolator characterized by a general pth power model for damping and qth power for stiffness. The input power flow spectrum was found not globally sensitive to the nonlinearity in damping and stiffness of the isolator except for local variations at some resonance frequency of the coupled system. Furthermore, the nonlinearity in stiffness was found to play an important role in determining the characteristics of power transmission. A nonlinear isolator with hardening stiffness but large damping index, p, was found to have the possibility of preventing the occurrence of jump phenomena in the neighborhood of the critical resonance frequency. It was concluded that a ship deck/hull built as rigid as possible is beneficial in reducing vibration transmission from the hull structure to the equipment. The utilization of a softening nonlinear stiffness in the low-frequency range and hardening nonlinear stiffness in the high-frequency range was found to produce benefits in controlling vibration transmission.

2.3. Chaotic response

Under harmonic excitation, a nonlinear isolator may exhibit chaotic behavior over a certain range of system and excitation parameters. A simple method for describing the arbitrary multi-axial loading process of vibration isolation with large nonlinear stiffness and damping was proposed by Ulanov and Lazutkin [34]. Qing et al. [35] studied the vibration isolation behavior of a nonlinear vibration-isolation system in a desired chaotic state. The transmitted force was characterized by a broad frequency band, although the excitation was sinusoidal. In order to control the system in a desired chaotic state, the isolator has to possess variable stiffness and damping.

Other types of nonlinear dynamic stiffness modeling were introduced by Kari [36,37]. Jiang and Zhu [38] analytically and numerically studied the vibration isolation of a nonlinear system. They estimated the

vibration isolation performance under different operating conditions and showed that the vibration isolation performance at the primary harmonic frequency is better than that of the linear system. Furthermore, the vibration isolation performance of the nonlinear vibration isolator in the chaotic states was found to be much better than that in the non-chaotic vibration states.

Liu et al. [39] took advantage of chaotic vibration isolation to eliminate the periodic component in water-borne noise and to improve the concealment capability of warships. The influence of hard stiffness nonlinearity on the performance of nonlinear isolators was numerically studied by Yu et al. [40]. Yu et al. [41] conducted numerical and experimental investigations to evaluate the performance of nonlinear vibration isolation system under chaotic state. They found that the nonlinear isolator exhibits excellent performance and can reduce the line spectrum when the system operates under chaotic state. The spectra of the radiated waterborne-noises of marine vessels constituted of a broad-band noise having a continuous spectrum superimposed on a line spectrum. At high-speed, the signature was found to be dominated by a broad-band noise, while at low-speed the signature was dominated by a line spectrum [32]. For soft spring nonlinearity both amplitude and transmissibility of displacement were found to outperform those observed in hard spring nonlinearity [42].

Ravindra and Mallik [43] extended their previous work [30] and considered both symmetric and asymmetric nonlinear restoring forces. Two typical routes to chaos, namely through period-doubling and intermittency, were found to be present with damping exponent values of $p = 2$ and 3. It was concluded that the bifurcation structure is unaffected by the damping exponent. However, the values of the damping coefficient required for complete elimination of the subharmonic and chaotic responses were found to depend on the value of p. It was shown that nonlinear damping can be used as a passive mechanism to suppress chaos.

2.4. Influence of internal resonance

Vibration isolation of nonlinear dynamical systems involving mixed coordinates was studied in Refs. [44–47]. These references considered the dynamic response of a rigid machine mounted on a foundation with Duffing-type stiffness. It was shown that the stiffness nonlinearity may cause unwanted coupling between the system modes. In addition, in the presence of 1:1 internal resonance mixed-mode periodic response was found to co-exist with single-mode linear and nonlinear oscillations. Yamamoto [48] and Chen and Chen [49] determined the response and transmissibility of nonlinear isolating systems using the incremental harmonic balance method.

The transient nonlinear vibration of a rigid body mounted on a three-degree-of-freedom vibration isolation system was examined in the presence of a 2:1:1 internal resonance [50]. The internal resonance is due to the interaction between vertical and horizontal vibrations of the rigid body and the rotational vibration about its center of gravity. The vibration of the rigid body passed through resonance when the rotation speed of an unbalanced rotor equipped with the rigid body was found to be significant. Special attention was given to the transient behavior of passage through resonance under the condition that a direct-current motor directly drives the unbalanced rotor with a limited electric current. Transient oscillations through resonance were observed and confirmed by analytical results for a few cases of limited currents.

2.5. Vibration protection under vibro-impact

Systems subjected to impact and shock loads exhibit severe vibration and they need special isolation means. Impact loading is encountered in many mechanical applications such as pneumatic hammers, slamming loads on water waves acting on ships and ocean structures, and vibro-impact systems with rigid or elastic stops. In order to protect a given object against these undesirable disturbances, a vibrating protecting system is placed between the vibration source and the object. In their research monograph, Alabuzhev et al. [51] introduced a number of vibration protection systems with quasi-zero stiffness. Fig. 5 shows schematic diagrams of selected systems whose load-bearing elastic elements possess constant positive stiffness as well as devices with negative-stiffness. This type of isolators has been used for vibration isolation of operators' seats in vehicles [52], impact action hand-held machines [53–55], and railway car suspensions [56,57]. Systems with negative-stiffness have

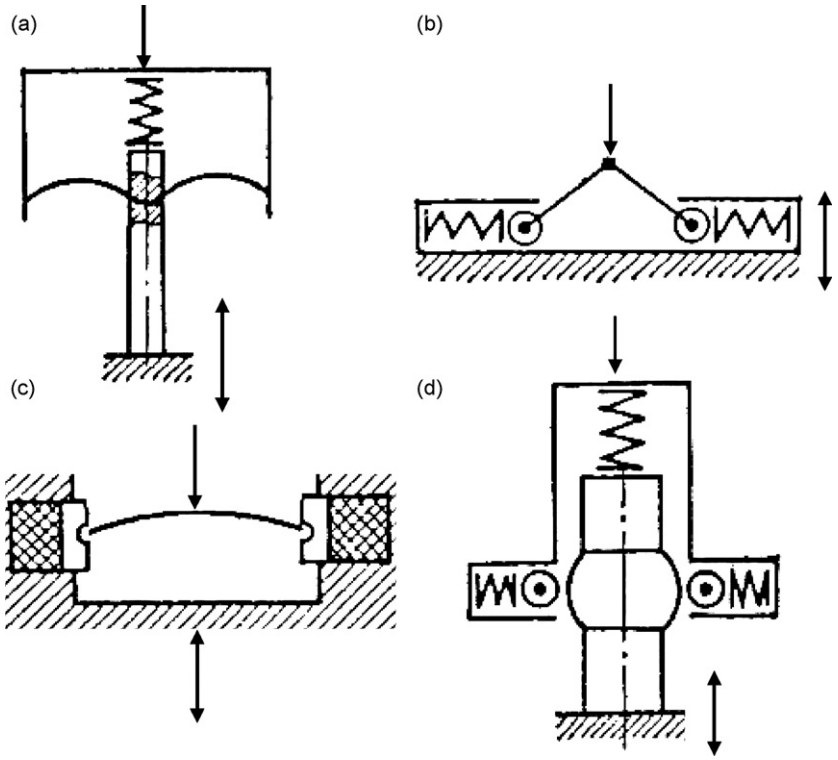

Fig. 5. Schematic diagrams of typical vibration protecting mechanisms: (a) vertical coil spring with two buckled beams, (b) links restraint against horizontal springs, (c) buckled beam isolator and (d) vertical and horizontal spring system [51].

been treated in Refs. [56,57] and the performance of such systems in the chaotic motion regime was addressed in Refs. [58–60].

Some modifications of the nonlinear characteristics of isolating mounts carrying rigid structures subjected to impact loads were proposed in the literature [61]. The modifications were adapted with respect to impact vibrations to achieve a well design behavior. The protection of workers against vibrations generated from hand-held tools requires special vibration isolation means. Dobry and Brzezinski [62] developed a strong elastic nonlinear isolator to minimize the interaction force between the tool and the handle. In an effort to prevent injuries from impact impulse loads, Balandin et al. [63] presented a review of research activities dealing with the limiting performance analysis of impact isolation systems. Zhiqing and Pilkey [64] conducted the limiting performance analysis to study the optimal shock and impact isolation of mechanical systems via wavelet transform.

A bumpered vibration protection arrangement of a gimbaled electro-optical device was developed by Veprik et al. [65]. This device was based on a split Sterling cry cooler for the cooling of an infrared focal array. The installation of bumpers with enlarged travel reduces the probability of accidental impacts and effectively reduces the excessive deflections. However, the presence of bumpers turns the vibration isolation arrangement into a potential strongly nonlinear vibro-impact system with unfavorable characteristics [66]. In an effort to eliminate these characteristics Babitsky and Veprik [67] introduced a novel concept based on the cooperation use of an undamped, low-frequency vibration isolator in combination with optimally damped bumpers installed with minimal free travel distance.

Some isolators experience a sudden change in the values of their parameters, which can be represented as piecewise linear or nonlinear functions. As stated earlier, soft isolators are best for isolation. However, nonlinear hardening is required to minimize relative displacement at high amplitude [68–70]. Patrick and Jazar [71,72] introduced a secondary suspension to limit high relative displacements. Mahinfala et al. [73] adopted a hyperbolic-tangent saturation function to study the frequency response of vibration isolators with saturating spring elements. Deshpande et al. [74,75] employed an adapted averaging approach to study highly nonlinear

systems described by piecewise linear representation. They obtained an implicit function for frequency response of a bilinear system under steady state. This function was examined for jump-avoidance and a condition was derived which ensures that the undesirable phenomenon of "jump" does not occur and the system response is functional and unique.

Orzechowski et al. [76] studied the behavior of nonlinear isolation mounts and measured their response to impulsive inputs. Their results showed the extent to which mounting linearity contributes to the shortening of the transient portion of the response to an impact without adding damping to the system. The presence of barriers is known to prevent a vibratory system from exceeding the relative amplitude particularly in the neighborhood of resonance. The effect of end stops in an isolator was studied by Narimani and Golnaraghi [77] and Narimani et al. [70]. They adopted a piecewise linear system and applied an averaging method to define from the analytical frequency response the range of the parameters, which minimize the relative displacement of the system. It was found that the damping ratio plays a more dominant role than stiffness in piecewise linear vibration isolators.

2.6. *Influence of random excitation*

Systems subjected to random excitation such as earthquake ground motion require special isolation means such as those discussed in Section 6. Fujiwara and Murotsu [78] estimated the optimum parameters of vibration isolators for systems subjected to stationary random force and/or foundation motion excitations. The vibration isolators consist of linear passive elements. Performance indices for these systems were expressed as nonlinear functions of the parameters of the vibration isolators. The procedure was illustrated for single- and two-degree-of-freedom systems with random excitation. Kirk [79] studied the influence of nonlinear spring stiffness characteristics on the effectiveness of vibration isolators with linear damping subjected to stationary random white noise ground acceleration. The probability density function of spring displacement was determined analytically by means of the Fokker–Planck equation and both the root-mean-square (rms) and mean peak values of spring displacement and mass acceleration were presented for three different types of spring nonlinearity: (a) cubic hard spring, (b) cubic soft spring, and (c) tangent spring. The usefulness of the cubic soft spring in reducing transmitted vibration was found to be of limited value, due to the need to avoid the possibility of snap-through buckling caused by a reduction of stiffness with increasing spring deflection. Miao and Liu [80] examined the random response of vehicles with a soft nonlinear spring to random excitation. It was found that damping material cannot effectively isolate the vibration of vehicles. The issue of isolating automotive components will be discussed in Section 7.

3. Ultra-low-frequency vibration isolators

The vibration isolation of mirrors in laser interferometers used in gravity wave detection is considered an important factor in the success of the Laser Interferometer Gravitational Wave Observatory (LIGO) and VIRGO projects [81–83]. The sensitivity of terrestrial gravitational detectors is limited at low frequencies by the resulting degree of seismic isolation. Efforts to improve this isolation have resulted in what is known as ultra-low-frequency isolators [83–87].

The concept of the negative-stiffness mechanism was adopted by Platus [88,89] for isolation against sub-Hertz vibrations. Zhang et al. [90] developed a combined positive- and negative-stiffness isolator based on an analysis of the mechanism of negative-stiffness, where negative-stiffness cancels much of the positive stiffness of the elastic element in the vicinity of the balance point. The stiffness at the balance point has a nonlinear characteristic and the net stiffness tends to be zero. This isolator was found to possess high support stiffness as well as low vibration stiffness. Its inherent frequency can be adjusted to zero by adjusting the initial deformation of the elastic elements of the negative-stiffness mechanism. Experimental results revealed that the inherent frequency of the isolator can be adjusted from 10 Hz down to 1 Hz. Zhang et al. [91] utilized the Euler column (will be described in Section 4) as a supporting spring in an ultra-low-frequency vibration isolator. The negative-stiffness spring and the Euler column spring were connected in parallel at the balance point.

Physicists introduced what is called a pre-isolator, which is in principle an isolation stage, which is designed to have a very low resonant frequency of suspension. The main distinction between a pre-isolator and normal

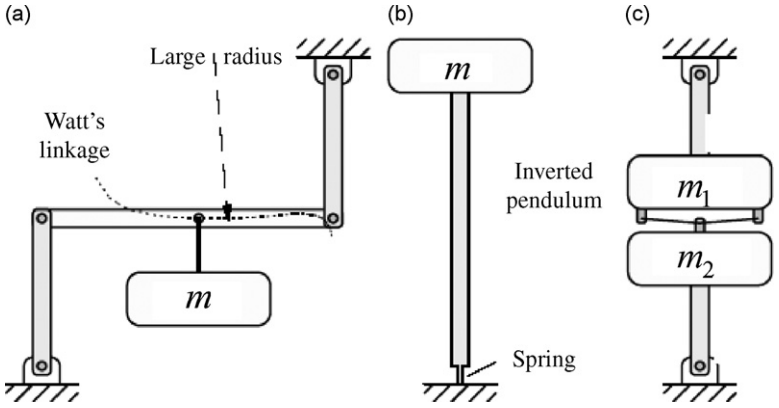

Fig. 6. Force and base motion nonlinear isolators: (a) Watt's linkage force isolator, (b) inverted pendulum retrained by a flat short spring, and (c) two opposite pendulums [95,96].

isolator is that structures that are designed to have very low resonant frequencies tend to be larger and more massive, and thus possess lower natural frequencies than normal isolator chain stages. As a result they generally do not provide useful isolation in the 10 Hz–1 kHz detection band but are included mainly to reduce residual motion at frequencies below the detection band [92]. The worst residual motion usually occurs close to 0.5–1 Hz at resonant frequencies of the lowest swinging modes of a standard isolation chain. Good design of a pre-isolation system can easily reduce the seismic drive to these modes and thus the residual low-frequency motion by two orders of magnitude. Lee et al. [93] described an ultra-low-frequency pre-isolator for micro-seismic noise isolation and reduction of suspension chain resonant mode amplitudes. The Australian Consortium for Interferometric Gravitational Astronomy applied reduction of seismic vibration to the main Fabry–Perot cavities test masses and to other mirror-like input optics. The isolator consists of an inverted pendulum horizontal stage [94].

Typical examples of ultra-low-frequency horizontal isolators are shown in Fig. 6. Fig. 6(a) shows the Watt's linkage with a mass suspended from an appropriate point which moves along a circle of very large radius. The inverted pendulum shown in Fig. 6(b) is restrained by a short flat spring to provide positive restoring moment. Pinoli et al. [95] and Saulson [96] studied the performance and mechanical properties of an inverted pendulum as an ultra-low-frequency vibration isolator. The third system, shown in Fig. 6(c), consists of two opposite pendulums.

3.1. Folded pendulum isolator

Ultra-low-frequency horizontal isolators must be carefully aligned to cancel the effect of gravity and may be designed so that minimum energy is stored in elastic elements. Vertical isolators, on the other hand, must support the entire weight against the gravitational force, and large energy storage in elastic elements is almost unavoidable. Blair et al. [97] and Liu et al. [99] designed the folded pendulum shown in Fig. 7(a) and its equivalent schematic diagram is shown in Fig. 7(b). It consists of a horizontal platform and two vertical rods hinged by foils under tension. The left rod, of mass m_{a1}, acts as a positive pendulum, while the right one, of mass m_{a2}, is an inverted pendulum. The two rods are of the same length, l. The distance between O and P is l_p and is the same as the distance between O' and P'. The platform is divided into two equivalent masses m_{p1} and m_{p2}. The points O, O', C, C', P, and P' have coordinates x_O, x'_O, x_c, x'_C, x_P, and x'_P, respectively. The angles of the two rods with the vertical are θ and θ'. For small angles one may assume, $\theta \approx \theta'$, $\dot{x}_C \approx \dot{x}'_C$, and $\dot{x}_P \approx \dot{x}'_P$. Under an external forcing excitation of the platform, $f(t) = F e^{i\Omega t}$, and setting $x_O(t) = X_O e^{i\Omega t}$, and $x_P(t) = X_P e^{i\Omega t}$, Liu et al. [98] obtained the following expressions for the force and base excited transfer functions:

$$\frac{X_P}{F} = \frac{1}{M_e \omega_r^2 (1 - \Omega^2/\omega_r^2)}, \quad \frac{X_P}{X_O} = \frac{1 - K(\Omega^2/\omega_r^2)}{1 - \Omega^2/\omega_r^2}, \tag{3a,b}$$

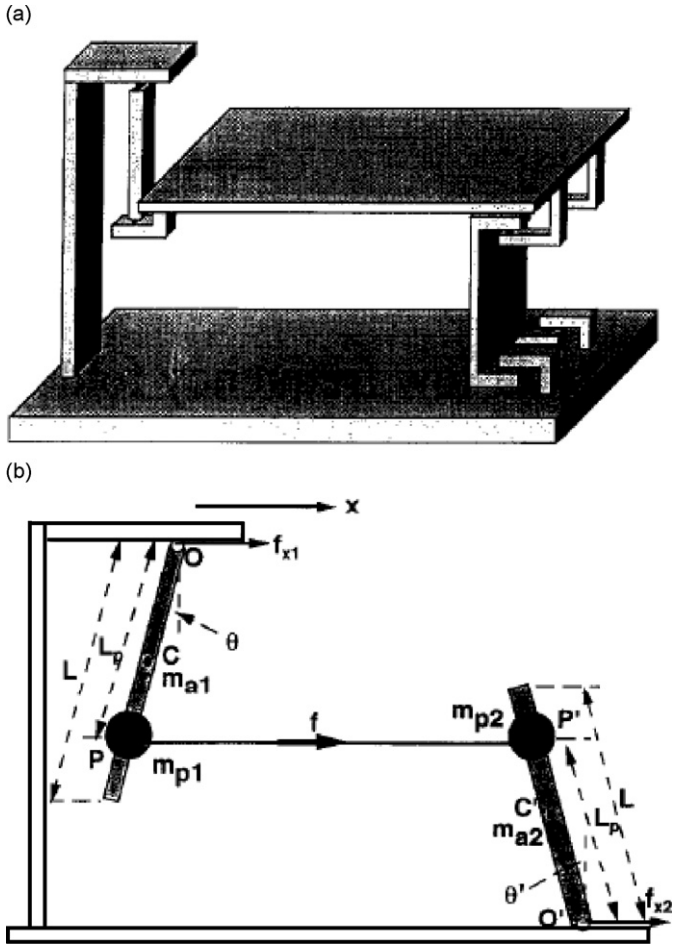

Fig. 7. Three-dimensional and projection diagrams of the folded pendulum: (a) three-dimensional of the folded pendulum and (b) equivalent system [98].

where

$$M_e = \frac{1}{3}(m_{a1}+m_{a2})\frac{l^2}{l_P^2}+(m_{P1}+m_{P2}), \quad \omega_r^2 = \frac{(1/2)(m_{a1}+m_{a2})(l/l_P)+(m_{P1}+m_{P2})}{(1/3)(m_{a1}+m_{a2})(l^2/l_P^2)+(m_{P1}+m_{P2})}\left(\frac{g}{l_P}\right),$$
$$K = \frac{(m_{a1}+m_{a2})\big((l/3l_P)-(1/2)\big)}{1/3(m_{a1}+m_{a2})(l/l_P)+(m_{P1}+m_{P2})(l_P/l)}. \tag{3c – e}$$

If the mass parameter $K=0$, then the system is converted into a simple pendulum of equivalent length

$$l_e = \frac{(1/3)(m_{a1}+m_{a2})(l^2/l_P^2)(m_{P1}+m_{P2})}{(1/2)(m_{a1}+m_{a2})(l/l_P)+(m_{P1}+m_{P2})}l_P. \tag{4}$$

In principle one can obtain any equivalent length by changing the masses in Eq. (4). In other words, one can reduce the pendulum resonant frequency to an arbitrary low value. This confirms the experimental results reported by Stebbins, Newell et al. [99]. The system forms a pre-isolation stage in the vibration isolation system for laser interferometer gravitational wave detectors. Liu et al. [98,100] found that the dynamic behavior of the folded pendulum closely approximates that of a simple pendulum of the same period of natural oscillation. At long periods the pendulum becomes susceptible to variations in the tilting of its base. The influence of base tilt was considered later by Winterflood et al. [101,102]. Fig. 8 shows the transfer function at a resonant frequency of 0.03 Hz for different values of K. The value of K vanishes if $l_P = 2l/3$, and this implies that the points P and

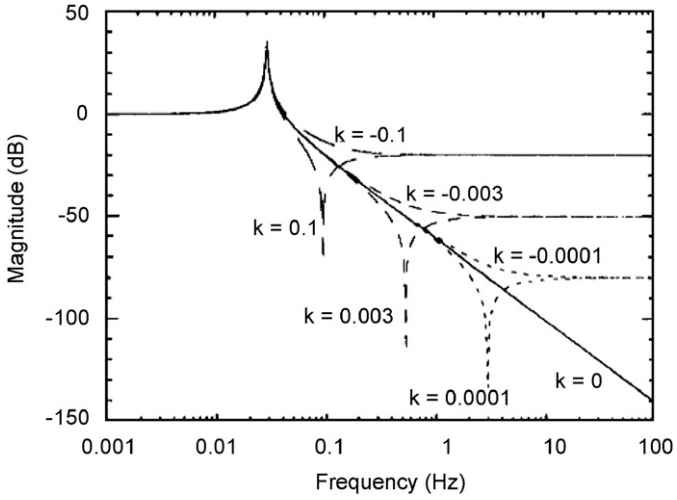

Fig. 8. Base excited transfer function of the folded pendulum for resonant frequency 0.03 Hz and different values of the parameter K: ____ $K = 0$, - - - $K = 0.0001$, __ __ __ $K = 0.003$, ____ ____ ____ $K = 0.1$ [98].

P' are on the centers of percussion of the two rods. Figs. 9(a) and (b) show the measured transfer functions of the folded pendulum with two different values of natural frequency, $f = 0.1$ and 0.029 Hz, respectively. It is seen that Fig. 9(b) exhibits better isolation performance.

3.2. The X-pendulum isolation table

Wire rope systems have found numerous applications in the shock and vibration isolation of military hardware, industrial machinery, and seismic protection of equipment in buildings [103–105]. Demetriades et al. [105] introduced the wire rope isolators and combination of them with locked casters for seismic isolation and found that their use in stiff configurations may substantially improve the seismic response of equipment in comparison to other installation methods. One form of wire rope isolator takes the shape of the X-pendulum vibration isolation table shown in Fig. 10(a). This system was studied in Refs. [106–108] and it uses typically four (but at least three) suspension wires to support an intermediate X-plate. The plate in turn supports the main test mass via a rigid structure such as a bar. The wires form an X-shape when viewed from the side. The X-mechanism acts as an elaborate but otherwise ordinary hinge, so that the bar and test mass move as an ordinary pendulum. However, the X-plate has the useful property of relaxing a small amount vertically when tilted off-center. This vertical motion tends to cancel the natural upward curvature of the locus of a point on the test mass due to the pendulum motion. If the dimensions are chosen to make the cancellation exact near the center of mass of the plate-bar-mass system, the potential well becomes arbitrarily flat (at least to second-order), and the natural frequency becomes arbitrarily small. Barton and Kuroda [107] showed that the X-pendulum behaves as a simple harmonic oscillator of an adjustable and very low frequency. The natural frequency of the lateral oscillation of the pendulum was given by the following expression:

$$\omega_n^2 = \frac{M_w g(H - H_H)}{M_w\{[(L_2 \tan \alpha_0)/2] + H\}^2 + I}, \tag{5}$$

where M_w is the mass of the test weight suspended by the bar, H is the distance of the center of mass of the pendulum, P, below the midpoint of the lower plate, L_2 is the distance between anchor points of the lower plate, I is the mass moment of inertia of the pendulum, α_0 is the acute angle of the wires and the horizontal when the pendulum is hanging centrally, and H_H is the critical value of H where the center of mass P moves horizontally and the pendulum is on the verge of stability. The value of H_H was given

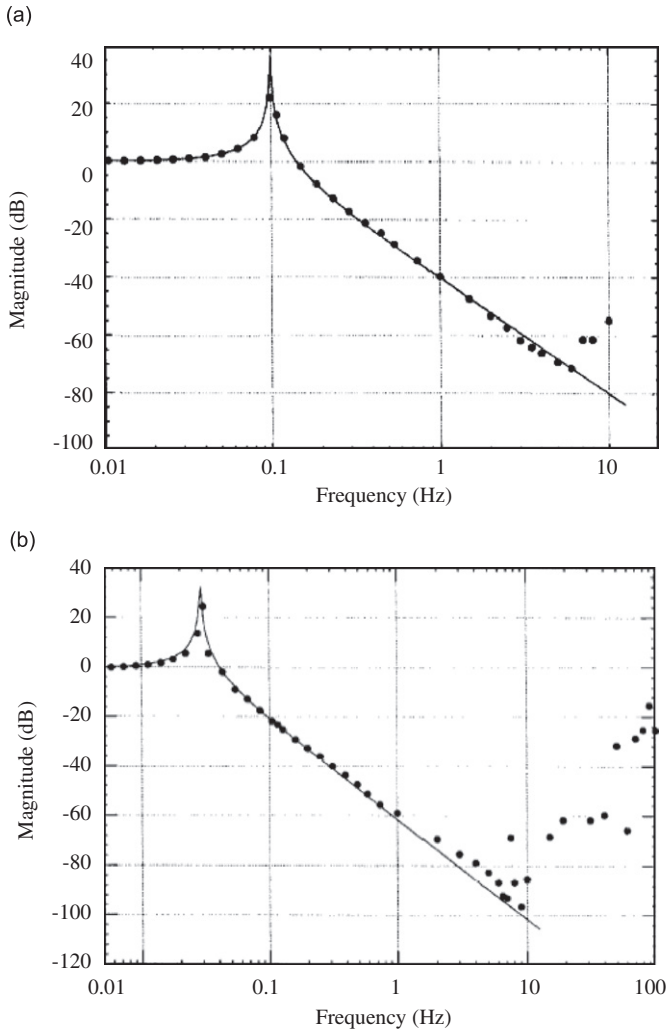

Fig. 9. Measured transfer functions of the folded pendulum for two different resonant frequencies: (a) $f = 0.1$ Hz, and (b) $f = 0.029$ Hz. The solid curves are for the equivalent simple pendulum of the same natural frequency [98].

by the expression

$$H_H = \frac{L_2}{4l \sin \alpha_0}\left[2l \cos \alpha_0 - (L_2/\cos^2 \alpha_0)\right], \tag{6}$$

where l is the length of each wire. The relationship between the tilt angle of the mass, θ, and the lateral displacement, x_P, of the center of mass P, was given by the following expression:

$$\theta = \frac{2x_P \cos \alpha_0}{L_2 \sin \alpha_0 + 2H \cos \alpha_0}. \tag{7}$$

Fig. 11 shows the dependence of the natural frequency, $f = \omega_n/2\pi$, on the weight position, d. The frequency monotonically increases with the position and approaches an asymptotic value as $d \to \infty$.

Barton et al. [108] extended the basic idea of the X-pendulum to a system of two or more X-pendulums. A load table is suspended using a combination of normal and upside-down X-mechanisms so that it moves freely with a very long period in both horizontal directions but is moderately stiff in all other degrees of freedom. Fig. 10(b) shows a schematic diagram of the two-dimensional X-pendulum. The combination of normal and inverted mechanisms was referred to as a corner unit, because the natural place to deploy it is at the corner of the

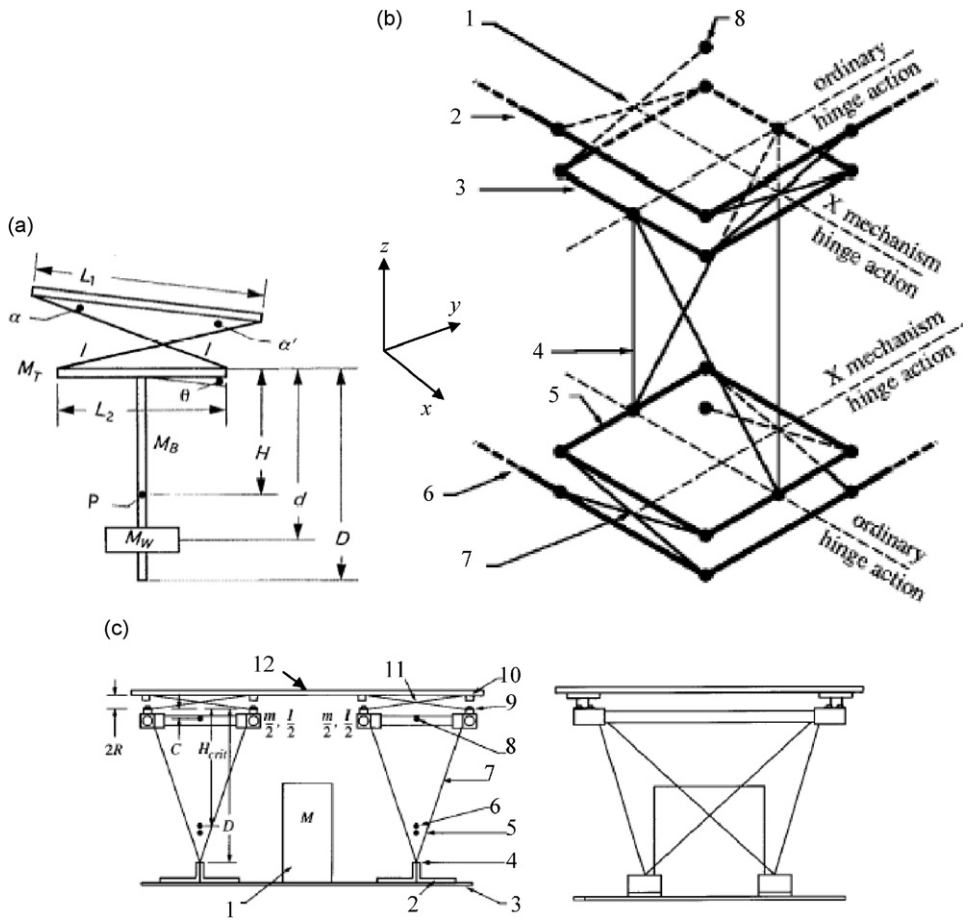

Fig. 10. Schematic diagrams of different versions of the X-pendulum: (a) schematic diagram of X-pendulum and (b) corner unit of a two-dimensional X-pendulum: 1—upper X-wires (slightly staggered), 2—support table corner, 3—upper X-plate, 4—intermediate wires (4), 5—lower, inverted X-plate, 6—load table corner, 7—lower X-wires (slightly staggered), 8—wire attachment point. (c) Side and end views of one-dimensional two X-pendulums supporting a table: 1—payload, 2—detachable clamp, 3—load table, 4—hinge point, 5—net center of mass, 6—critical point, 7—intermediate wire, 8—frame center of mass, 9—clamp screw with tuning spacer, 10—clamp block, 11—X-wires, 12—support table [87,107,108].

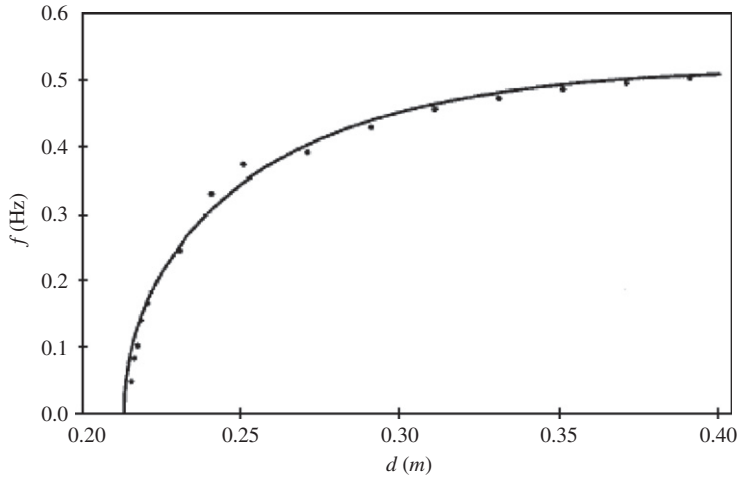

Fig. 11. Dependence of the natural frequency on the weight position: _____ analytical according to Eq. (5), •••• experimental measurements [107].

table to be supported. The corner units are oriented such that the normal X-mechanisms allow motion along the y-axis and the inverted X-mechanisms are responsible for the x-motion. Another type of low-frequency, but one-dimensional, vibration isolation system is shown in Fig. 10(c). A load table is supported by two X-pendulums from a support table, which moves horizontally due to seismic disturbances but is stiff against all other motions [108].

3.3. Conical pendulum

Winterflood and Blair [85] and Winterflood et al. [109] developed the conical pendulum based on the Scott–Russel linkage [110] schematically shown in Fig. 12(a). The system consists of a linkage arrangement,

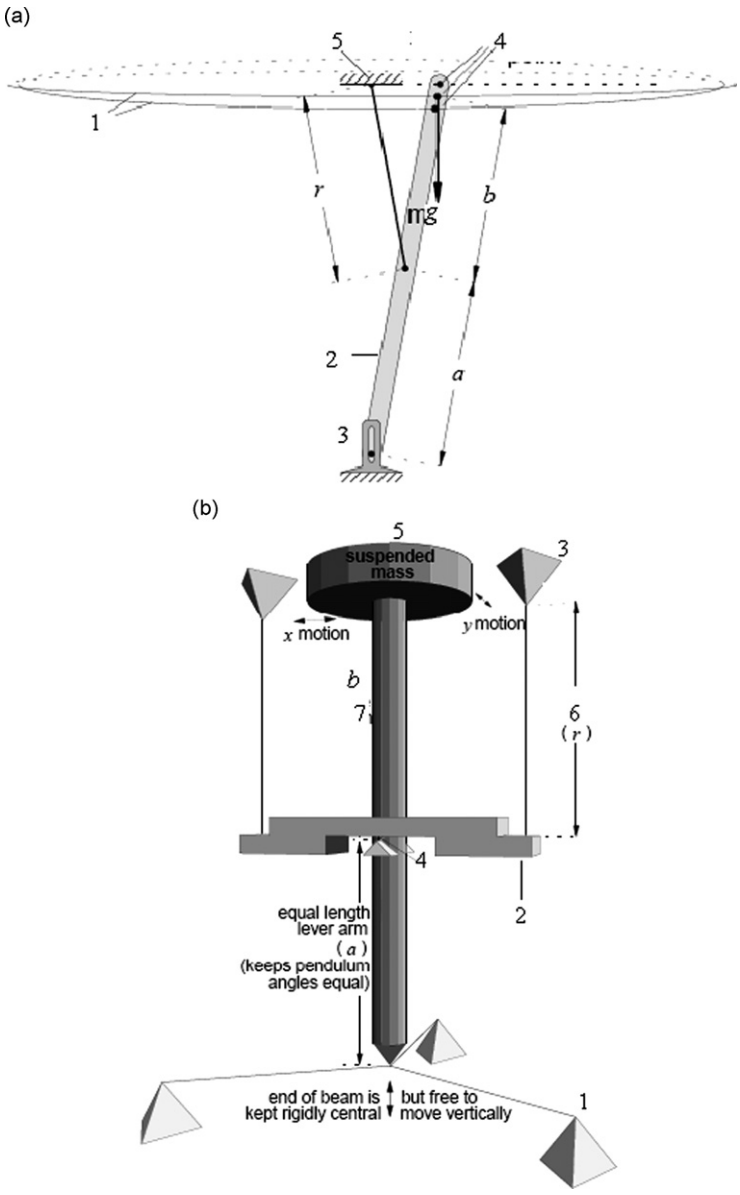

Fig. 12. The conical pendulum: (a) schematic diagram of the conical pendulum: 1—elliptical suspension point loci, 2—rigid beam, 3—vertical alignment motion constraint, 4—mass suspension point, 5—main fixed support. (b) Prototype arrangement: 1—taut wire fixings, 2—cross-beam (allows supporting at each side of mass avoiding spatial conflict in center, 3—main support, 4—central flex joint, 5—suspended mass, 6—normal pendulum, 7—inverse pendulum [85,92].

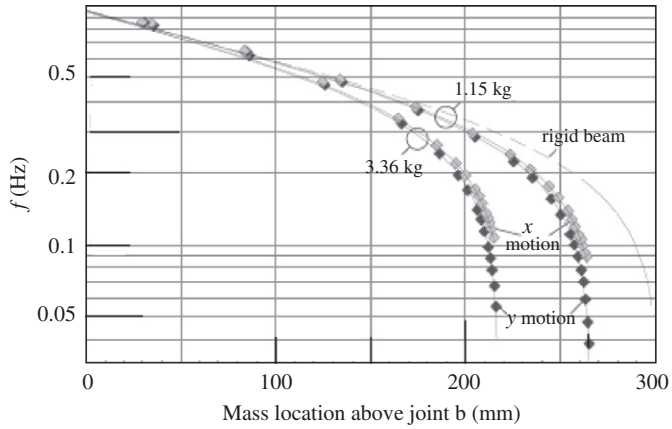

Fig. 13. Dependence of natural frequency on the height of mass above joint: ---, rigid rod, 1—1.15 kg, 2—3.36 kg [85,92].

which mimics the motion of a very long conical pendulum achieving x–y isolation in a single stage. A pendulum of length r is joined near the midpoint of a rigid rod of length $(a+b)$. The normal pendulum is under tension and supports the entire weight of the structure and suspended mass. The top section of the rod supports the suspended mass under compression and bending. The lower end of the rod is merely constrained to move in a vertical line directly under the main support. If $a = r$, then the upper section of the rod b may be considered as an inverted pendulum, which is constrained to follow the same angle of deflection as the normal pendulum, a. In addition, if $b = r$ then the effect of the normal and inverted pendulums cancel and the suspension point follows a straight horizontal line. On the other hand, if a slightly lower suspension point is chosen, then the suspension point follows an exact elliptical trajectory as shown in Fig. 12(a).

The idea was implemented by constructing a simple prototype shown in Fig. 12(b). Both the rod and mass were threaded to allow adjustment for the position of the suspension point. The vertical wires carry the entire weight of the structure as a simple pendulum and the vertical rod with its mass acts as an inverted pendulum. The mass was initially adjusted for maximum repeatable period and then moved down in small increments. For each location the resonant frequency for each direction was measured. The process was repeated with a much heavier mass for comparison and the results are shown in Fig. 13. The observed difference in the frequency curves for two different masses was attributed to the flexibility of the rod. The difference between the x- and y-directions was partly due to the 1-mm joint offset and partly due to differing rod flexibility from the flex joint construction in the center of the rod.

Garoi et al. [111] took advantage of the Roberts linkage [110] and built an ultra-low-frequency passive vibration isolation device as part of the pre-isolation stage for the Australian International Gravitational Observatory. Fig. 14 shows a schematic diagram of one-dimensional Roberts's linkage pre-isolator. It consists of a rigid frame attached to two wires in the form of a W-shape, where the sidelines represent the two suspension wires and the central inverted V is the rigid frame. The isolator works by causing the mass suspension point P to move in an almost flat horizontal plane, so that the suspended mass gravitational potential energy is almost independent of displacement. Small modifications in the geometry (such as moving point P slightly above or below the plane of the suspension points) allow point P to move in a very shallow arc.

4. Euler column isolators

4.1. Buckling and post-buckling of Euler column

An Euler spring is a column of spring steel material that is compressed elastically beyond its buckling load. The analysis of finite deflections of prismatic elastic columns after buckling was developed by Euler [112] using elliptic integrals. The shape of the elastic curve in the post-buckling state is referred to as the *elastica*.

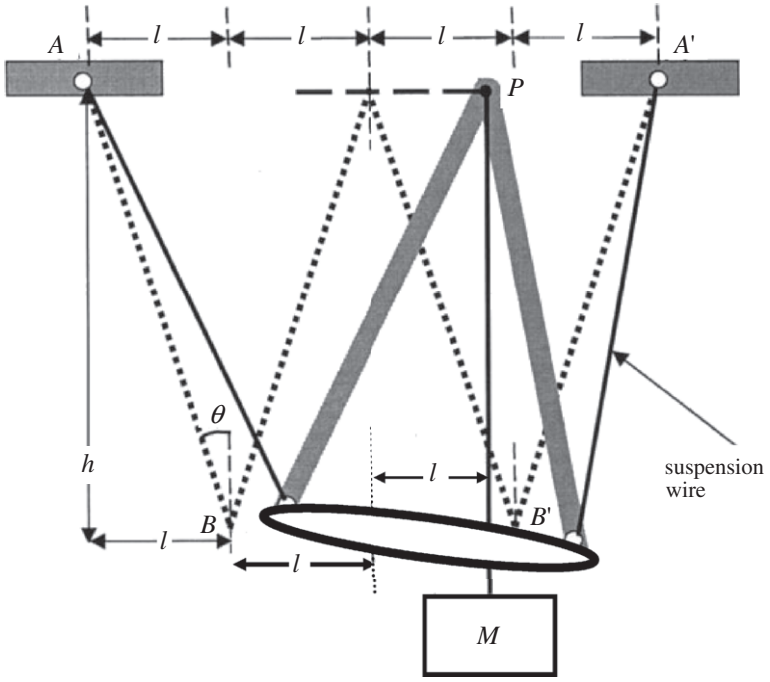

Fig. 14. Schematic diagram of the Roberts linkage isolator with a suspended load from the wire PM [111].

The stability theory of buckled and post-buckled elastic structural elements under static load is well documented in many Refs. [113–128]. It was demonstrated that the neighborhood of an equilibrium state could be explored analytically by means of a perturbation approach. The most important problems include the post-critical behavior, which involves stability analysis in the vicinity of bifurcation points. Schmidt and Da Deppo [129] presented an assessment of the classical work on large deflection of non-shallow arches. Traditionally, buckling is regarded as a failure criterion of structures. However, the post-buckling behavior of flexible rods is of practical interest if one considers the resulting axial displacement. Buckling loads and post-buckling behavior are very important to structural design.

The critical (Euler) buckling load, P_E, of a prismatic column primarily depends on their boundary conditions and the following four cases are well documented in the literature (see e.g., Ref. [115]):

(i) For the clamped–free column, $P_E = \pi^2 EI/4l^2$.
(ii) For the pin-ended column, $P_E = \pi^2 EI/l^2$.
(iii) For clamped–pin column, $P_E = 20.19\pi^2 EI/4l^2$.
(iv) For clamped-ended column, $P_E = 4\pi^2 EI/l^2$.

where E is Young's modulus of elasticity, I is the area moment of inertia, and l is the length of the column. The shape of a buckled pin-ended column is the same curve as the center section of the buckled clamped-ended column between the points of inflection, which in this case is half the length.

The mechanics of *elastica* of different geometries, including statics and dynamics problems, is treated in Refs. [130–132]. The dynamic elastic stability of the Euler beam under deterministic and random parametric (axial) excitations is also documented in Refs. [133–136]. Woinowsky-Krieger [137] determined the natural frequency for simply supported beam, with an axial load that is below the value of the critical buckling load. Burgreen [138] estimated the first mode natural frequency and its dependence on the amplitude for post-buckling of a simply supported column. Other cases with different boundary conditions were considered in several studies [139–144]. It was found that the nonlinear natural frequency of a beam with a constant axial load or with a constant distance between its ends increases with the amplitude of vibration.

Nonlinear analyses of post-buckling of rods include the determination of the critical buckling load for different types of boundary conditions and stability under high-frequency axial excitation [145–153]. Early works by Chelomei [154,155] showed that a buckled beam could be stabilized by adding a high-frequency axial excitation. A heavy mass was mounted on a simply supported elastic rod and caused the rod to buckle. However, with high-frequency axial excitation applied to the mass, the rod was reported to straighten out. Jensen [149] considered the same problem and developed a nonlinear analysis allowing the effect of high-frequency excitation on straight and buckled positions. The nonlinear analysis revealed that stable buckled (quasi-static) equilibria could co-exist for loads almost as low as the original buckling load. With co-existing straight and buckled positions, the actual configuration was found to depend on the initial conditions. For example, if the beam is situated in a buckled position, then adding high-frequency excitation will not have any apparent effect on the system apart from adding small fast vibrations. Only if the beam was guided away from the buckled position, it can attain the stabilized straight position. Yabuno and Tsumoto [153] experimentally clarified that high-frequency excitation changes the nonlinear property of the bifurcation from supercritical pitchfork bifurcation to subcritical pitchfork bifurcation. Then the stable steady state of the beam exhibits hysteresis as the compressive force is reversed.

One of the recent applications of the Euler spring is its utilization as a vertical isolator. A major advantage of the Euler spring is that it stores negligible static energy below its working range thereby minimizing both the stored elastic energy density and the spring mass required to support the suspended test mass [5,156]. This feature makes Euler springs an excellent candidate as a vertical isolator. A schematic diagram of the Euler spring isolator is shown in Fig. 15(a). As the flat spring blade starts to buckle, the bulk of the blade can be offset in either one of two directions. If it is mounted in the pivoted support structure shown in Fig. 15(a) then the effect of offset in one direction is markedly different from the effect of offset in the other direction. If the offset occurs towards the pivot then very low (and even negative or unstable) spring stiffness is obtained as indicated by curve 1 shown in Fig. 15(b). On the other hand, if the offset occurs away from the pivot then much higher spring stiffness is achieved as indicated by curve 4 in Fig. 15(b). If a pair of matched spring blades is employed with one going in each direction, then the spring stiffness shown by curve 3 is graphically indistinguishable from what it would have been if it had been constrained to move linearly rather than in the rotating support structure actually employed. It follows that by choosing an appropriate ratio between the bending stiffness of the blade(s) moving towards the pivot to those moving away, a suitable mix of curves 1 and 4 can be reached yielding a much reduced spring stiffness as given by curve 2. The next sub-section describes the *elastica* and axial stiffness of the Euler column.

4.2. Exact and approximate axial stiffness

In order to establish an accurate modeling of the Euler spring dynamic characteristics, the basic relations of *elastica* and axial stiffness of a simply supported column will be presented. The presentation includes both exact and approximate analyses. Some nonlinear analyses of *elastica* have been developed in Refs. [106,148,157,158].

4.2.1. Exact analysis

Consider a uniform straight beam of length l shown in Fig. 16(a). Under an axial compressive load P, the column buckles with deflection $v(x)$ and its end moves by distance e. Consider an elemental length δx whose original position is a–b, which assumes the position a'–b' and length δs under the action of the compressive load P as shown in Fig. 16(b). The x- and y-displacements are related as follows:

$$\left(\frac{\mathrm{d}s}{\mathrm{d}x}\right)^2 = \left(1+\frac{\mathrm{d}u}{\mathrm{d}x}\right)^2 + \left(\frac{\mathrm{d}v}{\mathrm{d}x}\right)^2. \tag{8}$$

The linear strain is

$$\varepsilon = \frac{\mathrm{d}s}{\mathrm{d}x} - 1. \tag{9}$$

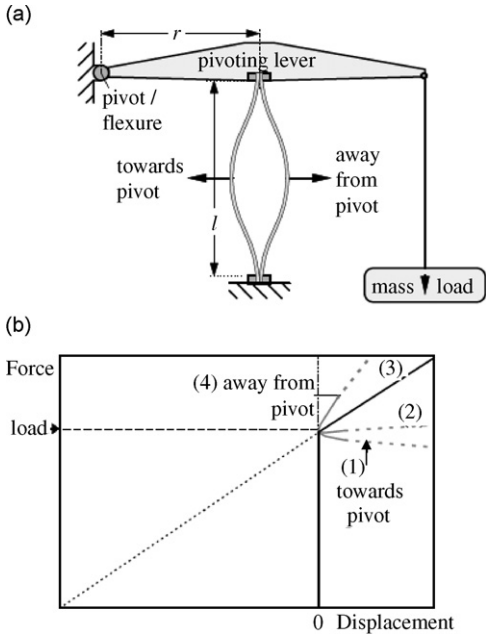

Fig. 15. Post-buckling Euler beam vertical isolator: (a) Euler column isolator showing its mount and its buckling columns is away from each other, (b) force–displacement relationship: 1—low or negative spring stiffness, 2—reduced spring stiffness, 3—linear spring stiffness and 4—high spring stiffness [5,168].

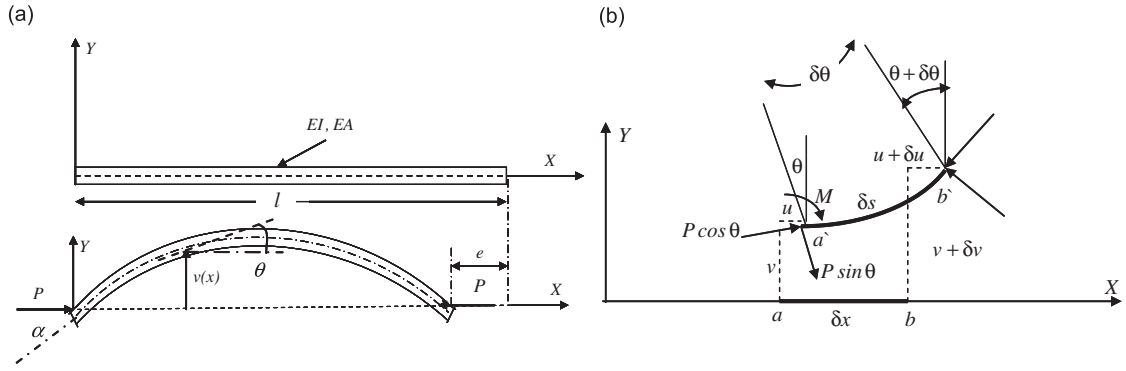

Fig. 16. Column under compressive axial load: (a) column before after buckling and (b) an element before and after buckling [121].

Let the tangent at any point make an angle θ with the x-axis. Since $\cos\theta = \left(1 + (\mathrm{d}u/\mathrm{d}x)\right)(\mathrm{d}x/\mathrm{d}s)$, Eq. (9) takes the form

$$\varepsilon = \left(1 + \frac{\mathrm{d}u}{\mathrm{d}x}\right)\frac{1}{\cos\theta} - 1 = -\frac{P\cos\theta}{EA}. \tag{10}$$

The bending moment equation is

$$EI\frac{\mathrm{d}\theta}{\mathrm{d}s} = EI\sin\theta\frac{\mathrm{d}\theta}{\mathrm{d}v} = -Pv. \tag{11}$$

From which one can write $EI\sin\theta\,\mathrm{d}\theta = -Pv\,\mathrm{d}v$. Let $c^2 = EI/P$, one can write

$$v\,\mathrm{d}v = -c^2\sin\theta\,\mathrm{d}\theta. \tag{12}$$

At $y=0$, the angle $\theta=\alpha$, and upon integrating Eq. (12), gives

$$v=c\sqrt{2}\sqrt{\cos\,\theta-\cos\,\alpha}. \tag{13}$$

Replacing $\sin\theta$ by $\mathrm{d}v/\mathrm{d}s$ in Eq. (12) gives

$$\mathrm{d}s=-c^2\frac{\mathrm{d}\theta}{v}=-\frac{c}{\sqrt{2}}\frac{\mathrm{d}\theta}{\sqrt{\cos\,\theta-\cos\,\alpha}}=-\frac{c}{2}\frac{\mathrm{d}\theta}{\sqrt{\sin^2(\alpha/2)-\sin^2(\theta/2)}}. \tag{14}$$

Introducing the transformation $k=\sin(\alpha/2)$ and $\sin(\theta/2)=k\sin\phi$, from which one can write $\cos(\theta/2)\,\mathrm{d}\theta/2=k\cos\phi\,\mathrm{d}\phi$. Substituting for $\mathrm{d}\theta$ in Eq. (14) gives

$$s=-c\int_{\phi}^{0}\frac{\mathrm{d}\phi}{\sqrt{1-k^2\sin^2\phi}}=c\int_{0}^{\phi}\frac{\mathrm{d}\phi}{\sqrt{1-k^2\sin^2\phi}}=cF(k,\phi), \tag{15}$$

where $F(k,\phi)$ is the elliptic integral of the first kind and is a function of the modulus, k, and the amplitude ϕ. Eq. (13) reduces to the form [121]

$$v=2c\sqrt{\sin^2\frac{\alpha}{2}-\sin^2\frac{\theta}{2}}=2ck\,\cos\,\phi. \tag{16}$$

To determine x in terms of ϕ we use the relationship $\mathrm{d}x=\cos\theta\,\mathrm{d}s$ or

$$\mathrm{d}x=(1-2k^2\sin^2\phi)\frac{c\,\mathrm{d}\phi}{\sqrt{1-k^2\,\sin^2\phi}}.$$

Upon integration one can write

$$\begin{aligned}x&=c\int_0^{\phi}\frac{2(1-k^2\sin^2\phi)-1}{\sqrt{1-k^2\sin^2\phi}}\,\mathrm{d}\phi=2c\int_0^{\phi}\sqrt{1-k^2\sin^2\phi}\,\mathrm{d}\phi-c\int_0^{\phi}\frac{1}{\sqrt{1-k^2\sin^2\phi}}\,\mathrm{d}\phi\\&=c[2E(k,\phi)-F(k,\phi)],\end{aligned} \tag{17}$$

where $E(k,\phi)=\int_0^{\phi}\sqrt{1-k^2\sin^2\phi}\,\mathrm{d}\phi$ is the elliptic integral of the second kind. At the ends of the rod, $\theta=\alpha$, the value of $\phi=\pi/2$, and at the column midpoint, i.e., at the maximum deflection, we have $\theta=\phi=0$. Thus, the distance between the ends of the rod, $2a$, is

$$2a=2c[2E(k)-K(k)]=l-e. \tag{18}$$

The maximum deflection and the total length of the rod are, respectively,

$$v_0=2ck=2\frac{l}{\pi}\sqrt{\frac{P_E}{P}}\sin(\alpha/2). \tag{19}$$

$$l=2cK(k), \tag{20}$$

where $K(k)=F(k,(\pi/2))$ and $E(k)=E(k,(\pi/2))$ are the complete elliptic integral of the first and second kind, respectively. The actual axial displacement, e, is

$$e=l-2a=2cK(k)-2c[2E(k)-K(k)]=4c[K(k)-E(k)]. \tag{21a}$$

For simply supported column, the above expression takes the form

$$e=4\frac{l}{\pi}\sqrt{\frac{P_E}{P}}[K(k)-E(k)]. \tag{21b}$$

One can estimate the axial stiffness $k_a=\mathrm{d}P/\mathrm{d}e$ from Eq. (21b), which gives

$$k_a=\frac{\pi}{2l}\frac{P}{P_E}\frac{\sqrt{P}}{[K(k)-E(k)]}. \tag{22}$$

The normalized displacement is

$$\frac{e}{l}=2\left[1-\frac{E(k)}{K(k)}\right]. \tag{23}$$

These exact results will be compared with the approximate analysis described in the next sub-section.

4.2.2. Approximate analysis

The approximate analysis is based on an approximate expression of the column curvature, $\kappa=\mathrm{d}\theta/\mathrm{d}x$. The bending moment may be written in the form [121]

$$M\approx EI(\mathrm{d}\theta/\mathrm{d}x)=-Pv. \tag{24}$$

Consider the sum of the energy due to contraction, bending, and the work done due to the axial load [121]

$$V=\frac{P^2}{2EA}\int_0^l\cos^2\theta\,\mathrm{d}x+\frac{1}{2}EI\int_0^l\left(\frac{\mathrm{d}\theta}{\mathrm{d}x}\right)^2\mathrm{d}x+P(u_l-u_0), \tag{25}$$

where u_0 and u_l are the end-displacements at $x=0$ and l, respectively. From Eq. (10) one can write

$$e=-(u_l-u_0)=\int_0^l\left[1-\cos\,\theta+\frac{P\cos^2\theta}{EA}\right]\mathrm{d}x. \tag{26}$$

Substituting Eq. (26) into Eq. (25), gives

$$V=\frac{1}{2}EI\int_0^l\left(\frac{\mathrm{d}\theta}{\mathrm{d}x}\right)^2\mathrm{d}x-\frac{P^2}{2EA}\int_0^l\cos^2\theta\,\mathrm{d}x-P\int_0^l(1-\cos\,\theta)\,\mathrm{d}x. \tag{27}$$

Expanding $\cos\theta$ in a power series and keeping terms up to fourth-order, gives

$$V=-\frac{P^2l}{2EA}+\frac{1}{2}EI\int_0^l\left(\frac{\mathrm{d}\theta}{\mathrm{d}x}\right)^2\mathrm{d}x-\frac{1}{2}P\left(1-\frac{P}{EA}\right)\int_0^l\theta^2\,\mathrm{d}x-\frac{1}{24}P\left(1-\frac{4P}{EA}\right)\int_0^l\theta^4\,\mathrm{d}x+\mathrm{HOT}, \tag{28}$$

where HOT stands for higher-order terms. For simply supported column, the shape function may be written in the form

$$\theta(x)=\alpha\cos(\pi x/l). \tag{29}$$

Substituting Eq. (29) into Eq. (28) and evaluating the integrals gives

$$V=-\frac{P^2l}{2EA}+\frac{l}{4}\left[P_E-P\left(1-\frac{P}{EA}\right)\right]\alpha^2+\frac{1}{64}Pl\left(1-\frac{4P}{EA}\right)\alpha^4+\mathrm{HOT}. \tag{30}$$

where $P_E=\pi^2EI/l^2$. Since the buckled mode is in static equilibrium, we have, $\partial V/\partial\alpha=0$, which gives

$$P_E-P\left(1-\frac{P}{EA}\right)+\frac{P}{8}\left(1-\frac{4P}{EA}\right)\alpha^2+\mathrm{HOT}=0. \tag{31}$$

To determine the axial displacement, e, Eq. (26) is used after replacing $\cos\theta$ and $\cos^2\theta$ in power series, i.e.,

$$\begin{aligned}e&=\int_0^l\left[1-\left(1-\frac{\theta^2}{2}+\frac{\theta^4}{24}\right)+\frac{P}{EA}\left(1-\theta^2+\frac{\theta^4}{3}\right)\right]\mathrm{d}x+\mathrm{HOT}\\&=\frac{Pl}{EA}+\frac{1}{2}\left(1-\frac{2P}{EA}\right)\int_0^l\theta^2\,\mathrm{d}x-\frac{1}{24}\left(1-\frac{8P}{EA}\right)\int_0^l\theta^4\,\mathrm{d}x+\mathrm{HOT}.\end{aligned} \tag{32}$$

Substituting Eq. (29) and evaluating the integrals gives

$$e=\frac{Pl}{EA}+\frac{l}{4}\left(1-\frac{2P}{EA}\right)\alpha^2+\mathrm{HOT}. \tag{33}$$

Ignoring higher-order terms, one can solve for α^2 and then substituting in Eq. (31) gives

$$P_E - P\left(1 - \frac{P}{EA}\right) + \frac{P}{2}\left(1 - \frac{4P}{EA}\right)\frac{\left((e/l) - (P/EA)\right)}{\left(1 - (2P/EA)\right)} = 0. \tag{34}$$

Solving Eq. (34) for e/l, gives

$$\frac{e}{l} = \frac{P}{EA} + 2\frac{\left(1 - (2P/EA)\right)}{\left(1 - (4P/EA)\right)}\left(1 - \frac{P}{EA} - \frac{P_E}{P}\right) \underset{EA\to\infty}{\longrightarrow} 2\left(1 - \frac{P_E}{P}\right). \tag{35}$$

Thus the axial stiffness, k_a, of the post-buckling curve at $P = P_E$ is

$$k_a = \left(\frac{\mathrm{d}P}{\mathrm{d}e}\right)_{P=P_E} = \frac{1}{2}\frac{P_E}{l}. \tag{36}$$

Comparing this approximate expression with the exact stiffness given by Eq. (22) reveals that the exact stiffness is a nonlinear function of the applied load.

The relationship between the axial displacement, e, and the lateral deflection, v, can be obtained by using the approximate relationship of the bending moment, Eq. (24), which gives after using Eq. (29)

$$v(x) = \frac{\pi EI}{Pl}\alpha\,\sin(\pi x/l) = v_0\,\sin(\pi x/l). \tag{37}$$

The maximum deflection, v_0, occurs at the mid-length of the column and has the value

$$v_0 = \frac{\pi EI}{Pl}\alpha. \tag{38}$$

For a very large value of EA the value of α is obtained from Eq. (33) in the form, after using Eq. (35)

$$\alpha = 2\sqrt{\frac{e}{l}} = 2\sqrt{2\left(1 - \frac{P_E}{P}\right)}. \tag{39}$$

Substituting Eq. (39) into Eq. (38) gives the dependence of the lateral deflection on the applied load

$$v_0 = \frac{\pi EI}{Pl}2\sqrt{2\left(1 - \frac{P_E}{P}\right)} = \frac{2l}{\pi}\frac{P_E}{P}\sqrt{2\left(1 - \frac{P_E}{P}\right)}. \tag{40}$$

Comparing the approximate Eq. (40) with the one given by the exact value of Eq. (19) reveals that as the applied load increases, the exact lateral deflection given by Eq. (19) is greater than the approximate one given by Eq. (40). Most of the analyses of Euler spring isolator reported in the literature are based on the approximate Eqs. (36) and (40). No attempt has been made to use the exact analysis.

Note that for the case of clamped–clamped column, the dependence of the applied load (normalized to the critical buckling load) on the axial displacement (normalized to the Euler spring length) beyond the initial onset of buckling at critical load is governed by the relationships

$$F = 4K(k)^2/\pi^2, \quad x = 2\left[1 - \frac{E(k)}{K(k)}\right], \tag{41}$$

where the modulus $k = \sin(\alpha_0/2)$, $K(k)$ and $E(k)$ are the complete elliptic integrals of the first and second kind, respectively, and α_0 is the maximum angle between the tangent at the inflection points and the axis between the two inflection points for the case of clamped–clamped column.

4.3. Techniques of reducing resonant frequencies

One of the basic requirements of vibration isolators is to reduce the system restoring force, which results in a reduction of the resonant frequency. Some techniques have been developed to reduce the isolator resonant frequency. These include the curved cantilever springs for gravitational wave applications [159,160] and the triangular pre-bent cantilever springs [83,161–164]. Figs. 17(a) and 17(b) show two examples for reducing the

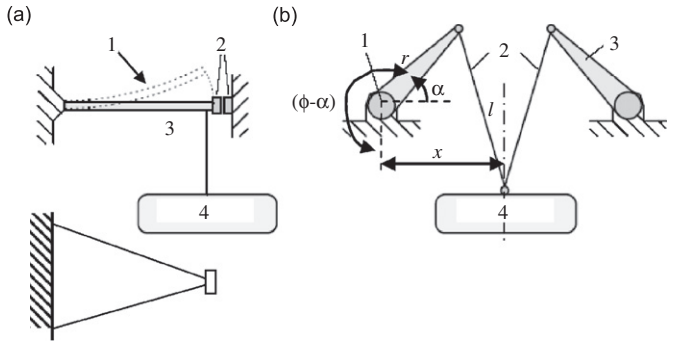

Fig. 17. Techniques of reducing resonance frequencies by using anti-spring and nonlinear mechanisms: (a) cantilever beam with end magnets: 1—static equilibrium position, 2—opposing magnets anti-spring, 3—smaller cantilever, 4—mass load. (b) torsional rod isolator: 1—torsion rod (end view), 2—suspension links, 3—crank arm, 4—mass load [5,168].

static energy stored in a cantilever beam and torsion-crank, respectively. The reduction of resonant frequency of these systems is discussed in the next sub-sections.

4.3.1. Cantilever with magnetic anti-spring

The cantilever beam can preserve constant stress over its surface if it has a triangular shape as seen from the top view with the wide base attached to the base and the triangle apex at the free end. This isolator was first proposed for use in gravitational wave detectors by Blair et al. [159] and later considered by Ju et al. [165] and Ju and Blair [160]. The free end of the cantilever beam is fitted with magnets, which strongly repel and try to drive the mass away from the normal operating position [166]. The issue of creep in metal cantilever spring suspension systems was considered together with some long-term observations of inelastic creep in carbon steel cantilever spring vibration isolators [167]. The vertical resonant frequency can be reduced by softening the cantilever around its working point by means of a magnetic system anti-spring mounted at the free end. The working principle of a magnetic anti-spring may be demonstrated by considering the system shown in Fig. 18, which consists of two magnets facing each other. When the magnets are perfectly aligned a repulsive force has a vanishing vertical component. If one of the magnets is moved in the vertical direction, a vertical component of the repulsive force emerges. For a vertical relative displacement, y, small with respect to the separation d of the magnets effective centers, the vertical component, F_y, of the repulsive force is proportional to y as

$$F_y = F_0 \sin \alpha \approx F_0 y/d, \tag{42}$$

where F_0 is the modulus of the repulsive force. This arrangement is equivalent to a vertical spring with a negative elastic stiffness (anti-spring) whose stiffness is F_0/d and the unstable equilibrium position is where the magnets are perfectly aligned. The anti-spring characteristics are governed by the anti-springs' position and temperature. Fig. 19 shows the dependence of the vertical resonant frequency on the magnets' vertical offset for three different horizontal separations between the two magnets at 30 °C. It is seen that the anti-spring system can be easily tuned so as to obtain the required natural frequency. When the separation between the magnets is reduced the minimum resonant frequency, obtained with perfectly aligned magnets, decreases and the frequency versus vertical offset parabola becomes sharper. When the horizontal separation between the magnets is too small the isolator becomes bistable, i.e., possesses two stable equilibrium vertical positions, which are symmetric with respect to the zero vertical offset. Fig. 20 shows the effect of environment temperature on the natural frequency of the isolator. The permanent magnetic field of the anti-spring magnets decreases when the temperature increases because of the thermal flipping of a fraction of magnetic domains. Note that the frequency fluctuation may arise because the isolator vertical equilibrium position experiences temperature-induced variations. The variations in the vertical resonant frequency of the isolator for small

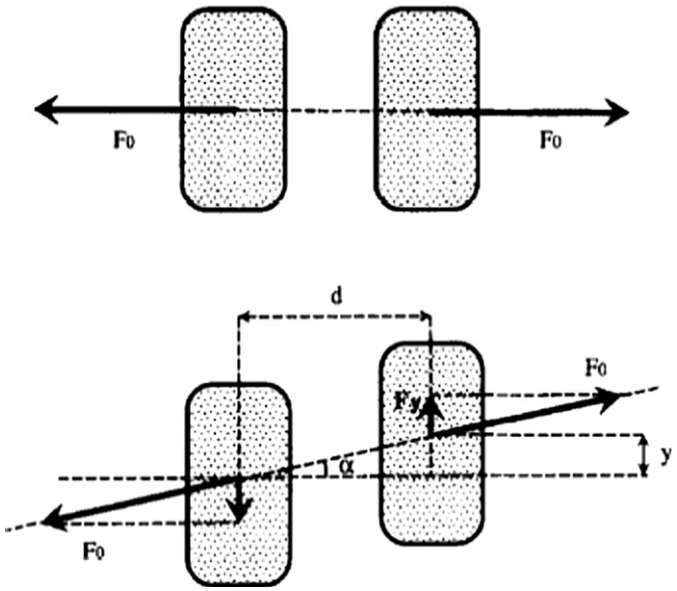

Fig. 18. Working principle of the anti-spring system: as the magnets are displaced one with respect to the other in the vertical direction, a vertical repulsive force component appears [166].

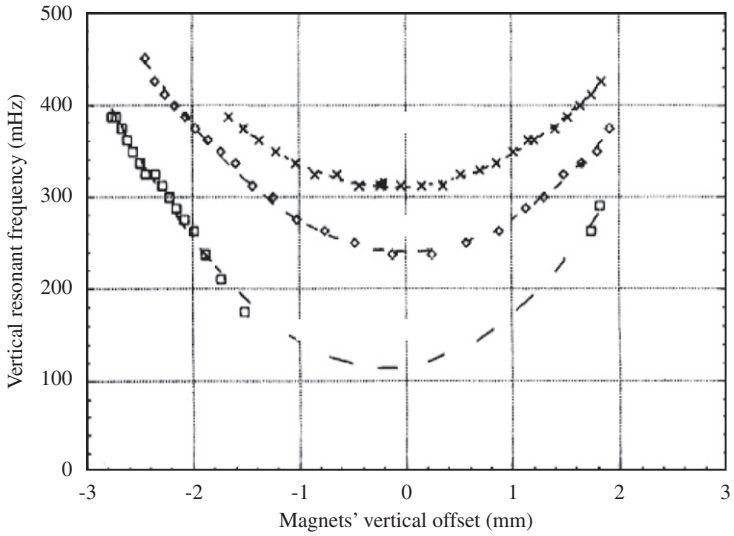

Fig. 19. Dependence of the natural frequency on the magnets' offset for different values of horizontal separations between: $\times\, d = 9.6$ mm, $\diamond\, d = 9.2$ mm, $\square\, d = 9.0$ mm [166].

variations in the temperature, ΔT, and the vertical offset, Δy, were evaluated by the formula

$$\Delta f_0 = \left.\frac{\partial f_0}{\partial y}\right|_{y_0,T_0} \frac{\Delta y}{\Delta T}\Delta T + \left.\frac{\partial f_0}{\partial T}\right|_{y_0,T_0} \Delta T. \tag{43}$$

The anti-restoring force, generated by the repelling force of the magnets, has a direct effect on the overall stiffness of the isolator. When this force is added to the normal restoring force of the cantilever beam, it produces a region of reduced gradient on the force displacement curve as shown in Fig. 21. It is seen that by operating over the flattened region of the curve, the natural frequency significantly drops. Winterflood and

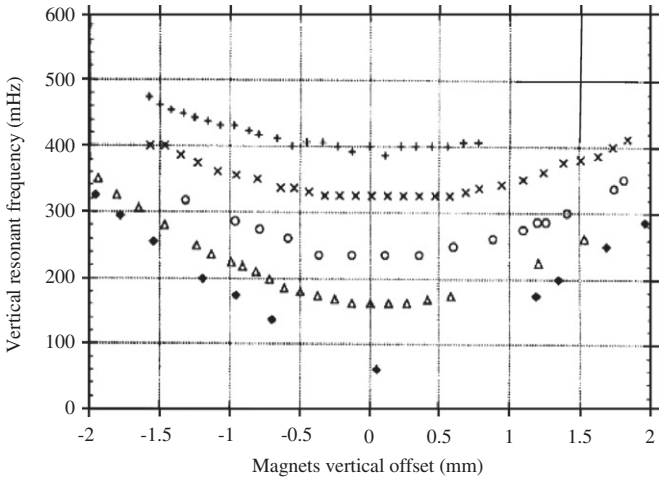

Fig. 20. Dependence of the vertical natural frequency of the isolator on the magnets' vertical offset for five values of different temperatures: ◆ $T = 24.8\,^{\circ}\mathrm{C}$, $\Delta T = 26.8\,^{\circ}\mathrm{C}$, ○ $T = 31.0\,^{\circ}\mathrm{C}$, × $T = 36.0\,^{\circ}\mathrm{C}$, + $T = 42.0\,^{\circ}\mathrm{C}$ [166].

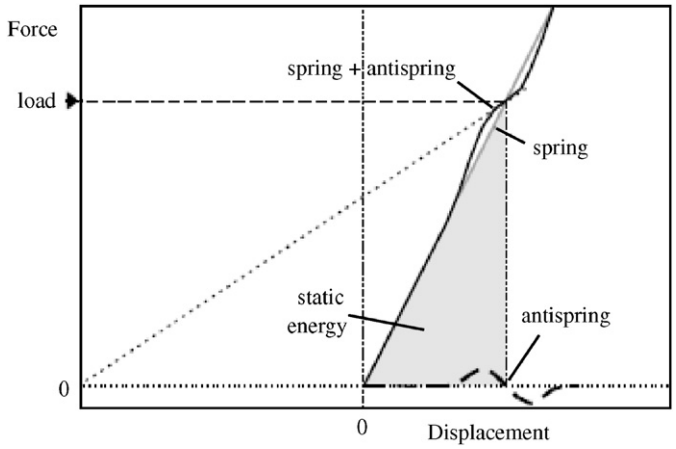

Fig. 21. Force–displacement relationship in the presence of anti-spring magnets [92,5].

Blair [168] pointed out some disadvantages of the magnetic anti-springs such as difficulty in achieving good spring stiffness neutralization over a wide range of operating conditions.

A vibration isolation system using a zero-power magnetic suspension system was proposed in Refs. [169–172]. A zero-power magnetic suspension system was shown to behave as if it has a negative stiffness. Furthermore, an infinite stiffness against disturbance on the isolation table can be achieved by combining it with a mechanical spring. The basic principle is based on a serial spring consisting of a normal spring in series with a spring whose stiffness is negative. If the absolute value of the stiffness of the normal spring is equal to that of the negative spring, the total stiffness of the serial spring becomes infinite. Accordingly, if a direct disturbance acts on the isolation table, the table will have no steady-state displacement.

4.3.2. Torsion-crank linkage

The torsion-crank linkage shown in Fig. 17(b) makes use of the nonlinearity produced by a torsion-sprung crank arm connected to a suspension link. The loaded end is constrained to move in a vertical line. The torsion rods are pre-stressed to provide an upward acting torque on the crank arms. By fixing the crank-arm length, r, the parameters that govern the force–displacement characteristics are (i) the length l of the supporting link,

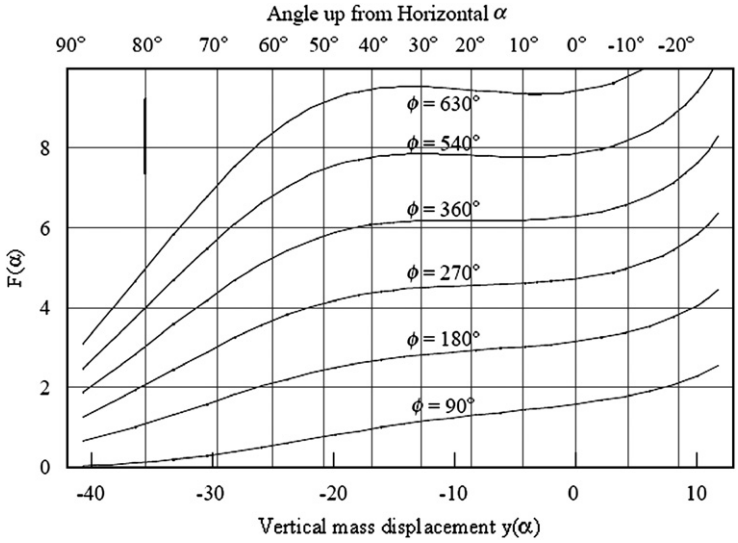

Fig. 22. Force–displacement relationship for different vales of pre-stress angle [92,168].

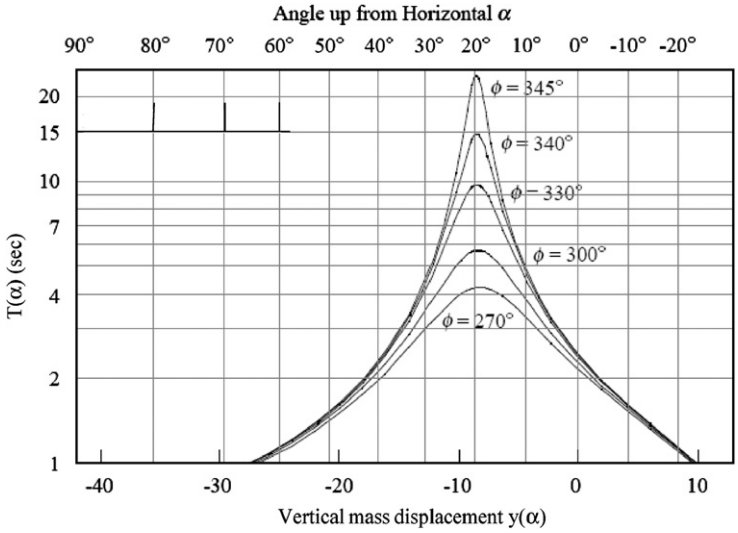

Fig. 23. Dependence of the resonant period on the mass displacement for different values of pre-stress angle [92,168].

(ii) the offset distance, x, from the crank-arm center to the vertical path followed by the end of the link, and (iii) the amount of pre-stress, ϕ, in the torsion rod. The pre-stress angle, ϕ, is the angle turned by the crank arm from being unstressed to being horizontal.

The dependence of the force on the vertical mass displacement, $y(\alpha)$, for different values of the pre-stress angle, ϕ, and for $l = x = r$, is shown in Fig. 22. It is seen that as the pre-stress angle is increased the degree of nonlinearity becomes more pronounced until $\partial F/\partial y$ becomes zero and then negative. Fig. 23 shows the dependence of resonant period on the vertical position of the mass for $l = x = r = 25\,\text{cm}$ and for different values of pre-stress angle. The nonlinearity observed in Fig. 22 owes its origin to the geometrical analysis of the vertical displacement. The vertical position, y, of the mass is related to the angle α through the relationship

$$y(\alpha) = \sqrt{1^2 - (x - r\cos\alpha)^2} - r\sin\alpha + \text{Const.} \tag{44}$$

The strain energy, $V(\alpha)$, stored in the torsion rod is

$$V(\alpha) = \frac{1}{2}k_\alpha(\phi - \alpha)^2, \tag{45}$$

where k_α is the angular stiffness of the torsion rod. The force acting in the vertical direction, $F(\alpha)$, is given by the gradient of the stored energy, i.e.,

$$F(\alpha) = \frac{\partial V}{\partial y} = \frac{\partial V}{\partial \alpha}\frac{\partial \alpha}{\partial y} = \frac{k_\alpha(\phi - \alpha)}{\partial y/\partial \alpha}. \tag{46}$$

The period of natural oscillation is

$$T = 2\pi\sqrt{\frac{[F(\alpha)/g]}{(\partial F/\partial\alpha)(\partial\alpha/\partial y)}} = 2\pi\sqrt{\frac{F(\alpha)y'(\alpha)}{gF'(\alpha)}}. \tag{47}$$

Note that both $F(\alpha)$ and $F'(\alpha)$ are proportional to the torsional spring stiffness, k_α. Accordingly, the period given by Eq. (47) is independent of k_α, but depends on $y'(\alpha)$ and the gravitational acceleration, g. In order to achieve a constant value of the resonant period for a small vertical motion, it is necessary to select an operating point where the resonant period is at a turning point, i.e., $\partial T/\partial y = (\partial T/\partial\alpha)(\partial\alpha/\partial y = 0)$. Since $\partial\alpha/\partial y$ is slowly varying and non-zero near the operating point, one may solve for $\partial T/\partial\alpha = 0$ as estimated from Eq. (47)

$$F'(\alpha)y'(\alpha) - F(\alpha)F''(\alpha)y'(\alpha) + F(\alpha)F'(\alpha)y''(\alpha) = 0. \tag{48}$$

Substituting Eqs. (44) and (46) in Eqs. (47) and (48) gives lengthy expressions. In an attempt to obtain an optimum geometry for which the resonant frequency is minimized over the largest possible vertical range, Winterflood and Blair [166] searched the space of solutions of Eqs. (47) and (48). It was found that the special geometry generated by a line of solutions with $\partial^3 F/\mathrm{d}y^3 = 0$, gives rise to a false optimum because it is associated with a horizontal instability over part of the operating region. Note that the symmetric opposing cranks become horizontally unstable over approximately the upper half of the vertical range. Horizontal motion occurs when both crank arms turn the same way allowing one arm to rise and the other fall. This horizontal instability was eliminated by adding constraints to limit motion to vertical translation only.

4.3.3. Monolithic geometric anti-spring system

Bertolini et al. [173] proposed the use of triangular cantilever blades coupled to inclined links to generate geometrical anti-spring effect. Fig. 24 shows a four-blade prototype in which the blade clamps are mounted on rotating and sliding supports. The load is attached to the disk center by means of a wire. The dependence of the system natural frequency on the vertical disk position is shown in Fig. 25 for different blade translations. The different curves correspond to different distances between the plate extremity to the clamped blade

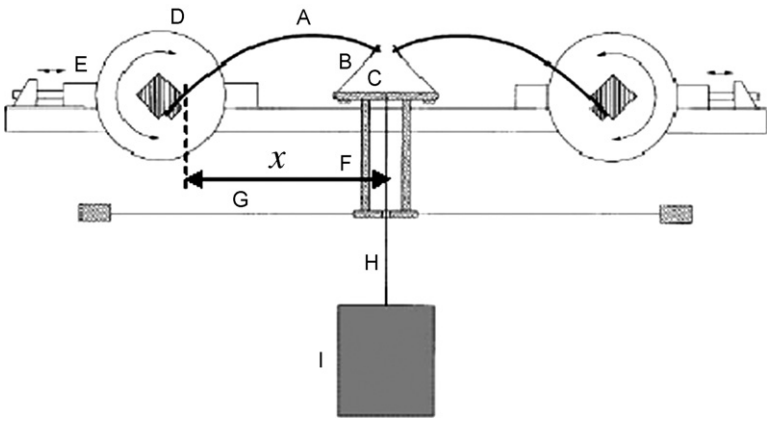

Fig. 24. Schematic diagram of a four-blade anti-spring prototype: "A" stressed blade, "B" link wire, "C" load disk, "D" angular movement of the blade base, "E" radial movement of the blade base, "F" anti-tilt tower, "G" anti-tilt centering wire, "H" suspension wire, "I" load [173].

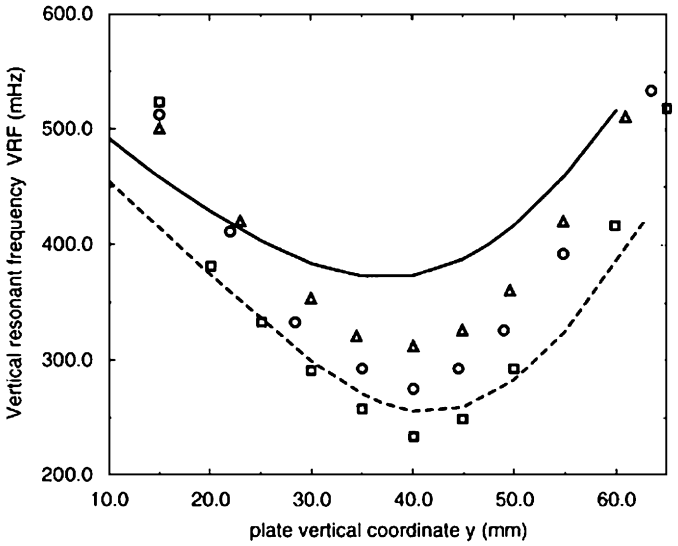

Fig. 25. Dependence of the vertical resonant frequency on the plate vertical distance of four-blade system: $\square x = 295 \pm 4$ mm, $\circ x = 296 \pm 4$ mm, $\triangle x = 297 \pm 4$ mm, ---- simulation with $x = 300$ mm, and — simulation with $x = 302$ mm [173].

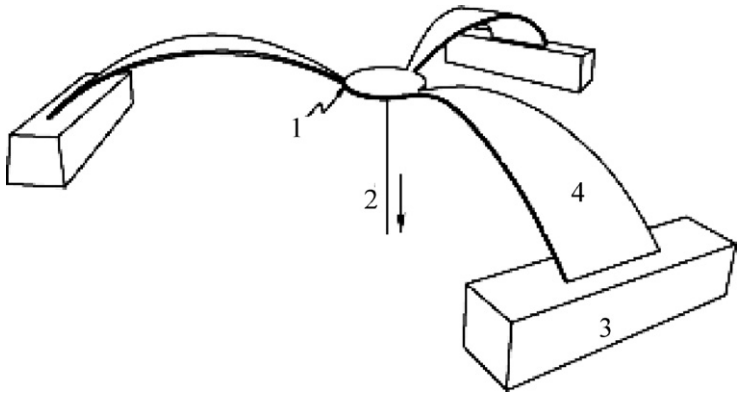

Fig. 26. Schematic view of a complete monolithic geometric anti-spring isolator for vertical noise attenuation [177].

extremity (the x-coordinate of the wire). It is seen that the frequency minima positions have a weak dependence on the blade positioning while the values of the vertical resonant frequency showed a rapid decrease. Passive isolation was achieved for all six degrees of freedom with an inverted pendulum and a chain of single wire pendulums whose masses were geometrically anti-spring filters [174,175]. Specifically the magnetic anti-spring concept allows significant increase in the vertical attenuation and thermal stability of a seismic attenuation system [173,175]. Wang et al. [176] developed a low-power non-contacting force actuator to control the advance Laser Interferometer Gravitational Wave Observatory and TAMA inverted pendulum motions and to damp the seismic attenuation systems.

The monolithic geometric anti-spring concept, introduced by Cella et al. [177], provided significant improvement of the performance of geometric anti-spring systems for vertical noise attenuation. Fig. 26 shows a schematic view of a complete monolithic geometric anti-spring filter made of three quasi-triangular blades radially disposed and connected together at their vertices. The base of the blade is clamped to a massive structure and subjected to an external force on the tip due to the load and the other radially arranged blades. The horizontal component compresses and bends the blade longitudinally. The low-frequency behavior of this isolator provides a singularity in the space of tunable parameters such as load and geometrical constraints, which are associated with a vanishing vertical stiffness. The fundamental limitations associated with the

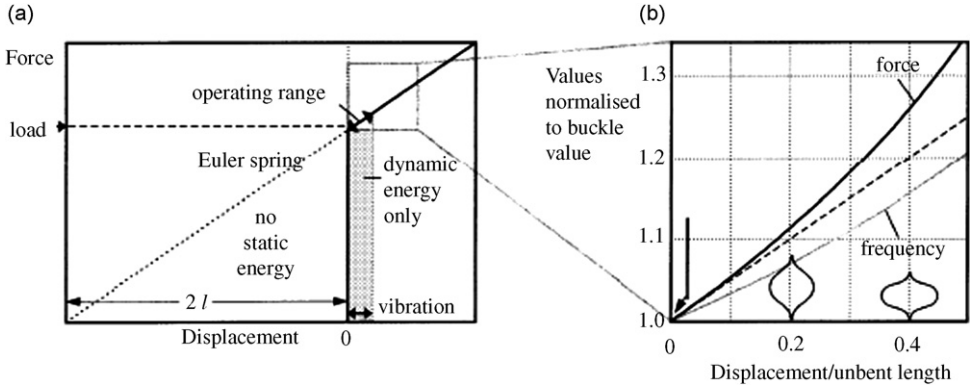

Fig. 27. (a) Force–displacement relationship, (b) expanded section of the gray area including the frequency characteristics of ideal buckling [5].

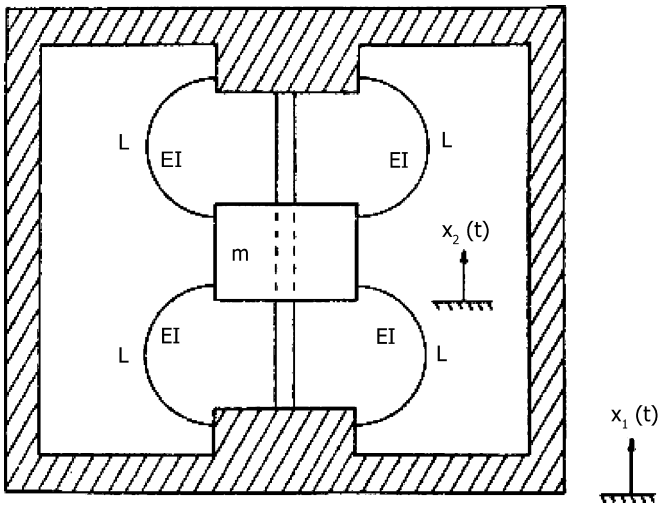

Fig. 28. Schematic diagram of two spring pairs in parallel of the elastica suspension isolator [179].

properties of the blade material such as Maraging[1] steel were explored by DeSalvo et al. [178]. It was reported that effects such as anomalous damping and hysteresis were caused by the movement of dislocations trapped between Maraging steel inter-metallic precipitates.

4.4. Natural frequency of Euler spring

Based on the approximate Eq. (36) of the axial stiffness of the Euler spring, the natural frequency under a weight equals to the critical buckling load, $P_E = mg$, is $\omega_e = \sqrt{g/2l}$, where l is the length of the Euler spring. Note that the natural frequency of a simple pendulum or mass–spring system is given by the well-known relation, $\omega_e = \sqrt{g/l}$, where l is the length of the pendulum or the static deflection of the coil spring. Thus, the suspended mass moves as though it was suspended by a linear spring whose static deflection is twice the length of the Euler spring. Fig. 27 demonstrates that if the working range is designed to begin just at the onset of buckling, then all of the energy stored by the spring is the dynamic energy within the gray area.

Shoup [179] developed a nonlinear elastic suspension vibration isolator consisting of a pair of flexible strips each having length L. The two strips are clamped in a semicircular shape as shown in Fig. 28. If the mass, m, is

[1]Maraging steel possesses superior strength and toughness without losing malleability.

forced downward by a load, P, the upper strip deflects into a shape called the *nodal elastica*, while the lower strip deforms into a shape known as the *undulating elastica*. The equations of these elastica curves are well documented in Frisch-Fay [116]. Shoup [179] utilized these equations to evaluate the load–deflection curves

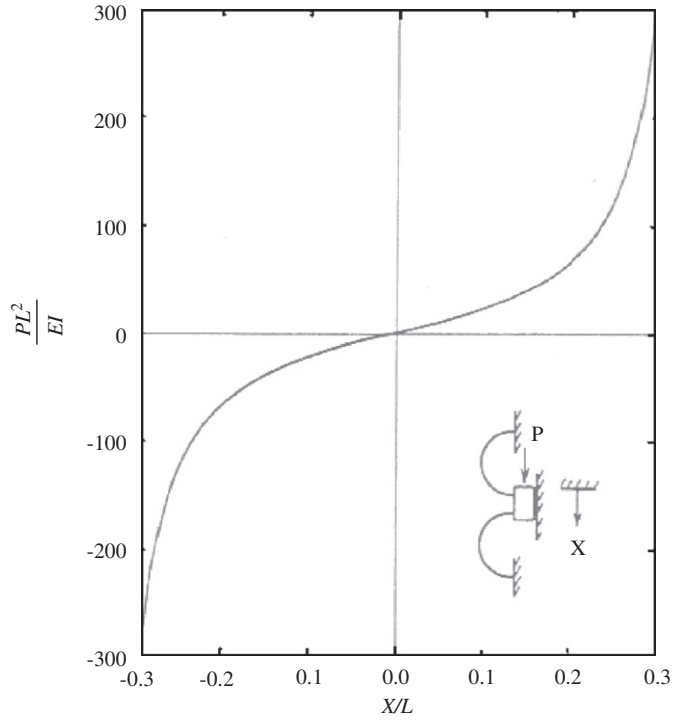

Fig. 29. Nondimensional load–deflection curve for the elastica suspension spring pair [179].

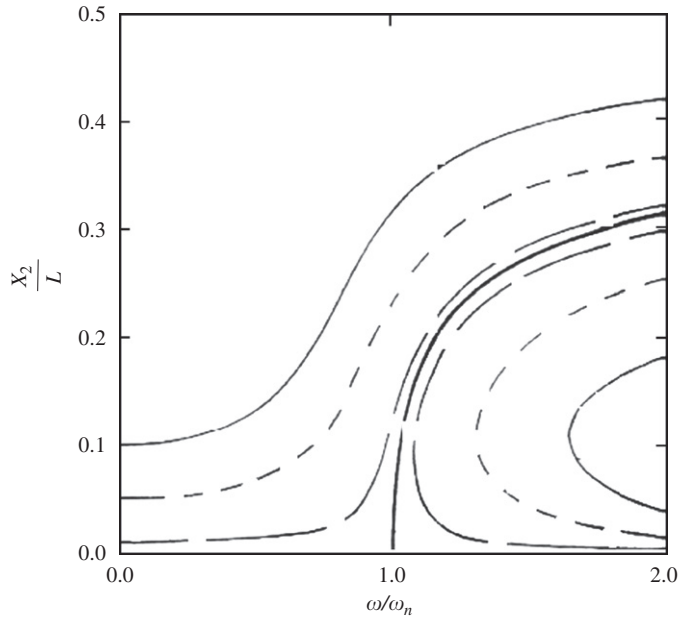

Fig. 30. Amplitude–frequency response of the elastica suspension system, the backbone curve represents the dependence of the natural frequency on the response amplitude: $X_1/L = 0.1$ ——, $= 0.1$ – – –, $= 0.1$ — —, $= 0.0$ ———— [179].

shown in Fig. 29. Note that the stress in the strips is caused by the combined effects of bending and simple tension or compression. The natural frequency for small deflection was given in the form

$$\omega_n = 285\sqrt{\frac{nEI}{mL^3}}, \tag{49}$$

where $n = 2$ is the number of spring pairs in parallel. The elastic springs are doubly clamped beams and possess a beam natural frequency apart from the suspension dynamics. However, elastica springs do not perform as desired when the frequency of suspension motion is near to the beam natural frequency. Shoup [179] numerically estimated the response of the elastica suspension under a sinusoidal excitation, $x_1(t) = X_1 \sin \omega t$, and his results are shown in Fig. 30. The backbone curve represents the dependence of the natural frequency on the response amplitude and it exhibits hard nonlinearity.

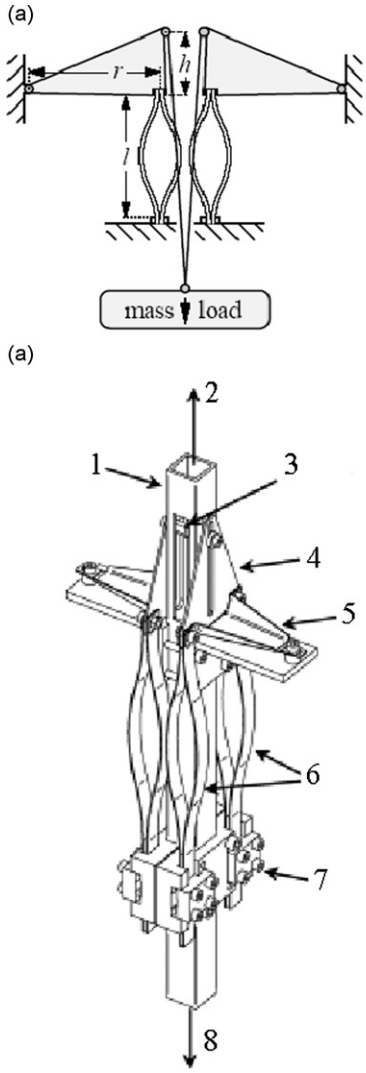

Fig. 31. Anti-spring concept: (a) anti-spring (inverted pendulum) to reduce the resonant frequency of Euler springs, (b) assembly drawing of the vertical Euler isolator showing the geometric inverted pendulum plates: 1—central tube, 2—to supporting platform, 3—suspension point, 4—tall plate, 5—rotational arm, 6—Euler springs, 7—lower spring clampless attached to the central tube, 8—to suspended mass [5,183].

The results of large deflection of a flexible bar were utilized to evaluate the deformation of an elastic ring subjected to two opposite radial compressive loads [116]. Later, Shoup and Simmonds [180] developed nonlinear suspension systems with adjustable stiffness rate.

Fig. 31(a) shows a schematic diagram of the Euler spring isolator and an inverted pendulum of height h as an anti-spring to reduce the resonant frequency of the isolator. Fig. 31(b) shows the assembly drawing of the isolator with eight Euler springs [181,182]. The reduction of the effective spring stiffness was explained by Winterflood et al. [5]. The arrangement of Fig. 31(a) has the merit that only very small forces are placed on the pivot allowing a lightweight structure and a very thin flexure to serve as the pivot. Under a vertical force, f, acting in one suspension wire, the inverted pendulum produces an anti-rotational spring rate of $fh\alpha/\alpha = fh$. The normal rotational spring-rate due to the Euler springs is $r\alpha(f/2l)r/\alpha = r^2(f/2l)$. Upon equating the two rates one obtains the required design to achieve spring-rate cancellation, i.e., $(h/r) = (r/2l)$.

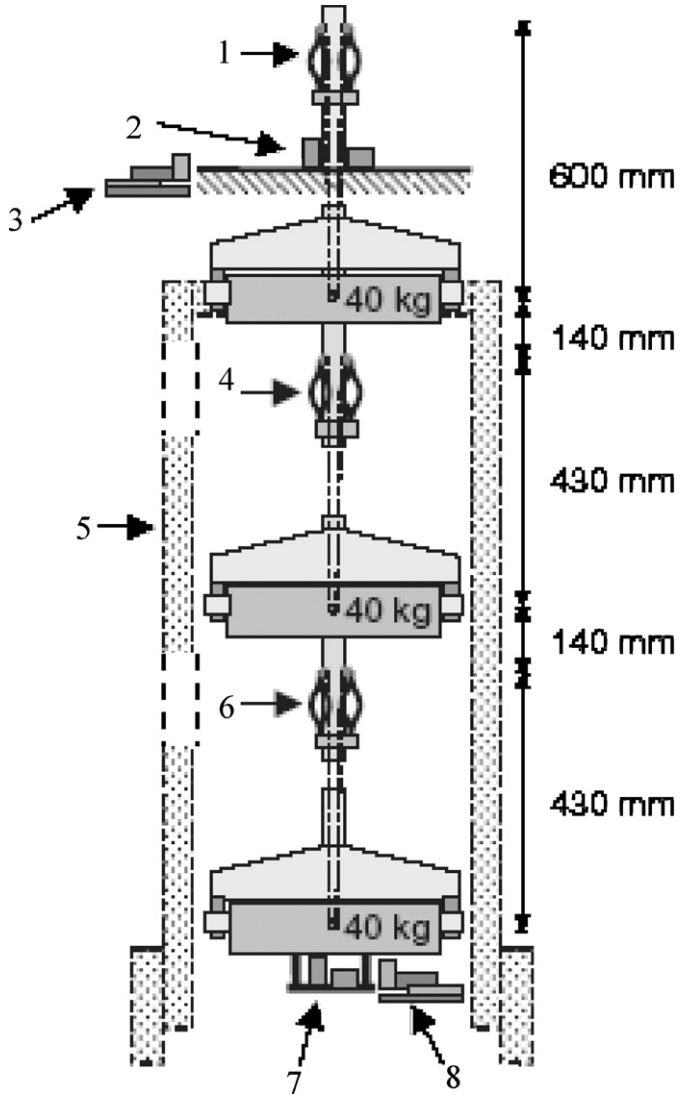

Fig. 32. Schematic diagram of a three-stage low-frequency isolator: 1—0.8 mm thick, 8 springs 140 mm long each, 2—input geophones (vertical and horizontal), 3—shadow sensor, 4—8 springs (0.7 mm thick and 148 long), 5—beam weights (added in latter part of experiment to increase moment of inertia of top masses, 6—8 springs (0.6 mm thick, and 166 mm long, 7—output geophones cradle, 8—shadow sensor [183].

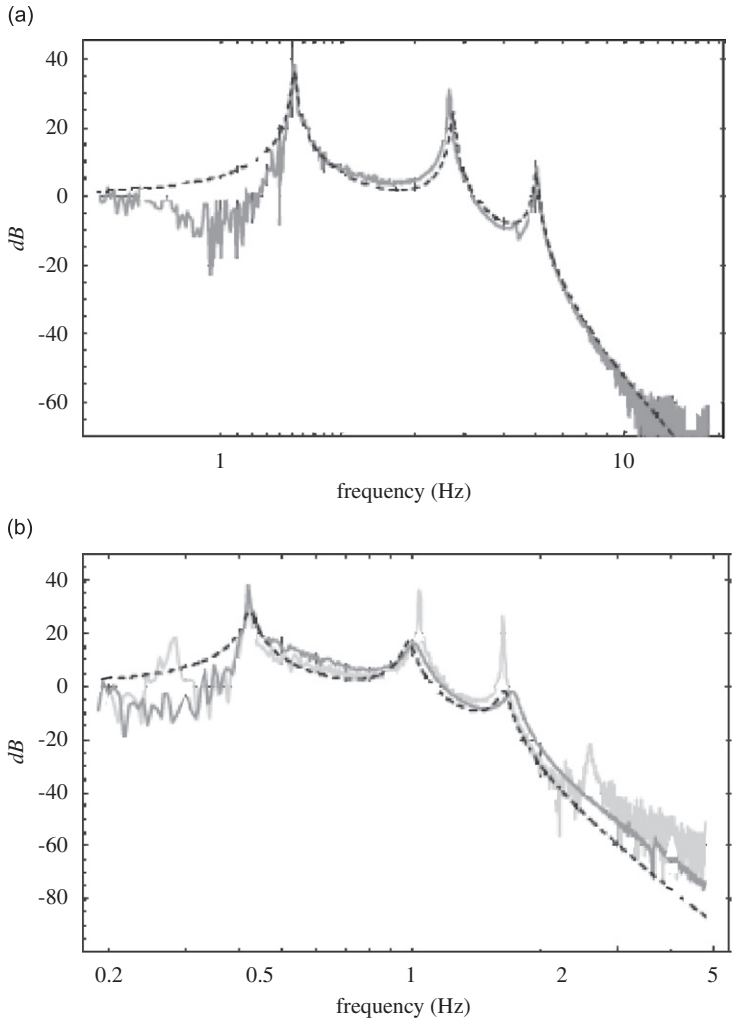

Fig. 33. Transfer functions of the vertical and horizontal isolation performance: (a) vertical frequency response: _____ measured, ---- model, (b) horizontal frequency response ━━━━ with self-damping, _____ without self-damping, ---- Model assuming $Q = 20$ [183].

Dumas et al. [183] presented the performance of a three-stage low-frequency vibration isolation chain as shown in Fig. 32. The isolator was originally developed for use in the Australian International Gravitational Observatory, where each stage was a combination of a vertical Euler-spring stage and a self-damped pendulum. Experimental results demonstrated that all horizontal normal modes including the fundamental pendulum mode were strongly damped. The transfer functions of the vertical and horizontal isolations are shown in Figs. 33(a) and (b), respectively. The plots show measured and predicted transfer functions based on assumed quality factor $Q = 50$. Fig. 33(b) shows the dashed curve for $Q = 20$. The self-damping mechanism was found to significantly reduce the pendulum normal mode peaks except for the lowest mode.

The buckled or pre-bent column with fixed ends, used as a vibration isolator, was analyzed by Virgin and Davis [184] and Plaut et al. [185]. The column was modeled as an extensible elastica, which allows large displacements in equilibrium. Small axial base excitations were considered. It was found that for sufficiently low damping and sufficiently high column stiffness, the axial transmissibility curves exhibit an infinite number of peaks. Plaut et al. [186] considered another system consisting of two bars hinged together through a rotational spring and a rotational dashpot with one end subjected to axial excitation. The equation of motion of the system included nonlinear inertia and nonlinear parametric excitation. The equation of motion was

found to possess no stable trivial solution if the static axial load is greater than the critical load. The bifurcation diagram exhibited chaotic motions, which occur for most of the frequencies over the range $\omega_n<\Omega<2\omega_n$, where ω_n is the natural frequency and Ω is the excitation frequency.

5. Gospodnetic–Frisch-Fay beam isolator

The static deflection curve of a thin elastic beam forced to deform by three symmetrical frictionless knife-edged supports, was analyzed by Gospodnetic [187] and documented by Frisch-Fay [116]. Since the beam is inextensible, there is no limitation on its deflection, and a closed form solution for the deflection curve was given in terms of elliptic functions. Fig. 34 shows a schematic diagram of a beam similar to the Gospodnetic–Frisch flexible beam. It is free to slide on two knife-edged supports under the action of the load P. This beam can be used as a resilient isolator between the machinery and the base in marine vessels. The beam can also model a load carrying bearing for pressure pipelines against earthquake ground motion [188,189].

As the load, P, increases both the beam length, L, and the end slope angle, ψ_0, increases simultaneously. d denotes the displacement at the mid-span, $x=l/2$. The two supports A and B are knife edged supports separated by distance l. Note that L and l are only equal when the beam is horizontal without any sag. The deflection of the beam may be written in terms of the slope angle ψ as [116]

$$\frac{\mathrm{d}\psi}{\mathrm{d}s}=\frac{M}{EI}=\frac{P}{2EI}[(l/2-x)+(d-y)\tan\psi_0], \tag{50}$$

where M is the bending moment. Taking the derivative with respect to s, gives

$$\frac{\mathrm{d}^2\psi}{\mathrm{d}s^2}=-k^2\left[\frac{\mathrm{d}x}{\mathrm{d}s}+\frac{\mathrm{d}y}{\mathrm{d}s}\tan\psi_0\right], \tag{51}$$

where $k^2=P/2EI$. Integrating both sides with respect to ψ, gives

$$\frac{1}{2}\left(\frac{\mathrm{d}\psi}{\mathrm{d}s}\right)^2=-k^2[\sin\psi-\cos\psi\ \tan\psi_0]+C. \tag{52}$$

At $x=l/2$, the bending moment vanishes, i.e., $(\mathrm{d}\psi/\mathrm{d}s)_{\psi=\psi_0}=0$, and thus $C=0$. Accordingly, Eq. (52) can be written in the form

$$\frac{\mathrm{d}\psi}{\mathrm{d}s}=k\sqrt{2(\cos\psi\ \tan\psi_0-\sin\psi)}=\sin\psi\frac{\mathrm{d}\psi}{\mathrm{d}y}=\cos\psi\frac{\mathrm{d}\psi}{\mathrm{d}x}. \tag{53}$$

From Eq. (53) it is possible to write

$$\mathrm{d}x=\cos\psi\,\mathrm{d}s=\cos\psi\frac{\mathrm{d}\psi}{k[2(\tan\psi_0\cos\psi-\sin\psi)]^{1/2}}, \tag{54}$$

$$\mathrm{d}y=\sin\psi\,\mathrm{d}s=\sin\psi\frac{\mathrm{d}\psi}{k[2(\tan\psi_0\cos\psi-\sin\psi)]^{1/2}}. \tag{55}$$

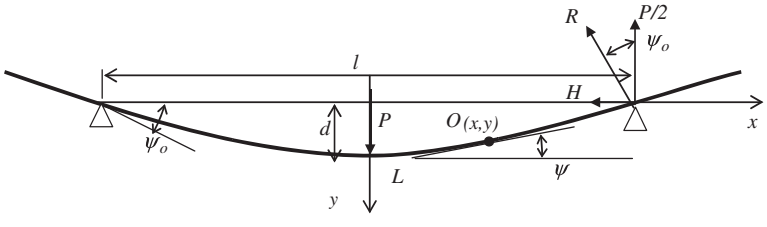

Fig. 34. Schematic diagram of deflected under static load of a flexible beam and free to slide at two knife edge supports.

Introducing the transformation of variables $\cos\phi = \sqrt{\sin(\psi_0 - \psi)}$ and $\cos\phi_0 = \sqrt{\sin\psi_0}$, and integrating Eqs. (54) and (55) gives

$$l = \frac{2\sqrt{\cos\psi_0}}{k}\left(\sqrt{2}\cos\psi_0\cos\phi_0 + \sin\psi_0\Phi\left(1/\sqrt{2},\phi_0\right)\right), \tag{56}$$

$$y = d = \frac{\sqrt{\cos\psi_0}}{k}\left(\sqrt{2}\sin\psi_0\cos\phi_0 - \cos\psi\Phi\left(1/\sqrt{2},\phi_0\right)\right), \tag{57}$$

where $\Phi(\phi_0) = 0.8472 + F\left(1/\sqrt{2},\phi_0\right) - 2E\left(1/\sqrt{2},\phi_0\right)$. In order to define the force–deflection relationship, Eqs. (56) and (57) may be written in the form

$$\frac{Pl^2}{EI} = 8\cos\psi_0\left(\sqrt{2}\cos\psi_0\cos\phi_0 + \sin\psi_0\Phi\left(1/\sqrt{2},\phi_0\right)\right)^2, \tag{58}$$

$$\frac{d}{l} = \frac{1}{2}\frac{\sqrt{2}\sin\psi_0\cos\phi_0 - \cos\psi_0\Phi\left(1/\sqrt{2},\phi_0\right)}{\sqrt{2}\cos\psi_0\cos\phi_0 + \sin\psi_0\Phi\left(1/\sqrt{2},\phi_0\right)}. \tag{59}$$

The non-dimensional load, Pl^2/EI, and deflection, d/l, are plotted in terms of the end slope angle ψ_0 in Fig. 35, [190]. It is seen that by increasing the load the end slope angle is increased and reaches a point where the vertical component of the support reaction is no longer able to support the vertical load. When this happens the beam will slip through without return. It is seen that the maximum load $(Pl^2/EI)_{\max} = 6.672$ is reached at the end slope angle $\psi_0 = 38.3^\circ$. For every load less than the maximum value there are two different values of the slope angle, $\psi_{01} < 38.3^\circ$ and $\psi_{02} > 38.3^\circ$. For all values of the slope angle $\psi_{01} < 38.3^\circ$, the beam strain energy is larger than the work done by the static load, and thus the beam is stable. On the other hand, for all values of $\psi_{02} > 38.3^\circ$ the work done of the static load exceeds the corresponding elastic restoring energy and thus the beam enters into the unstable state. For any load greater than the maximum value $(Pl^2/EI) > (Pl^2/EI)_{\max}$ the beam becomes unstable and begins to slide and slips off the supports in the absence of friction or constraint forces. Note that the restoring elastic force of the beam is analogous to the roll restoring moment of ships where it vanishes when the value of the roll angle reaches the capsizing value (see, e.g., Refs. [191,192]).

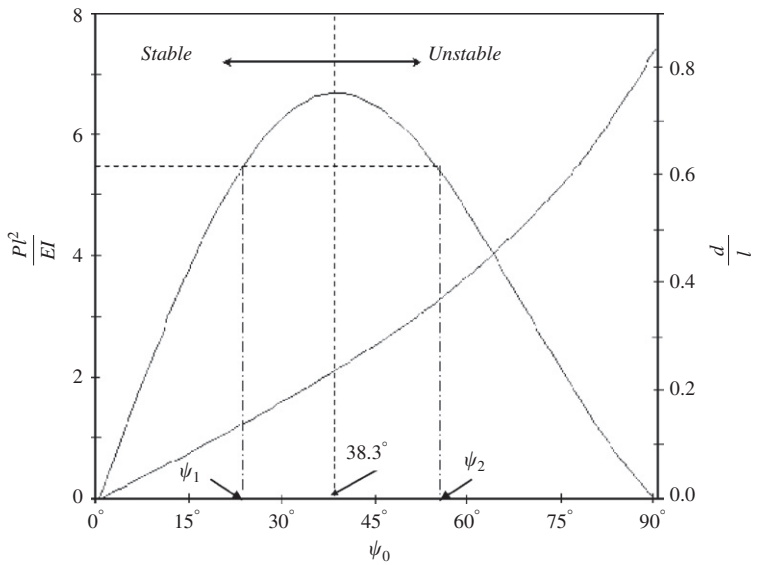

Fig. 35. Dependence of load and deflection on the end slope angle based on the exact solution showing the critical angle $\psi_{0_{cr}} = 38.3^\circ$ at which the beam becomes unstable [190].

The above analysis provides the load and deflection in closed form in terms of elliptic functions. For the dynamic analysis and to develop the equation of motion, Somnay et al. [190] expressed the load in terms of the beam deflection rather than elliptic functions of the end slope angle. They found that the best is to be of order 11 in the form

$$\frac{Pl^2}{EI} = a_1\left(\frac{d}{l}\right) + a_3\left(\frac{d}{l}\right)^3 + a_5\left(\frac{d}{l}\right)^5 + a_7\left(\frac{d}{l}\right)^7 + a_9\left(\frac{d}{l}\right)^9 + a_{11}\left(\frac{d}{l}\right)^{11}, \tag{60}$$

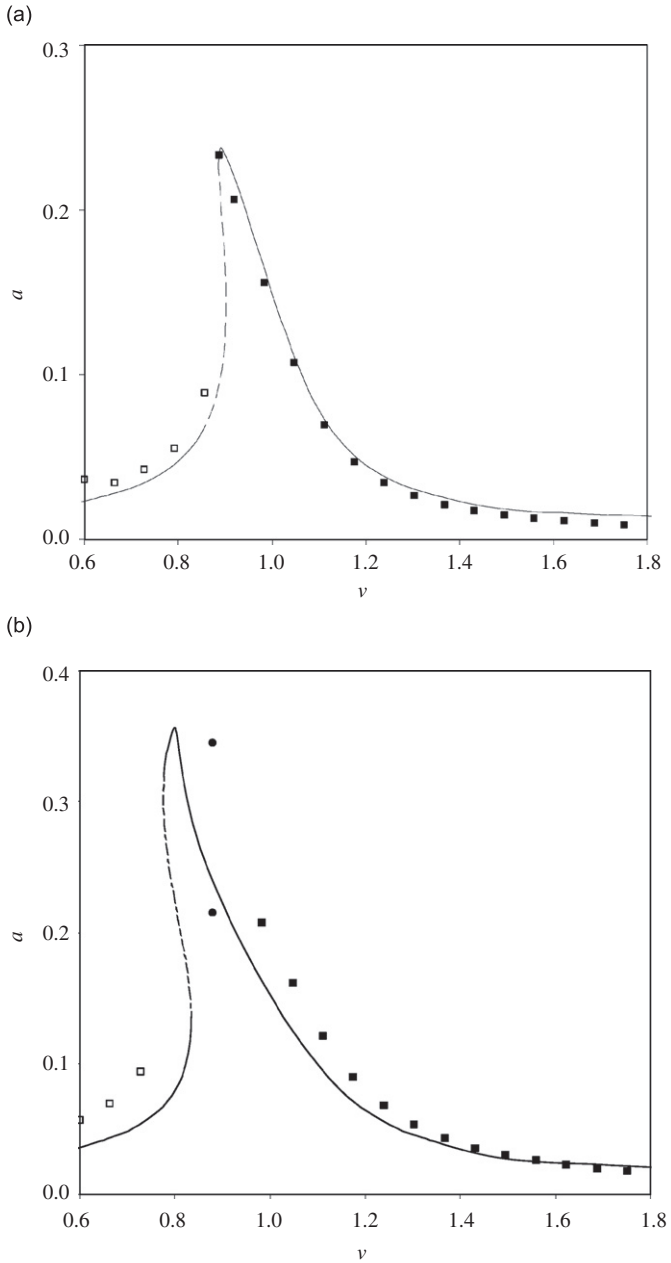

Fig. 36. Amplitude–frequency response for different values of excitation amplitude: □: mono-periodic symmetric response, ■: mono-periodic asymmetric response, ●: period-doubling response, numerical integration. ———: response from multiple scales solution: (a) excitation force amplitude $f_0 = 0.02$ and (b) excitation force amplitude $f_0 = 0.04$ [190].

where a_i are constants. Under a sinusoidal dynamic unbalance force, $F(t) = F_0 \sin \Omega t$, where F_0 and Ω are the excitation amplitude and frequency, respectively, the equation of motion of the system is

$$m\ddot{d} + \frac{EIa_1}{l^3}d + \frac{EIa_3}{l^5}d^3 + \frac{EIa_5}{l^7}d^5 + \frac{EIa_7}{l^9}d^7 + \frac{EIa_9}{l^{11}}d^9 + \frac{EIa_{11}}{l^{13}}d^{11} = mg + F(t), \tag{61}$$

Alternatively, Eq. (61) can be written in terms of the displacement measured from the static equilibrium position, S, i.e., $y = d - S$. The static component is obtained from the static equilibrium position. The equation of motion in terms of the dynamic displacement, $\tilde{y} = y/l$, takes the form

$$\ddot{\tilde{y}} + 2\zeta\dot{\tilde{y}} + \tilde{y} + c_2\tilde{y}^2 + c_3\tilde{y}^3 + c_4\tilde{y}^4 + c_5\tilde{y}^5 + c_6\tilde{y}^6 + c_7\tilde{y}^7 + c_8\tilde{y}^8 + c_9\tilde{y}^9 + c_{10}\tilde{y}^{10} + c_{11}\tilde{y}^{11} = f_0 \cos \nu\tau, \tag{62}$$

where $\tau = \omega_n t$, $f_0 = F_0/(ml\omega_n^2)$, $\nu = \Omega/\omega_n$, ω_n is the linear natural frequency of the beam, and ζ is a linear damping factor introduced to account for energy dissipation. Figs. 36(a) and (b) show the dependence of response amplitude, a, on excitation frequency ratio for two different values of excitation level, $f_0 = 0.03$ and 0.04, respectively using the multiple scales method (solid and dashed curves). The unstable branches of the response are shown by dashed curves while the stable manifold by solid curves. It is seen that for small excitation amplitude, the response exhibits soft nonlinear characteristics. As the excitation amplitude increases the soft behavior predominates and at $f_0 = 0.04$ the trend is mixed between soft and hard characteristics. Fig. 36 shows numerical simulation plots where empty squares refer to symmetric single frequency response in the time domain. This behavior is preserved over excitation frequency range $0 < \nu \leqslant \nu^*$, where ν^* is the excitation frequency at the first saddle (turning) point. The numerical simulation reveals a jump to asymmetric single frequency response designated by the solid square points. Asymmetry of the response was manifested by a non-zero mean response in the time history record. As the excitation amplitude increases, say at $f_0 = 0.04$, the response experiences bifurcation to period doubling designated by solid circle points as shown in Fig. 36(b).

The existence of multiple solutions is dependent on initial conditions. This is realized from the numerical simulation of the system original equation of motion. For different initial conditions the response can be periodic symmetric with period one, or periodic asymmetric with period one or with period two, or chaotic.

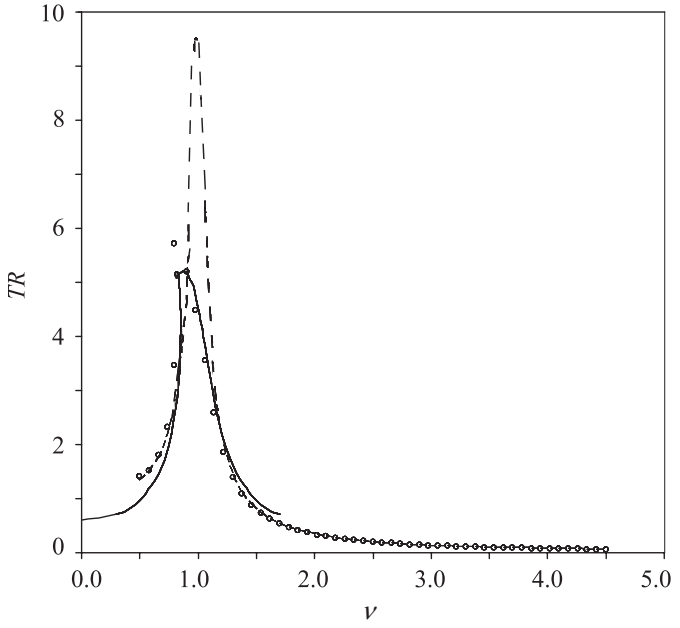

Fig. 37. Comparison of transmissibility of the nonlinear isolator and the linear isolator as a function of excitation frequency ratio: — multiple-scales solution, ○ ○ ○ numerical simulation, – – – linear isolator [190].

It was found that the periodic symmetric response covers the entire range of excitation amplitude parameter, while the periodic asymmetric occurs over a limited range of excitation amplitude $0.02<f_0<0.028$ for $v=0.75$. The chaotic regime is noticed over a very narrow window of excitation amplitude $0.028\leqslant f_0\leqslant 0.02875$.

The system transmissibility, is given by the ratio

$$\mathrm{TR}_{nl}=\frac{F_t}{f_0}=\frac{\sqrt{F_{\mathrm{te}}^2+F_{\mathrm{td}}^2}}{f_0}, \tag{63}$$

where F_{te} is the elastic transmitted elastic force expressed in terms of the main harmonic component of $(v\tau+\phi)$, and F_{td} is the damping transmitted force.

Fig. 37 shows comparison of the transmissibility of the nonlinear and linear isolators. The transmissibility of the nonlinear isolator was predicted by the multiple-scales solution (shown by the solid curve) and numerical simulation (shown by empty circles). It is seen that the nonlinear isolator outperforms the linear one only over frequency range close to the system resonant frequency, i.e., $v\approx 1$. For $v\gg 1$ the transmissibility of the two isolators is almost the same.

The influence of friction at the beam supports was considered by Ibrahim and Somnay [193] and it was shown that when the excitation frequency is increased beyond resonance, the friction at the sliding supports improves the transmissibility. The dependence of the response on initial conditions establishes the basins of attraction for different values of friction coefficient and excitation parameters.

6. Base isolation of structures

6.1. Concept of base isolation

Seismic isolation of ground structures such as multi-storey buildings, nuclear reactors, bridges, and liquid storage tanks are designed to preserve structural integrity and to prevent injury to the occupants and damage to the contents by reducing the earthquake-induced forces and deformations in the super-structure. The performance of these systems depends on two main characteristics:

(1) The capacity of shifting the system fundamental frequency to a lower value, which is well remote from the frequency band of most common earthquake ground motions.
(2) The energy dissipation of the isolator.

Basically, all isolation systems can be classified into two main categories:

(1) Laminated-rubber bearing isolators with and without lead-core.
(2) Frictional-type sliding isolators.

The first category has several practical applications while the second is still in the early stage of development. The idea of friction-base isolation is based on decoupling a structure from the damaging components of earthquake motion by introducing flexibility and energy absorption capacity through a system placed between the structure and its foundation [194]. Note that damping effect of friction-base isolators is created by nonlinear mechanisms and the behavior of the structure is amplitude dependent. The compliant elastomeric bearings and frictional sliding mechanisms installed in the foundations of seismically isolated structures protect these structures from strong earthquakes through a reduction of stiffness and an increase in damping [195]. Although rubber bearings have been extensively used in base-isolation systems, sliding bearings have found increasing applications (see, e.g., [196–201]). Another class of base isolation of flexible multi-storey shear-type buildings was proposed by Lin and Hone [202], Jangid [203,204] and Jangid and Londhe [205] who introduced rolling rods with a re-centering device.

Several base isolation systems have been proposed and developed for various types of structures. The design of base-isolated structures, including various types of materials to develop supplemental energy devices and

the concept of energy dissipation, has been the subject of many studies [206–215]. Deb [216] presented an overview of seismic base isolation.

Damper-bracing assembly has been recognized as one of the best schemes to be implemented for individual buildings. In the case of adjacent buildings, damping devices are perhaps better utilized if they could be installed between buildings because relative displacement between distinct structures is normally larger than their respective inter-storey drifts provided the fundamental periods of the structures are quite different. This coupling control was originated by Klein et al. [217] for large structures exposed to wind forces, and later it was the subject of several studies [218–223]. Kobori et al. [224] provided a typical example of seismic control between adjacent buildings in the form of bell-shaped hollow connectors.

Takeda et al. [225] evaluated the probability of failure of buildings and equipment for two fusion-reactor-like buildings, with and without seismic base isolation. The probability of failure was calculated by considering nonlinearity and rupture of isolators. While the probability of building failure for both buildings on the same site was almost equal, the base-isolated building was found to have higher reliability than the non-isolated building. Even if the base-isolated building alone is located on a higher seismic hazard area, it could compete favorably with the ordinary one in reliability of equipment.

The next two sub-sections will address laminated-rubber bearing isolators and friction-base isolators.

6.1.1. Laminated-rubber isolators

Several studies considered the translational response analysis of two-dimensional idealized models of structural buildings. This studies include parametric investigations of a base isolated building for different types of isolation devices such the laminated-rubber bearing, the laminated-rubber bearing with lead core known as the New Zealand system, the Electricite de France system [226], the resilient-friction-base isolator system [227], and sliding resilient-friction (SR-F) system [228]. The resilient-friction-base isolator system uses the parallel action resiliency of rubber and the friction of Teflon-coated steel plates. Hernried and Lei [229] conducted comprehensive parametric studies to examine the effect of isolator friction coefficient, subsystem (equipment, structure, isolator) natural period, subsystem damping, and the equipment/structure mass ratio on the equipment response. It was shown that the resilient-friction-base isolator is, in general, effective in reducing the accelerations in lightweight equipment components from the corresponding fixed base case.

The influence of parameter variations on the stochastic response of an asymmetric building isolated by a resilient-friction-base isolator system was found to be less sensitive [230]. Jangid [231] obtained the optimum damping of the resilient-friction-base isolator system under parameter variations, such as the coefficient of friction of the resilient-friction-base isolator system, the period and damping of the superstructure, and the effective period of base isolation. The criterion was based on minimizing the top floor rms acceleration. For the purpose of accurately predicting the seismic response of base-isolated structures, Kikuchi and Aiken [232] proposed an analytical hysteresis model for elastomeric seismic isolation bearings. The proposed model is capable of predicting the mechanical properties of each type of elastomeric bearing into the large strain range. In order to show the validity of the proposed model, nonlinear dynamic analyses were conducted to simulate the earthquake simulator test results. Experimental and analytical results revealed that the model could be an effective tool to predict not only the peak response value but also the force–displacement relationship of the isolators and floor response spectra for isolated structures. The reader may consult Soong [233] for the state-of-the-art of active control approaches.

Elasto-plastic dampers possess material nonlinearity as reflected from the hysteresis of the load–deflection plot. The nonlinear vibration system composed of a linear spring–mass–damper structure system of any order and a hysteresis damper. The responses for seismic excitation were examined by Fujita et al. [234] by using two typical models of the hysteresis element, a bilinear model and a Ramberg–Osgood model. The effects of the second stiffness of the dampers and the amplitude of the excitation motion were investigated using an actually recorded earthquake motion.

The effects of the horizontal stiffness nonlinearity and the decrease in the vertical stiffness of rubber bearings on seismic response during large deformation in a horizontal isolation system of nuclear island buildings were studied by Kurihara et al. [235]. In order to examine the horizontal and vertical stiffness of full-scale bearings, rubber bearings of 4900-kN (500-ton) rated load were tested within the allowed value of horizontal deformation. The design of rubber bearings involves the influence of nonlinear behavior during

large deformation and the increase in stiffness due to aging. A combination of laminated rubber bearings, viscous dampers and friction elements was considered to seismically isolate a building of 11 levels [236]. A smooth approximation of discontinuous characteristics friction was introduced in the analytical modeling of the structure. It was found that the dynamics of the superstructure largely influence the entire system's response.

Villaverde [237] and Villaverde and Mosqueda [238] proposed to mount a building's roof on elastomeric bearings. Flexible laminated-rubber bearings were inserted between a building's roof and the columns that support the roof. Viscous dampers were connected to the roof and a structural element below the roof. It was found that the suggested device effectively reduces the seismic response of the frame, although the extent of this reduction depends on the magnitude of nonlinear deformations.

The reliability of a two-dimensional hysteretic shear-beam-type structure with viscoelastic bracing dampers subjected to uni-directional horizontal ground motion was studied by Guo et al. [239]. They estimated the statistical response functions of the structure with deterministic parameters and with random parameters. Reliability indices and failure probabilities of a building model were also determined under five different earthquake records for cases with and without dampers. It was found that the use of dampers would significantly increase the reliability of the structure. Alhan and Gavin [240] addressed the problem of seismic risk of critical facilities by specifying the required reliability of components of vibration isolation systems for an improved performance and the reliability of isolated sub-systems with respect to earthquake hazards. In their study, they considered a four-storey structure with an isolation floor at the second floor level.

6.1.2. *Friction-base isolators*

Friction in support boundaries acts as a source of energy dissipation. However, the associated slip results in irregular variations in system dynamic properties, such as natural frequencies and damping coefficient [241,242]. Because the stick and the slip phases take place alternately, depending on the magnitude of the shear forces at the interface of the sliding bearings, the dynamic behavior of a sliding structure can be highly nonlinear. Note that there is always maximum dissipation of energy, such that the dynamic response of the structure can be significantly reduced. The energy dissipation is reflected by the measured hysteresis curve, as obtained, for example, by Filiatrault and Cherry [209] and Ni et al. [243]. Friction-base isolators have been adopted as a means of passive control [207,209,227,244] of structures subjected to ground motion.

A number of overviews of the applications and performance of seismic isolation of structural systems were presented in Refs. [199,245–249]. A numerical algorithm for distribution of friction devices along the height of different structural systems was presented by Dimova et al. [250]. The response of a rigid structure with frictional-base isolation system to a random earthquake excitation was the focus of many studies (see, e.g., Refs. [251–258]). These studies provided a comparison of the rms displacement and velocity responses as predicted analytically with those estimated by Monte Carlo simulations. It was concluded that the frictional-base isolators are highly reliable in reducing structural displacements and accelerations.

Kircher et al. [259] estimated the nonlinear earthquake time history records of seismically isolated buildings. Their analysis included the lateral-force-resisting systems of two building types: a four-storey braced-frame building and a four-storey moment-frame building. For each building type, four isolation systems, with varying degree of stiffness, were modeled and evaluated using spectrum-compatible earthquake time histories. Peak displacements in the isolation system and peak displacements in the first storey of the superstructure were calculated for each building.

Multi-storey buildings constructed with a low-rise podium structure form a major shortcoming in view of seismic design. For example, Shahrooz and Moehle [260] experimentally and numerically demonstrated that relatively large inter-storey drifts of the setback structure were localized at the level just above the podium structure, and was accompanied by a moderate increase in damage. Ng and Xu [261] explored the possibility of using passive friction dampers to connect the podium structure to the main building to prevent their seismic response enlargement without violating the architecture features. It was found experimentally that unfavorable seismic response amplification did occur in the building complex in the rigidly connected case. This was in contrast with the friction damper, which exhibited effectiveness in reducing absolute acceleration and inter-storey drift responses of both buildings if friction level was appropriately applied.

Chen and Ahmadi [262] examined the sensitivity of base-isolated structures to fluctuating components of wind disturbance. They found that these structures were less sensitive to wind excitation as compared to conventional excitation systems. Jangid [263] reported that sliding systems are less sensitive to the effects of torsional coupling in asymmetric base-isolated structures. Comparative studies of base-isolation systems, conducted by Chen and Ahmadi [264] and Su et al. [228], revealed that the response of the sliding system does not vary with the frequency content of earthquake ground motions. Jangid [265] investigated the optimum friction coefficient of sliding base isolation supporting a linear flexible multi-storey structure subjected to earthquake excitation. The minimization of the rms of the top floor absolute acceleration was adopted as a criterion for optimality.

Numerical simulations performed by Dimova [266] showed that friction devices used in steel frame structures exhibit an equally stable response during both the short and long periods of seismic excitations. Hirata and Somaki [267] and Dimova and Hirata [268,269] presented a simplified method for fragility analysis of structures with friction devices. The effect of randomness of the friction forces was estimated by Monte Carlo simulations based on Gaussian distribution of the friction force. Dimova and Elenas [270] extended the work of Dimova and Hirata [268,269] and estimated the correlation coefficient between the response parameters of nonlinear systems with energy dissipating devices and the seismic intensity parameters. They found that the correlation coefficient does not relate to the sequence of the fragility curves.

Simple and slotted bolted connections for energy dissipation, which takes place during structural dynamic response were examined in Refs. [271–273]. Excellent isolation performance was achieved in conventional sliding-type systems if the friction coefficient is small, due to the reduction in the transmitted ground acceleration. On the other hand, if the friction coefficient is large, the structure will be isolated only during large earthquakes, and the sliding system will not be activated by small to moderate earthquakes. The idea of displacement-proportional friction was theoretically proposed by Tadjbakhsh and Lin [274]. This type of frictional resistance can be provided by tightening together a set of friction plates by compression forces that increase with relative separation of the building and the foundation. It was shown that in comparison with dry friction alone significant reductions in acceleration transmissibility and relative displacement transmissibility can be achieved.

Sliding base isolation systems may not be able to maintain the same value of friction coefficient under a prolonged inactivity [275,276]. Furthermore, these isolators may suffer from excessive displacements under strong earthquakes. It was demonstrated that the use of variable friction dampers improves structural response characteristics. Dowdell and Cherry [277] introduced two semi-active control methods for improving the performance obtained from constant slip friction dampers by varying the slip forces as a function of the response of the structure as it performs over time during external excitation. These methods were referred to as the off-on friction damper and the variable amplitude semi-active friction damper. The main objective of these schemes is to minimize the rms inter-storey drift. Alhan and Gavin [278] investigated the performance limits of passive linear and nonlinear isolation systems. The levels of heavy isolation damping, which increases structural acceleration and inter-storey drifts, were identified. They were able to define appropriate combinations of isolation parameters, which reduce base displacements without significantly increasing floor accelerations and inter-storey drifts. Filiatrault and Cherry [279] and Dorka and Conversano [280] implemented friction devices for seismic retrofitting of existing buildings, as they require a limited structural intervention.

The reliability of these isolators has been of great concern to civil engineers. For example Pradlwater et al. [281] used the Monte Carlo simulation to assess the reliability of a three-storey structure equipped with two-dimensional frictional devices under bi-directional earthquake loading. Their results revealed that the friction can reduce structural displacements by half and structural velocities by two-thirds. Shenton and Holloway [282] examined the effect of the isolator stiffness variability on the response of the structure. The stiffness was assumed to be random variable with Gaussian distribution.

6.2. Base isolation of bridges

Bridges are usually constructed to have horizontal stiffness bearings that allow thermal deformations of the deck. The use of multi-layer elastomeric bearings for seismic protection is a natural extension of rubber pads

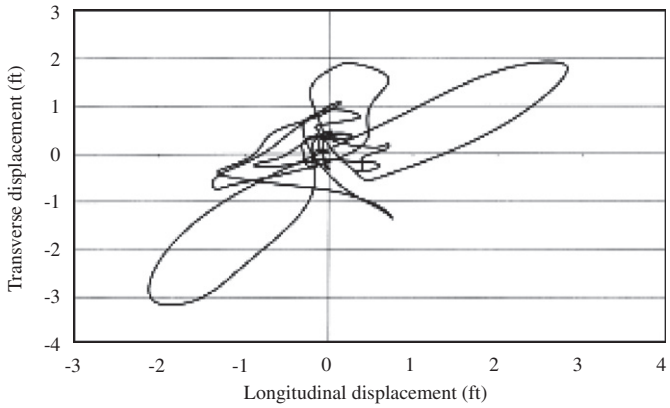

Fig. 38. Trajectory plot of typical friction-pendulum bearing displacement from the bridge global nonlinear time history analysis [297].

for thermal expansion. Several studies were devoted to investigate the effect of various types of isolation pads on the dynamic characteristics of bridges under different environmental conditions [283–293]. These studies indicated that the presence of the isolation pads considerably reduces the amplitude of longitudinal deck motions with respect to those at top of the pier except at the first natural frequency of the system. Delis et al. [294] considered friction bearings and friction bearings with nonlinear fluid viscous dampers. They performed nonlinear three-dimensional time history analyses using several ground input motions. The increased displacement demands at abutments were accommodated with specially designed expansion joints that allow large seismic movements in both horizontal directions.

Dowdell and Cherry [295] and Antonucchi et al. [296] developed a set of criteria for design of structures with friction-damped bracings. The design criteria for the retrofit design were based on the desired level of serviceability. In terms of performance, Mutobe and Cooper [297] indicated that the analysis and subsequent design of the Benicia-Martinez Bridge require that the retrofit should prevent any damage following the maximum seismic event. The retrofit design of this particular case relied on the use of friction-pendulum bearings, which will be described in Section 6.4. The use of nonlinear analysis was required to account for the bearing's inherent nonlinear behavior. The implementation of the global Automatic Dynamic Incremental Nonlinear Analysis (ADINA) for a bridge model revealed that the friction-pendulum bearing underwent large displacements. However, forces in the superstructure were kept at acceptable levels. Fig. 38 shows the displacement trajectory at one of the piers with the largest displacement excursion for the postulated earthquake event. Savage Eddy and Orsolini [298] discussed the use of ADINA as an analytical tool for the development of a retrofit project of the Three Mile Bridge. Ingham [299] presented a nonlinear time history analysis in support of the seismic retrofit of the Million Dollar Bridge. The retrofit included the installation of friction-pendulum system.

Shinozuka et al. [300] proposed the retrofit use of dynamic restrainers at the expansion joint for preventing the collapse of bridges in the event of a severe earthquake. The proposed dynamic restrainer consisted of a nonlinear viscous damper and an elastic spring connected in parallel. They performed two-dimensional nonlinear finite element analysis using bilinear hysteretic models for the bridge substructure joints and nonlinear gap elements for expansion joints. The numerical simulation revealed that the dynamic restrainers are substantially effective in reducing the relative opening displacements and impact forces due to pounding at the expansion joints.

Equivalent linearization techniques have been used to study the behavior of isolation systems. Equivalent linear models are based on the effective stiffness at the design displacement and the equivalent viscous damping is evaluated from the area of the hysteresis loop. The response characteristics of equivalent linear models were compared with those of actual nonlinear models of base-isolated bridges with lead–rubber bearings [283,301–303]. It was shown that the equivalent linearization could be used for predicting the actual nonlinear response of the system. These studies assumed the bridge to be a rigid body and the nonlinear behavior of the isolator was limited to the lead–rubber bearings represented by bi-linear characteristics. This

also agrees with other studies [262,304–306]. It was reported that the equivalent linearized model of a bi-linear hysteretic system overestimates the design bearing displacement and underestimates the superstructure acceleration [306].

The isolation of the majority of US bridges consists of lead–rubber bearings [307] and the rest being sliding isolation systems [308,309]. The vast majority of Italian bridges are isolated using lubricated sliding bearings and yielding mild steel dampers [310]. Tsopelas and Constantinou [311,312] and Tsopelas et al. [313] found that such systems restrict the force transmitted to elements of the substructure to a predetermined level, which is independent of the seismic action. They are also characterized by a large dispersion in peak displacements and the development of permanent displacements. In Japan, Kawashima and Unjoh [314] reported a different approach called 'Menshin', which utilizes isolation bearings to enhance energy dissipation capability and to distribute the lateral forces to elements of the substructure.

Constantinou and Symans [212] and Tsopelas et al. [313,315] conducted experimental investigations on a seismically isolated bridge. The isolation system consists of sliding bearings and rubber restoring force devices. Fluid viscous dampers were utilized to withstand the strong and long period level design motions. The transmitted force to the substructure did not exceed one-third of the deck weight. The guide specifications for seismic isolation design provide procedures for the analysis and design of isolation systems, and full-scale testing of seismic isolators.

Warn [316] and Warn and Whittaker [317] determined the increase in the maximum isolator displacement of isolated bridge structures due to bi-directional seismic excitation. It was shown that maximum isolator displacements were significantly larger than those considering uni-directional seismic excitation. The effect of structural details on seismic performance of four multi-span, continuous base-isolated bridges in Japan was examined from recorded seismographs by Chaudhary et al. [318]. Experimental values of stiffness and damping revealed that the behavior of the bridges is significantly altered by structural/non-structural details such as metallic bearings, side stoppers, and bearing keeper plates. Friction in metallic bearings, which are used at the end spans of two bridges, was found to be the major cause for substantial increase in stiffness and damping of superstructure of these bridges. This effect was found to diminish with increasing seismic amplitude.

6.3. Isolation of liquid storage tanks

Liquid storage containers are usually mounted on the ground either unanchored or anchored. Large unanchored tanks with flat bases usually experience different kinds of damage under the action of ground motions. The most known damage is the elephant foot bulge, which takes the form of buckling at the bottom part of the tank, and cracking at the corner of the bottom plate-shell. Both classes are related to the uplifting of bottom plate and thus involve strong nonlinearity due to the associated large displacement and the separation between the bottom plate and foundation for unanchored tanks. The liquid–structure interaction of a reactor vessel subjected to a horizontal excitation was studied using combined computational schemes. For example, the finite element method was used for the structure and boundary element method for the liquid [319]. Seismic isolation of liquid storage tanks and pool-type nuclear spent fuel storage tanks require careful investigation to enhance their safety under earthquake motion. An overview of liquid sloshing interaction with the tank elastic structure is documented in Ibrahim [320].

In order to increase the seismic resistance of liquid storage tanks, engineers incorporated base isolators to isolate the tank structure from the earthquake ground movement. Chalhoub and Kelly [321,322] conducted an experimental investigation of two similar cylindrical liquid tanks. One of these tanks was directly fixed to the earthquake simulator and the other was mounted on the base of a sealed nine-storey steel structure. The structure was isolated on eight multi-layered elastomeric bearings. Due to the reduction in the ground accelerations, the dynamic pressure was reduced for the tank in the isolated structure. The free-surface liquid elevation was slightly increased due to the lower frequency that characterizes the motion of base-isolated structures. It was recommended to appropriately select an isolation system or to introduce dampers at the location of maximum water particle velocities. The seismic isolation of liquid storage tanks was also studied in Refs. [323–326], while the response of base-isolated liquid storage tanks was estimated numerically in Refs. [327–336].

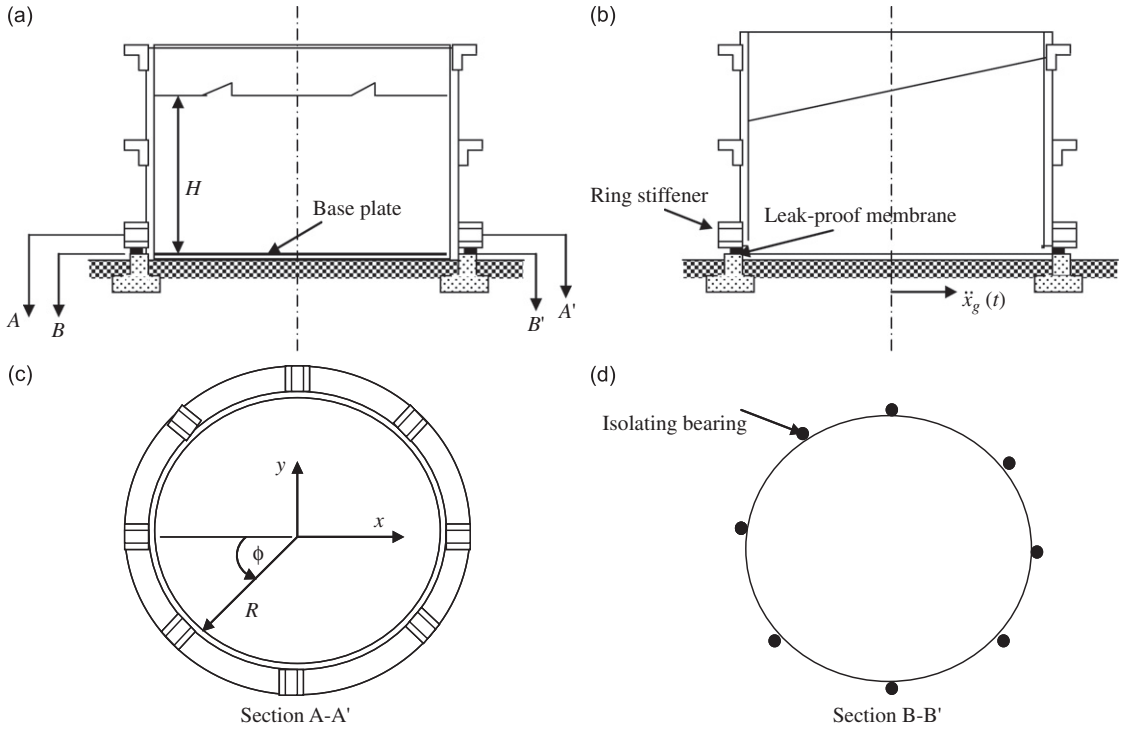

Fig. 39. Liquid-storage tank with a ring flexible bearing [340].

Kim and Lee [337] studied the horizontal seismic performance of the base-isolated liquid storage tank system with different types of base isolator stiffness and tank geometry. It was recommended to adjust the dominant frequency of the base-isolated tank to be in the effective frequency range of the isolated system. The effects of lead–rubber bearings on the seismic response of flexible liquid storage tanks were investigated by Bo and Jia-Xiang [338]. The isolator was in the form of a lead–rubber with steel-reinforced multi-layer elastomeric bearing, which has a hole in its center to facilitate the insertion of a lead plug. It was shown that the yielding instability has a close relationship with the liquid sloshing. The coupling effects among liquid sloshing dynamics, shell vibration modes, and isolator motion were considered. The hysteretic loop of the lead–rubber bearing was represented by the reduced hysteretic model.

Malhotra [339,340] proposed a seismic base isolation of ground supported cylindrical liquid-storage tanks by disconnecting the wall of the tank from the base plate and supporting it on a ring of horizontally flexible bearings as shown in Fig. 39. The base plate is supported directly on the ground. The gap between the wall and the base plate is closed with a flexible membrane, which prevents the loss of fluid from the tank and allows the tank wall to move freely in the horizontal direction. The effect of isolation on impulsive and convective (sloshing) responses of the liquid was examined for broad and slender steel tanks. It was shown that isolation can reduce dramatically the hydrodynamic base shears, overturning moments, and axial compressive stresses in the tank wall without significantly increasing the free surface liquid motion.

The use of a seismic isolation system under the superstructure of pool-type tanks can enhance its safety [341–344]. It was shown that seismic isolation results in a reduction of dynamic responses. However, the base isolation system can cause adverse effects on the free surface sloshing motion and on the relative displacement of the isolator to the ground. The relative displacement of the isolator to the ground was found to increase when the isolator becomes more flexible [345]. Park et al. [346] considered the cost-effectiveness of seismically isolated pool structures taking into account the effects of fluid-structure interaction. It was found that the seismically isolated pool tanks are highly cost-effective in low-to-moderate seismic regions.

The friction-pendulum system has been proposed to isolate liquid storage tanks by Tsai et al. [347] and Wang et al. [348]. The friction-pendulum system will be described in the next subsection. It was found that the

seismic isolation could effectively reduce the impulsive pressure while barely affecting the convective dynamic pressure.

For liquefied natural gas storage tanks, Eibl et al. [349] conducted performance tests on high-damping steel-laminated seismic isolation bearings. Baumann et al. [350] compared different methods to describe the nonlinear behavior of the seismic isolators. Three models were developed and their effect on the seismic response was considered for typical earthquakes. Baumann et al. [350] discussed different types of energy dissipated within an earthquake and provided instructive insights into the mode of operation of the base isolation. Computational simulations of high-damping rubber bearings were performed by Baumann and Boehler [351]. Their results confirmed the beneficial effect of the dissipation by hysteretic damping for the global behavior of the dynamic system. However, the random characteristic of different types of energy dissipation was found to be impractical for seismic design. Fornl [352] conducted shaking table tests to examine the effectiveness of new devices (fiber-reinforced isolators, and buckling-reinforced braces) for protecting liquid-filled structures (product storage, spherical and liquefied natural gas tanks). Different configurations were tested including fixed base, isolated base with high-damping rubber bearings, fiber-reinforced rubber bearings, and lead–rubber bearings. Furthermore, each configuration was tested for both time histories and three different levels of filling. Analytical studies of seismically isolated cylindrical offshore storage tanks were conducted by Masten-Zada and Yazici [353]. For the rubber base isolation system, the seismic response caused by the medium and short period earthquake can be effectively reduced [354].

6.4. Friction-pendulum system

While most base-isolated buildings utilize laminated-rubber bearings, non-rubber types and friction-pendulum systems have lately been developed. Zayas et al. [192,355,356] and Constantinou et al. [357] introduced friction-pendulum system in the form of sliding bearings that make use of a spherical concave surface to provide a restoring force and friction force to dissipate earthquakes energy. Fig. 40 shows the cross-section of the friction-pendulum system with a spherical concave facing up or down. The friction-pendulum system was assessed to be feasible and cost effective for improving the seismic resistance of new buildings. The flexibility to select any isolator period makes the approach suitable for a wide range of applications. Note that

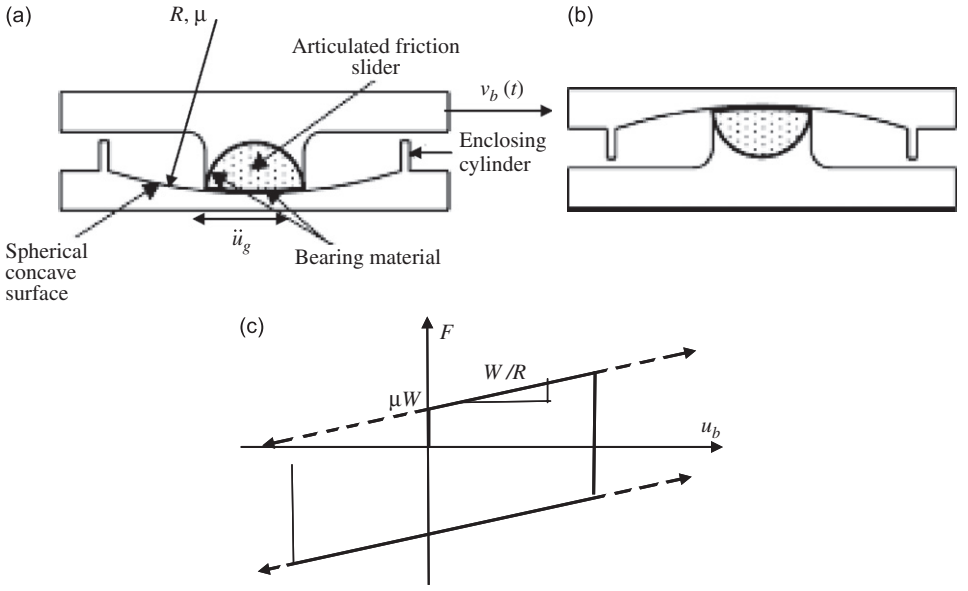

Fig. 40. The cross-section of the friction-pendulum system: (a) spherical concave up, (b) down, (c) rigid-plastic force–displacement relation for uniaxial excitation [355,385]).

isolators using friction-pendulums shift the natural period, T, of oscillation of the support structure such that

$$T = 2\pi\sqrt{R/g}, \tag{64}$$

where R is the radius of the spherical concave. The force–displacement relationship may be expressed by the following expression [358–360], see Fig. 40(c):

$$F = \frac{W}{R} v_b + \mu W \operatorname{sgn}(\dot{v}_b), \tag{65}$$

where W is the total weight carried by the friction-pendulum system, v_b is the sliding displacement (relative to the ground) in the x- and y-components for bi-axial excitation, μ is the coefficient of friction on the sliding surface, $\dot{v}_b$ is the sliding velocity, and sgn(.) is the signum function. The first term in Eq. (65) is the component of the pendulum weight directed toward the centered position, and the second term is the friction force that opposes the instantaneous velocity. The lateral restoring stiffness of the friction pendulum was given by the following equation [355]:

$$k_b = \frac{W}{R}. \tag{66}$$

Practical sliding isolation systems utilize teflon sliding bearings in which the coefficient of friction exhibits a strong dependency on the sliding velocity [361–366]. The coefficient of the sliding friction of teflon–steel interfaces was expressed by the following relationship:

$$\mu_s = \mu_{\max} - (\mu_{\max} - \mu_{\min})\mathrm{e}^{-a|\dot{v}_b|}, \tag{67}$$

where $\mu_{\max}$ and $\mu_{\min}$ are the maximum and minimum mobilized coefficients of friction, respectively, and a is a constant parameter that controls the variation of the friction coefficient with the sliding velocity.

Significant studies of friction-pendulum systems have focused on the seismic behavior of base-isolated structures subjected to near-fault ground motions (see, e.g., [367]). Tsai et al. [368] considered a special class of friction-pendulum system characterized by variable curvature. The radius of curvature of the variable curvature was lengthened for an increase of the isolator displacement. Thus, the fundamental period of the base-isolated structure can be shifted further away from the predominant period of near-fault ground motion. Tsai et al. [369,370] proposed another version of friction-pendulum system known as the trench friction-pendulum system. They conducted a series of shaking table tests for a scaled steel structure equipped with trench friction-pendulum isolators. It was found that the trench friction-pendulum system could adjust the curved trench surface radius to meet the structure's stiffness, thus providing a good protection during strong earthquake ground motion.

Abrahamson and Mitchell [371] used lead–rubber bearings and a friction-pendulum system with constant and variable friction coefficients. The lead–rubber-bearing element has a nonlinear elastic longitudinal spring and a bi-axial kinematic hardening spring in the transverse place. On the other hand, the friction-pendulum system element was formulated as point-to-point contact element, including velocity and pressure-dependent friction, and coupled vertical/horizontal displacements. Ryan and Chopra [370,372] adopted an algorithm to estimate the isolator deformations and force due to ground motions characterized by a design spectrum with its intensity defined by the median value of peak ground velocity. The algorithm was used for a system isolated with lead–rubber bearings and for a system isolated by the friction-pendulum bearing. Jangid [373] estimated the optimum parameters of the friction-pendulum system for minimum earthquake response of the base-isolated buildings under near-fault motions.

Analytical solutions of the stochastic response of such practical sliding systems were verified by extensive Monte Carlo simulations by Constantinou and Papageorgio [251]. Amin and Mokha [374] reported that the friction-pendulum system was chosen for a full-scale seismic upgrade of the US Court of Appeals building on the basis of highest technical rating and lowest cost. Fujita et al. [375,376] conducted shaking table tests to investigate the performance of isolation and restoring force characteristics of the friction-pendulum bearing. It was found that the friction-pendulum system with poly-curvature satisfies some commercial constraints. Tsai [377,378] examined the performance of the friction-pendulum system using an advanced analytical model and finite element formulation. It was found that the local bending moment, which results from the movement of

the isolator, is an important factor in the design process. Wang et al. [379,380] and Kim and Yun [381] employed the friction-pendulum system for multi-storey structures and bridges subjected to earthquake excitations. The dispersion of friction coefficient in friction-pendulum system was examined by Okamura and Fujito [382]. Okamura et al. [383] studied the rotational dynamic motion of isolated structures mounted on four friction-pendulum bearing systems subjected to earthquake motion. It was found that the rotational motion was generated due to the friction coefficient differences in the friction-pendulum bearing system.

The idea was employed for seismic protection of bridges by Constantinou et al. [309], Tsopelas and Constantinou [312], and Ates et al. [384,385]. An isolated structure behaves as a fixed base flexible single-degree-of-freedom system when there is no sliding in the friction-pendulum system. When the intensity of earthquake is large enough to take place in the friction-pendulum system, the equation of motion of the isolation system during the sliding phase was derived by Papageorgiou and Constantinou [386] and Jangid and Banerji [387] in the form

$$m_b\ddot{v}_b + c_b\dot{v}_b + \mu_5 W\,\mathrm{sgn}(\dot{v}_b) + k_b v_b = -m_b\ddot{v}_{sg}, \tag{68}$$

where m_b, c_b, and k_b are the mass, damping, and stiffness of the base isolation system. Note that Eq. (68) is strongly nonlinear differential equation due to the friction force term. The signum function was replaced by a smooth function approximated by the expression [244]

$$\mathrm{sgn}(\dot{v}_b) \approx a_1\dot{v}_b + a_3\dot{v}_b^3, \tag{69}$$

where the coefficients a_1 and a_3 are determined by minimizing the mean square error

$$E[e^2] = \int_{-\infty}^{\infty} \left[\mathrm{sgn}(\dot{v}_b) - a_1\dot{v}_b + a_3\dot{v}_b^3\right]^2 p(\dot{v}_b)\,\mathrm{d}\dot{v}_b. \tag{70}$$

The conditions for minimizing the above error are

$$\frac{\partial E[e^2]}{\partial a_1} = 0 \quad \text{and} \quad \frac{\partial E[e^2]}{\partial a_3} = 0. \tag{71}$$

The process of satisfying these conditions yielded the following values of the coefficients a_1 and a_3:

$$a_1 = \frac{E[\dot{v}_b^6]E[\dot{v}_b\,\mathrm{sgn}(\dot{v}_b)] - E[\dot{v}_b^4]E[\dot{v}_b^3\,\mathrm{sgn}(\dot{v}_b)]}{E[\dot{v}_b^2]E[\dot{v}_b^6] - \left(E[\dot{v}_b^4]\right)^2}, \tag{72a}$$

$$a_3 = \frac{E[\dot{v}_b^4]E[\dot{v}_b^3\,\mathrm{sgn}(\dot{v}_b)] - E[\dot{v}_b^4]E[\dot{v}_b^3\,\mathrm{sgn}(\dot{v}_b)]}{E[\dot{v}_b^2]E[\dot{v}_b^6] - \left(E[\dot{v}_b^4]\right)^2}, \tag{72b}$$

Dicleli and Mansour [388] took advantage of the friction-pendulum system for retrofitting typical seismically vulnerable bridges in the State of Illinois. Roussis and Constantinou [389–391] extended the idea of friction-pendulum for building structure isolation and developed an uplift-prevention friction-pendulum

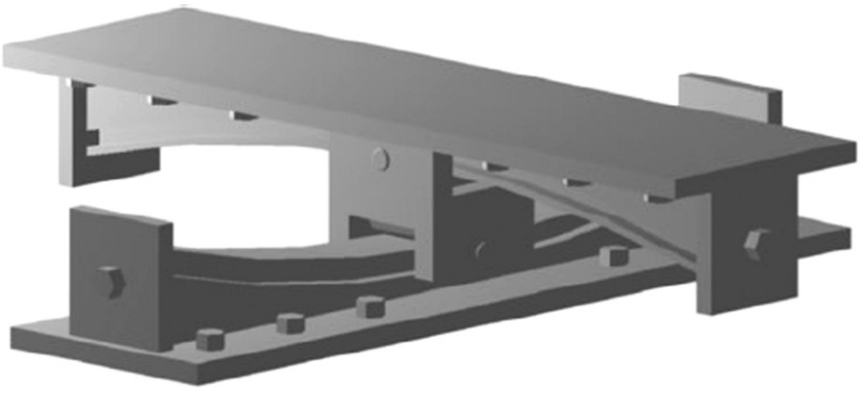

Fig. 41. Three-dimensional view of the uplift-restraining XY-PF isolator [387].

isolator known as the XY-FP shown in Fig. 41. It consists of two orthogonal opposing concave beams interconnected through a sliding mechanism that permits tension to develop in the bearing, thereby preventing uplift. The effectiveness of the XY-FP isolator was experimentally studied using a slender five-storey scale-model frame seismically isolated with four XY-FP isolators subjected to simulated horizontal and vertical ground motions. The XY-FP isolator was shown to provide effective uplift prevention regardless of the state of displacement in the bearing. In addition, it allows for decoupling of the bi-directional horizontal motion along two orthogonal directions. The system has the capability to provide distinct stiffness and energy dissipation along the principal directions of the bearing. The friction-pendulum bearing was utilized for seismic isolation of liquid storage tanks, as demonstrated by Wang et al. [348].

Pranesh and Sinha [392–394] and Murnal and Sinha [395] developed another isolator known as the variable frequency pendulum isolator. The isolation period of this isolator was found to continuously decrease with increasing the horizontal sliding displacement.

7. Nonlinear viscoelastic and composite isolators

7.1. Characteristics of viscoelastic materials

Viscoelastic materials are widely used for vibration isolation in automotive and aerospace industries. It is well known that the shear modulus and loss factor of rubber materials depend on frequency, ω, as well as temperature, T, [396–399]. Thus one can express the complex shear modulus, $G^*(\omega, T)$, in the form

$$G^*(\omega, T) = G'(\omega, T) + \mathrm{i}G''(\omega, T) = G'(\omega, T)[1 + \mathrm{i}\eta(\omega, T)], \tag{73}$$

where $G'(\omega, T)$ is the shear modulus and $G'(\omega, T)\ \eta(\omega, T)$ is the loss factor. The dependence of these two parameters on the temperature and frequency is shown in Fig. 42. Fig. 42 shows the optimum regions of viscoelastic materials for different types of damping devices. For example, region A is optimum for free-layer treatments, having a high modulus and high loss factor. On the other hand, region B is optimum for constrained-layer treatments, possessing a low modulus and high loss factor. Region C is optimum for tuned-mass dampers possessing a low modulus and low loss factor.

With reference to Fig. 42 one can see that at the so-called rubber-to-glass transition, the loss factor passes through a maximum value that lies approximately in the frequency or temperature range through which the

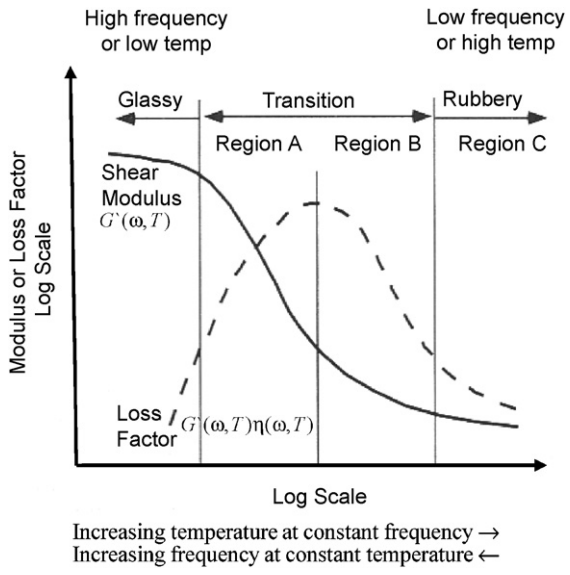

Fig. 42. Dependence of shear modulus and loss factor on temperature at constant frequency/or frequency at constant temperature [418].

shear modulus changes rapidly. The frequency at which the shear modulus increases rapidly as the excitation frequency increases is called the transition frequency. On the other hand, the temperature at which the shear modulus decreases rapidly as the temperature increases is called the glass transition temperature. The glass transition state is a non-equilibrium state at which the nonlinear viscoelastic nature of structural recovery can lead to surprising behavior [400]. Thus, one can use the temperature and frequency as control parameters to study such phenomena as bifurcation and other complex dynamic characteristics.

The transition frequency of low-damping rubber typically occurs at very high frequencies in the typical operating temperature range. Through the range of frequencies normally encountered in automotive isolators and other applications, the loss factor and shear modulus vary slowly with frequency. Furthermore, the transition frequency of high-damping materials usually occurs in or near the typical operating frequency ranges, so the dynamic modulus of high-damping materials changes very rapidly with frequency [2]. The transition frequency is dependent on temperature, so the concept of temperature–frequency equivalence [401] is extremely important, and nonlinear analysis of rubber isolators should include the effects of temperature and frequency. The temperature–frequency equivalence can be used to superimpose modulus curves covering a limited frequency range at different temperatures.

Schallamach et al. [402] and Harwood and Schallamach [403] examined the dynamic behavior of two different vulcanized elastomers, natural rubber, and acrylonitrile–butadiene rubber under strain cycling at various strain rates. The effect of amplitude, temperature, and frequency on the mechanical behavior of rubber under compressive loading was studied by McCallion and Davies [404]. However, these studies did not consider the influence of excitation amplitude under shear. Rubber is more compliant when loaded in shear than it is when loaded comparatively in compression, although energy storage capacity is relatively smaller [405].

When memory effects are neglected, the nonlinear characterization of viscoelastic materials, at the limits of the time and frequency ranges, approaches the nonlinear elastic theory [406]. However, the concept of a strain energy function cannot be carried over directly from the elastic to viscoelastic characterization. Some attempts [407] replaced the strain energy by a stored energy functional, which depends on the entire past history of deformation. The constitutive relation that defines the stress matrix in terms of the left Cauchy–Green strain measure was expressed nonlinearly in terms of scalar functions of strain invariants.

The time-stress superposition principle cannot be used to model the entire range of loading from low stress to the yield point as indicated by Skrypnyk et al. [408,409]. This is due to the fact that the storage modulus of a vulcanized material can increase very significantly at very low strains. Furthermore, the transition from linear to nonlinear dynamic properties occurs at decreasing strain amplitude with increasing filler content. For example, for butyl material at 23.2% high-abrasion the nonlinear region begins at double strain amplitude (peak-to-peak) of approximately 0.002, which is very small [410].

These studies motivated others [411–413] to further investigate the characteristics of nonlinear viscoelastic behavior, which is commonly observed in creep and relaxation. Furthermore, Lazan [399] introduced various nonlinear models by combining nonlinear dampers with nonlinear springs possessing either strain-hardening or strain-softening characteristics. Ferry [396] developed a nonlinear model where the time-dependent tensile stress was expressed by a power series and the Boltzmann superposition principle was extended to higher-order odd terms. In general, these models have been used to study nonlinear material behavior and stress–strain relations.

Gong et al. [414,415] considered a vibration isolator with hysteresis behavior and presented a method for modeling the isolator. They proposed a dynamic model of a wire-rope vibration isolator and reconstructed a force–displacement hysteresis loop. Their results revealed that the theoretical loops and the experimental measurements are close to each other in performance. They used their model to examine the nonlinear damping behavior of the isolator. It was demonstrated that the damping in the isolator varies with the amplitude and excitation frequency. The model reflected the damping characteristics of the nonlinear isolator.

Predicted transmissibility of a rubber-like mount may be in error when the physical dimensions of the elastomer coincide with half wavelengths of the elastic wave traveling in the material [416]. This so-called wave effect occurs at many frequencies, the first of which is in the region of 200 Hz for most commercial isolators. It may vary with frequency depending on dimensions of the mount and the hardness of the

elastomer. Many commercial isolators use rubber in compression, in shear, or in combination. When used in combination, loads producing small deflections are satisfactorily carried in shear. During large deflection produced by overload, the rubber becomes loaded in compression, thus acting as compression spring to the motion.

Viscoelastic isolators are often designed using primary and secondary stiffness values based on geometry changes. The primary value, k_{d1}, is taken as the first load–deflection slope, and the secondary value, k_{d2}, is taken as the second slope for a higher load. Some optimization codes used with many commercial nonlinear finite element programs determine the geometric shape of a mount that satisfies the stiffness requirements of engine mounts. The dynamic stiffness is expressed as $k_d = \varsigma k_s$, where k_d and k_s are the dynamic and static stiffness, respectively, and ς is a correction factor in the range 1.2–1.4 [417–420]. Even though the steps (k_{d1}, k_{d2}, …) are introduced in the analysis, the stiffness used in the model is assumed to be linear and damping is ignored. Furthermore, the relation $k_d = \varsigma k_s$ appears to be inconsistent with experimental observations that the dynamic stiffness depends on frequency and excitation amplitude.

Snowdon [2] and Ver [421] reported that the mean static load results in an increase of the dynamic stiffness. In effect, the mean static load shifts the value of dynamic loading to dwell in the nonlinear zone. The role of nonlinearity in the dynamic behavior of rubber components was addressed by Harris and Stevenson [422]. The transient response of linear structures mounted on nonlinear viscoelastic mounts was examined under impact loading by Gjika et al. [423]. The experimental characterizations of elastomers provided the definition of the quasi-static load deflection curves. The instantaneous stiffness and modal damping factors, deduced from experimental measurements, were used to model the nonlinear behavior of the elastomer mount. A nonlinear system with a power curve loading formula such as $F = kx^n$, where k is the stiffness, x is deflection, and n is exponent in the loading curve, has been used for both the spring and damper-loading characteristics of body mounts in computer aided engineering crash modeling [424]. Despite the fact that the power curve loading was used to express material nonlinearity, the stiffness and damping were assumed to be independent of excitation frequency and amplitude.

7.2. Isolator material and modeling

7.2.1. Nonlinear natural rubber

The dynamic properties of both neat rubber and filled rubber with filler content $\phi < \phi_c$ are linear viscoelastic, while those of filled rubber with filler content $\phi \geqslant \phi_c$ are strongly strain-dependent and nonlinear viscoelastic, where ϕ_c is a critical volume fraction of the filler content. Note that for neat rubber or filled rubber with small filler content, the storage modulus G' and loss shear modulus G'' (where the complex shear modulus $G^* = G' + \mathrm{i}G'' = G'(1 + \mathrm{i}\eta)$, and η is the loss factor) are correlated by the Kramers–Kronig relationship [396,425]

$$G'(\omega) = G_e + \frac{2\omega^2}{\pi}\int_0^\infty \frac{G''(\tau)}{\tau(\omega^2 - \tau^2)}\,\mathrm{d}\tau, \tag{74a}$$

$$G''(\omega) = \frac{2\omega^2}{\pi}\int_0^\infty \frac{G'(\tau) - G'_e}{(\omega^2 - \tau^2)}\,\mathrm{d}\tau. \tag{74b}$$

Eqs. (74a) and (74b) state that the storage modulus and loss shear modulus depend on each other. The limitation of the linear viscoelasticity described by Eqs. (74a) and (74b) was discussed by Lin and Lee [426] who considered four basic types of G': constant G', a step function for G', a ramp function for G', and a three-element spring-dashpot model.

Nonlinear viscoelasticity of filled rubbers arises from the breakdown and recombination of the secondary aggregate of filler network during vibration [427]. As the filler content becomes greater than the critical volume content, a secondary aggregate of filler network is formed and the dynamic mechanical properties become nonlinear viscoelastic. According to the study of Lin and Lee [427,428], the storage modulus, G'_T, and the shear loss modulus, G''_T, of the filled rubber are

$$G'_T(\omega, \varepsilon_0, \phi) = G'_F(\omega, \varepsilon_0, \phi) + G'_\infty(\omega, \phi), \tag{75}$$

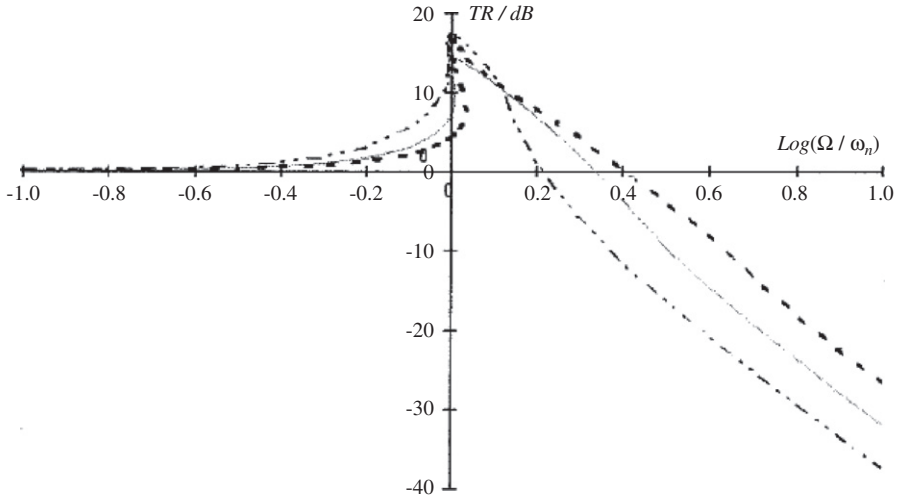

Fig. 43. Dependence of transmissibility of excitation frequency ratio for a carbon black filled natural rubber (NR-75 system) driven at a constant stress condition: – · ·– · ·– · ·– $\varepsilon_n = 0.002$, ····· $\varepsilon_n = 0.01$, and – – – – – $\varepsilon_n = 0.05$ [426].

$$G''_T(\omega, \varepsilon_0, \phi) = G''_F(\omega, \varepsilon_0, \phi) + G''_\infty(\omega, \phi) + \left[G''_0(\omega, \phi) - G''_\infty(\omega, \phi) \int_{\varepsilon=2\varepsilon_0}^{\infty} g_{1a}(\varepsilon)\, \mathrm{d}\varepsilon \right], \tag{76}$$

where G'_∞, G''_∞, G'_F, and G''_F are dynamic shear moduli,

$$G'_F(\omega, \varepsilon_0, \phi) = \xi_p^{2-d} \frac{Q\varepsilon_b}{a^2} \left[\int_{\varepsilon=2\varepsilon_0}^{\infty} \frac{f_{1a}(\varepsilon)}{\varepsilon}\, \mathrm{d}\varepsilon \right], \quad \varepsilon_{\mathrm{app}} = \left[\frac{mQ + 2\bar{G}}{4d\bar{G}} \right] \varepsilon_b,$$

$$G''_F(\omega, \varepsilon_0, \phi) = \xi_p^{2-d} \frac{Q\varepsilon_b}{2\pi a^2} \left[\frac{1}{\varepsilon_0^2} \int_{\varepsilon=2\varepsilon_0}^{\infty} \varepsilon f_{1a}(\varepsilon)\, \mathrm{d}\varepsilon \right],$$

$Q\varepsilon_b/a^2$ is the failure stress of single connected bonds, a is the length of a single connected bond, ε_b is the failure strain amplitude for breaking the contact between the particles, ε_0 is the failure strain amplitude, and $\varepsilon_{\mathrm{app}}$ is the apparent yield strain amplitude, which corresponds to the on-set point of breakdown of the secondary aggregate as the strain amplitude increases. When the strain amplitude is greater than $\varepsilon_{\mathrm{app}}$, G'_T starts to decrease, while G''_T starts to increase. Q and $\overline{G}$ are local elastic constants. $\overline{G}$ is controlled by the rubber phase around fillers and Q is controlled by van der Waals force between fillers. d and m are fractal parameters, ξ_p is the critical length of the links-nodes-blobs model [429,430]. $f_{1a}(\varepsilon)$ is the density distribution function of the number of singly connected bonds in the links-nodes-blobs model, $g_{1a}(\varepsilon)$ is the density distribution function that accounts for breakdown of the secondary aggregate attributed to the nonlinear phase deformation. Both $f_{1a}(\varepsilon)$ and $g_{1a}(\varepsilon)$ are exponential functions.

Two types of constraints are usually encountered in vibration isolation. One is the constant strain and the other is the constant stress condition. For a force driven at constant strain level on a filled rubber isolator, the behavior of the isolator is similar to a linear viscoelastic vibration isolator. The case of constant stress condition is usually considered to study the performance of a filled rubber isolator. As a vibration isolator drives different stress levels, different transmissibility behaviors are obtained due to the nonlinear behavior of filled rubber. Fig. 43 shows the simulation results of transmissibility dependence on excitation frequency ratio Ω/ω_n for three different values of strain amplitude, $\varepsilon_n = 0.002$, 0.01 and 0.05. All three cases exhibit a jump phenomenon near $\Omega/\omega_n = 1$. For the case of $\varepsilon_n = 0.002$, the system attenuates at the greatest rate near the natural frequency because G'_n is higher than the other two cases. However, all three cases have the same attenuation rate of 40 dB/log(Ω/ω_n) at high frequencies.

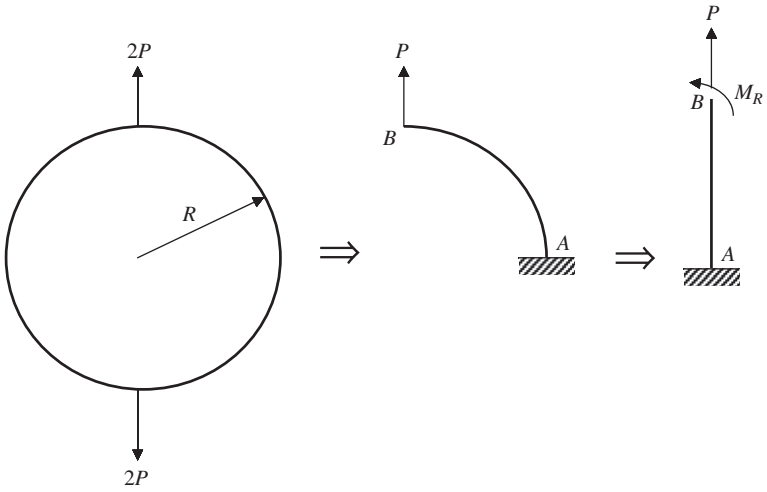

Fig. 44. Equivalent analysis of a ring in tension.

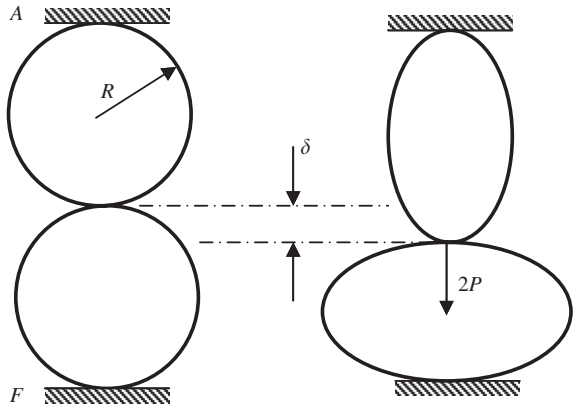

Fig. 45. Push–pull system of two elastic rings.

7.2.2. Composite springs

In view of the excellent properties of composite materials, engineers developed composite springs for automotive vehicles [431–437]. Scowen and Hughes [433] introduced the sulcated[2] spring in order to utilize the high tensile strength of fiber-reinforced plastic in spring systems. The elliptic composite springs described by Mallick [431,432] represent another generation of composite spring development. Tse et al. [438] and Tse and Lung [439] presented a large deflection analysis on orthotropic mid-plane symmetric laminated circular springs under vertical uni-axial tension and tension-push loading.

With reference to Fig. 44, the circular ring of radius, R, is subjected to two equal and opposite radial tensile loads, $2P$, and due to the symmetry only one quadrant is considered for the analysis. This deformed quadrant can be regarded as an originally straight rod AB of length $l = \pi R/2$ and subjected to a vertical load, P, and a bending moment, $M_R = bD/R$, at the free end, where D is the equivalent rigidity per unit width, b. Tse et al. [436,438] developed the equivalent flexural rigidity and obtained an expression for the stiffness of the ring in terms of elliptic integrals.

Tensile and push–pull tests were conducted by Tse et al. [438] on thin walled circular composite springs fabricated from E-glass woven cloth/Ciba-Geigy epoxy resin (XH750A/HY956) with nominal width of 51-mm and internal diameter of 114 mm. The push–pull tests were conducted on the combination of two rings shown

[2]A sulcated spring is characterized by long, narrow grooves or channels.

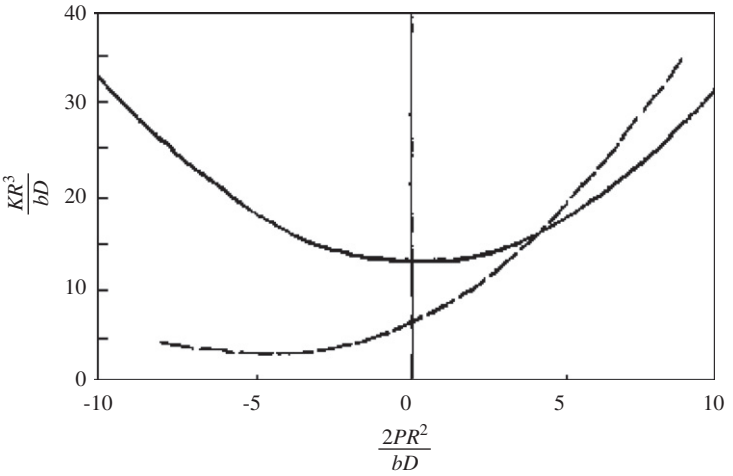

Fig. 46. Dependence of stiffness on load for spring ring and push–pull arrangement —— push–pull arrangement, - - - - single ring [438].

in Fig. 45. The spring stiffness was determined from the initial linear portion of their respective load–deflection curves. The equivalent flexural rigidity per unit width, $D = E_{11}h^3/12$, was evaluated by substituting the experimental spring stiffness into the spring stiffness expression

$$K = \frac{8\pi}{3(\pi^2 - 8)} \frac{E_{11} b h^3}{(2R + h)^3}, \tag{77}$$

where h is the thickness of the ring and E_{11} is the Young's modulus in the major principal direction.

Fig. 46 shows the dependence of the spring stiffness on the applied load for a spring ring and push–pull arrangement shown in Fig. 45. It is seen that for a spring ring the compressive region is much softer than the tensile one, as the same amount of load will produce larger deflection in the compressive region. Thus the spring can be classified as soft in the compression region and hard in the tensile region. For the arrangement of Fig. 45 of two similar ring springs the characteristics of the stiffness is changed to a symmetrical hard spring. The stiffness increases with deflection throughout the entire range of the load. This feature was found to satisfy the requirements of softness for steady-state vibration isolation and stiffness for transient and shock endurance.

7.3. Phenomenological modeling and transmissibility

It has been reported that methodologies based on dynamic mechanical tests and analysis accurately characterize the linear viscoelastic properties. However, these methods are only valid for small strains or loads. Other tests adopted high strain amplitudes of up to 20% as in American Society for Testing and Materials (ASTM) D-945 [440]. Dynamic properties measured at high strain amplitude cannot be used to design a vibration isolator that will work under low strain amplitude and vice versa. In some applications such as the front end cooling systems of road vehicles their isolators must work under a wide range of strains and loads. For that reason Shaska et al. [441] conducted experimental tests to measure the nonlinear behavior of rubber isolators as a function of excitation amplitudes. Based on these measurements, they developed phenomenological models under different conditions.

A wide spectrum of test techniques has been developed for measuring the complex modulus properties of viscoelastic materials [401,442–446]. It is frequently accepted that no single technique offers the range necessary to overcome the broadly varying nature in viscoelastic material properties. The techniques used to obtain the data evaluated in Ref. [441] were the forced resonance vibration and the impedance tests. Both tests carried out measurements in shear by using the same sample. The disadvantage of the forced resonance vibration test is the need for careful frequency adjustment and control. Determination of dynamic properties

over an extended frequency range is not practical with that test. For a given specimen the only variable available to change the resonant frequency is the mass and it is not practical to change it frequently. Furthermore, the static load due to the mass has an effect on the observed dynamic properties. The main advantage of the forced resonance vibration test is its simplicity. On the other hand, the impedance test yields a low signal-to-noise ratio. The signal-to-noise ratio can be of a concern at low excitation amplitude and high frequency. However, the frequency and the static load are relatively easy to control. It is important to use both tests and compare results for a better understanding of the effects of static load and frequency. The excitation amplitude can be controlled in both tests.

Tedesco [447] developed a mathematical model for the T22-AB-2 elastomeric vibration isolator. The isolator was tested both statically and dynamically to determine its response characteristics. It was found that the static stiffness as determined from force–deflection curves is significantly less than the stiffness determined from vibration testing. The dynamic modulus and loss factor were found to be nonlinear functions of the isolator displacement.

Chandra et al. [448,449] considered the nonlinear effects on the performance of isolators under shock excitations. Experimental characterization that reveals nonlinear behavior is essential to better understand rubber isolator dynamics under different static and dynamic loading conditions. Richards and Singh [450–452] and Mallik et al. [453] developed analytical models that describe the nonlinear characteristics of different rubber isolators. Static stiffness experiments conducted by Richards and Singh [442] presented time-invariant load–deflection curves. Dynamic excitations under random, frequency-sweep and mono-frequency were conducted to examine the behavior of each isolator under each excitation type.

Biejers and De Boer [454] developed a numerical algorithm to model rubber vibration isolators. Shaska et al. [441] conducted a series of impedance tests on a tubular sample of butyl rubber (Type II). The tests were conducted at room temperature, constant excitation frequency of 170 Hz and different values of excitation amplitude. The same measurements were performed at different temperatures and at different frequencies. The energy loss, ΔW, was estimated from each particular measurement and the loss factor was calculated from the area enclosed by the hysteresis loop, $\Delta W = \pi\eta_H X_0^2$, where η_H is the hysteretic damping constant (dimensional) and X_0 is the response amplitude. The dependence of the peak force amplitude, F, on the corresponding peak displacement amplitude, X_0, measured from hysteresis loops for three different values of temperature -10, 20, and 50 °C was generated for each temperature using a polynomial curve-fit. The following phenomenological relationships were obtained:

$$F = 2245X_0 - 12\,999X_0^2 + 25\,063X_0^3 \quad \text{at} \quad T = -10\,^\circ\text{C}, \tag{78a}$$

$$F = 1103X_0 - 4987X_0^2 + 7982X_0^3 \quad \text{at} \quad T = 20\,^\circ\text{C}, \tag{78b}$$

$$F = 780X_0 - 3645X_0^2 + 6941X_0^3 \quad \text{at} \quad T = 50\,^\circ\text{C}. \tag{78c}$$

The linear transmissibility at temperature T_i was calculated using the natural frequency, $\omega_n^2 = k_0/m$, where k_0 is the first term of Eqs. (78) at temperature T_i.

The dependence of the shear loss factor, η, and the shear storage modulus, G', at 20 °C, on the shear strain amplitude, γ, were given by the following relations:

$$\eta = 0.29 + 6.788\gamma + 1772\gamma^2 - 14,8075\gamma^3, \tag{79a}$$

$$G'(\text{MPa}) = 19.4 + 1065\gamma - 213,361\gamma^2 - 2\times10^8\gamma^3 + 4\times10^{10}\gamma^4 - 3\times10^{12}\gamma^5 + 7\times10^{13}\gamma^6. \tag{79b}$$

Fig. 47(a) shows the measured transmissibility using the forced resonance test for different values of excitation acceleration amplitude $|\ddot{Y}|$. The transmissibility is plotted versus the excitation frequency ratio, Ω/ω_n, where $\omega_n^2 = k_0/m$, and k_0 is the dynamic stiffness measured at the lowest excitation amplitude. Each curve is associated with a specific constant acceleration magnitude. It is seen that as the excitation amplitude increases the stiffness decreases and damping increases. The peaks are shifted to the left and the peak magnitudes are reduced as the excitation magnitude increases. The stiffness and transmissibility at resonance decrease approximately 40% and 25%, respectively, as the excitation acceleration increases from $\ddot{Y} = 2.5\,\text{m/s}^2$ to $\ddot{Y} = 39.2\,\text{m/s}^2$. The same feature is observed during transmissibility measurements for two

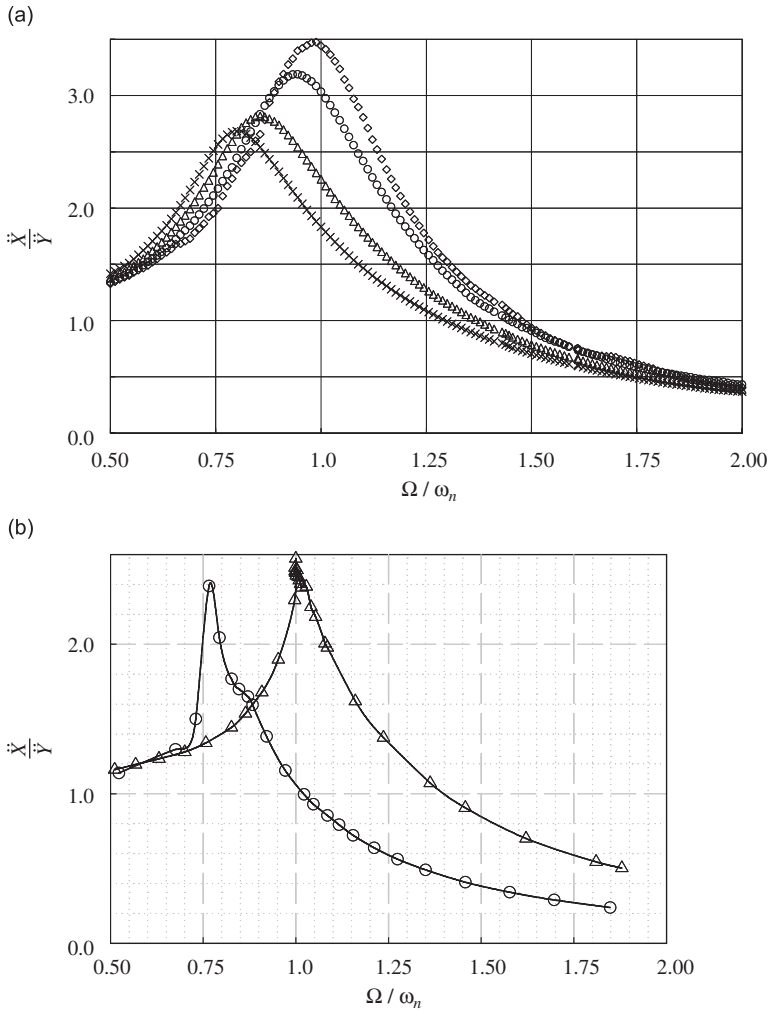

Fig. 47. Transmissibility as measured by the forced response vibration test at 20 °C: (a) different values of excitation acceleration: $\ddot{Y} = 2.5\,\mathrm{m/s^2}$ ◇, $\ddot{Y} = 9.8\,\mathrm{m/s^2}$ ○, $\ddot{Y} = 29.4\,\mathrm{m/s^2}$ Δ, $\ddot{Y} = 39.2\,\mathrm{m/s^2}$ × (b) Two different excitation amplitudes: $Y = 0.03$ in ○, 0.01 in Δ [441].

excitation displacement amplitudes: 0.25 mm (0.01-in) and 0.76 mm (0.03-in), as shown in Fig. 47(b). The stiffness decreases by 44% as the excitation amplitude increases by a factor three.

The reduction in stiffness and the associated increase in damping with excitation level is a phenomenon that appears for all values of temperature. To demonstrate the effectiveness of the nonlinear isolator, the normalized transmissibility, TR_{visc}/TR_{lin}, given by the ratio of the transmissibility of the viscoelastic mounts, TR_{visc}, to the one of a linear spring-dashpot mount, TR_{lin}, is given in Figs. 48(a)–(c) for three different temperatures: 20, 50, and 85 °C, respectively. The linear transmissibility is obtained by using linear parameters measured at the corresponding temperatures 20, 50, and 85 °C, respectively. Thus, any drop of the normalized transmissibility below unity is an indicative of the superiority of the viscoelastic isolator. This normalization method shows the combined effect of temperature and excitation amplitude. It is seen that the transmissibility at 20 °C and low excitation amplitude, $2.5\,\mathrm{m/s^2}$, is approximately the same as the linear prediction as shown in Fig. 48(a). However, as the excitation amplitude increases the transmissibility displays a significant departure from unity and the peaks are shifted to the left and reduced as the excitation amplitude increases. It is obvious that the rubber isolators under large excitation amplitudes lead to lower natural mounting frequencies. The transmissibility decreases rapidly with frequency as compared with linear isolators.

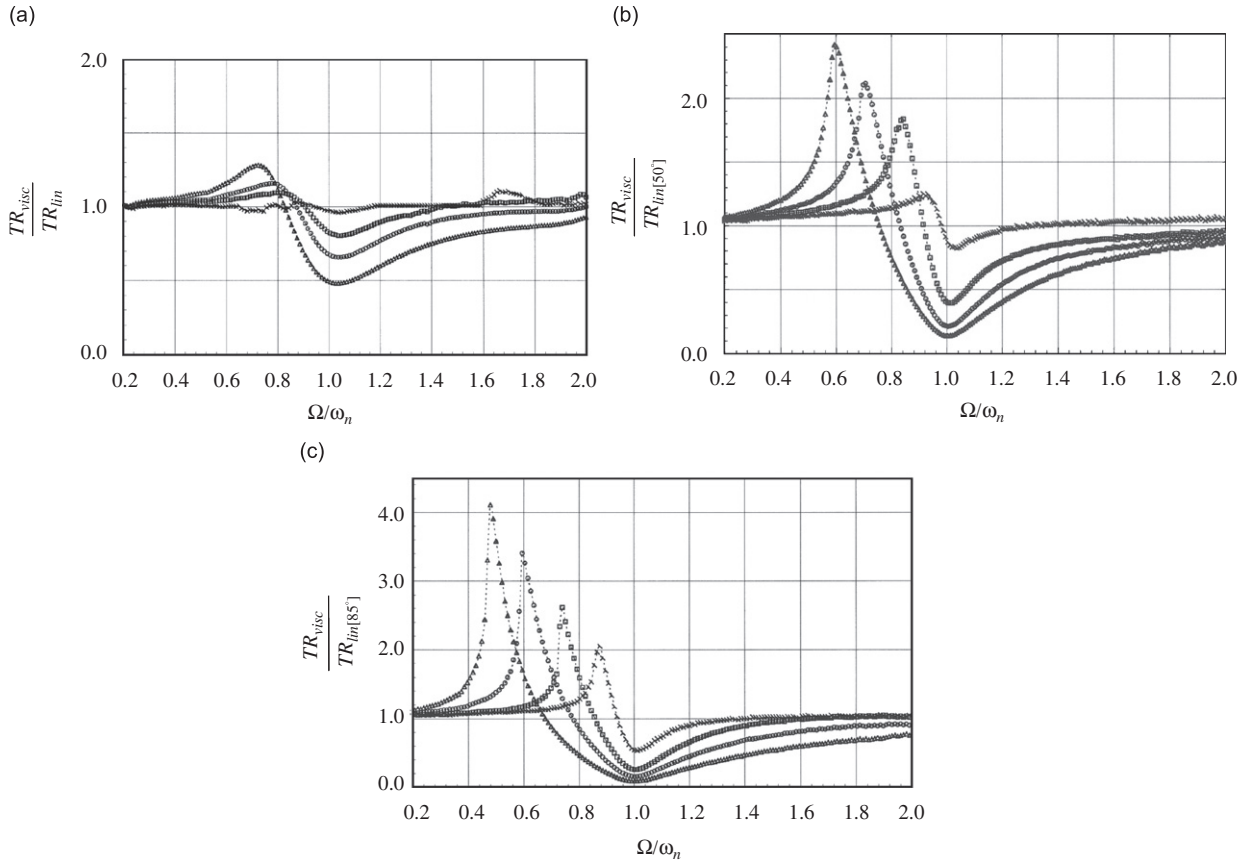

Fig. 48. Normalized transmissibility for different values of excitation acceleration at different temperatures (effect of temperature of shifting natural frequency is removed): (a) $T = 20\,^{\circ}\mathrm{C}$, (b) $T = 50\,^{\circ}\mathrm{C}$, (c) $T = 85\,^{\circ}\mathrm{C}$: $\ddot{Y}(m/s^2) = 2.5 \times$, $\ddot{Y}(m/s^2) = 9.8\,\square$ $\ddot{Y}(m/s^2) = 29.4\,\circ$, $\ddot{Y}(m/s^2) = 39.2\,\Delta$ [441].

7.4. Viscoelastic fractional modeling

Kari [36,37,455] introduced the nonlinear shape factor-based models that account for the increasing shape factor resulting from decreasing thickness of the rubber cylindrical isolator during compression. His results agreed with those of a cylindrical neo-Hookean hyper-elastic rubber isolator model. Padovan and Sawicki [456] studied the steady-state response of a nonlinear Duffing isolator with fractional derivative damping to harmonic excitation. They used an energy-constrained Poincaré–Lindstedt perturbation method with a diophantinized fractional derivative[3] representation. Sjöberk and Kari [457] included nonlinear friction in a fractional Kelvin–Voigt model in studying the nonlinear behavior of a rubber isolator.

Sjöberk and Kari [458] considered a nonlinear dynamic model of a cylindrical carbon black filled rubber isolator by combining a nonlinear shape factor-based stiffness, a fractional derivative and a generalized friction model. The total force, F, consists of the sum of elastic, F_e, viscoelastic, F_{ve}, and friction, F_f, forces. The viscoelastic compression force was described by the fractional time derivative of order α

$$F_{\mathrm{ve}} = b\frac{\mathrm{d}^{\alpha}u}{\mathrm{d}t}, \tag{80}$$

[3]Diophantinized fractional derivative is a type of differential-integro representation of structural hysteresis.

where u is the compression displacement under the total force F, $0<\alpha<1$, and $b>0$ Ns^{α}/m are model constants. The fractional derivative is defined as

$$\frac{\mathrm{d}^{\alpha}u}{\mathrm{d}t^{\alpha}}=\frac{1}{\Gamma(1-\alpha)}\frac{\mathrm{d}}{\mathrm{d}t}\int_0^t\frac{u(\tau)}{(t-\tau)^{\alpha}}\mathrm{d}\tau, \tag{81}$$

where the Gamma function $\Gamma(\beta)=\int_0^{\infty}s^{\beta-1}\mathrm{e}^{-s}\,\mathrm{d}s$.

Note that the fractional derivative operator is a non-local operator in a temporal sense for $0<\alpha<1$. In other words, it depends on the displacement history, not only on the current value, in line with components made of materials with memory such as rubber isolators. Numerically, Sjöberk and Kari [458] found that the viscoelastic force, given by Eqs. (80) and (81), is

$$F_{ve}(t_n)\approx b\frac{\Delta t^{-\alpha}}{\Gamma(-\alpha)}\sum_{j=0}^{n-1}\frac{\Gamma(j-\alpha)}{\Gamma(j+1)}u_{n-j}. \tag{82}$$

The friction force of carbon black filled rubber was given by the smooth representation

$$F_f=F_{f_s}+\frac{u-u_s}{u_{1/2}\left[1-\mathrm{sgn}(\dot{u})(F_{f_s}/F_{f_{\max}})\right]+\mathrm{sgn}(\dot{u})(u-u_s)}\left[F_{f_{\max}}-\mathrm{sgn}(\dot{u})F_{f_s}\right], \tag{83}$$

where $F_{f_{\max}}$ is the maximum friction compression force, $u_{1/2}$ is the displacement at half of that force, and $\mathrm{sgn}(\dot{u})$ denotes the signum of the compression displacement rate. The parameters F_{f_s} and u_s are updated each time the displacement changes direction at $\dot{u}=0$.

The elastic compression force was given by the definition

$$F_e(u)=\int_0^u\frac{\mathrm{d}F_e(u)}{\mathrm{d}u}\,\mathrm{d}u=\frac{3\pi}{4}\frac{\mu D^2u}{L-u}\left[1+\frac{D^2(2L-u)}{16L^2(L-u)}\right], \tag{84}$$

where L and D are the length and diameter of the rubber cylinder, respectively. μ is the static shear modulus

The linearized elastic force contribution at vanishing compression was given by the expression

$$F_e^{\mathrm{lin}}(u)=k_e(0)u=\frac{3\pi}{4}\frac{\mu D^2}{L}\left(1+2S_0^2\right)u, \tag{85}$$

where $S_0=D/4L$ is the shape factor.

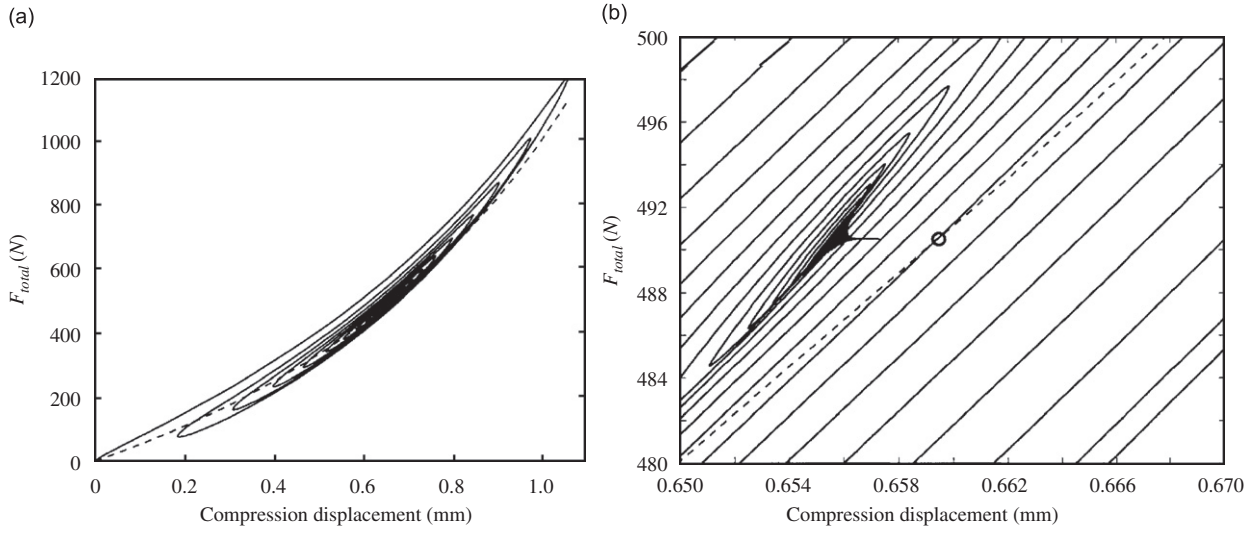

Fig. 49. Force–displacement contours of a freely oscillating mass mounted on cylindrical rubber isolator: (a) Full response _____ freely oscillating mass, --- elastic force only, (b) magnification around the focal point, ⊙ focal point [458].

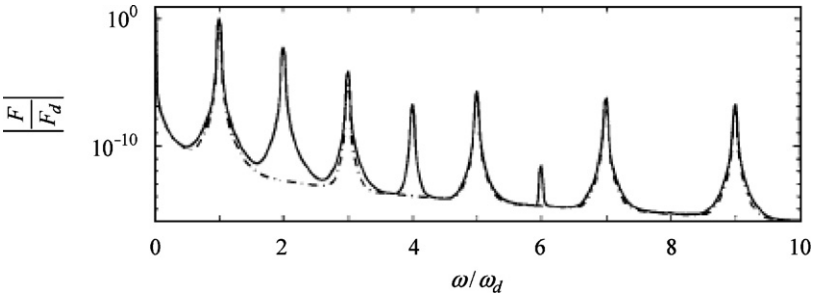

Fig. 50. Normalized total force FT versus excitation frequency ratio for excitation pre-compression and amplitude of 0.8 mm and excitation of 100 Hz. Solid curve is fully nonlinear model, and dashed-dot curve is the linearized mode [458].

The system considered by Sjöberk and Kari [458] was described by the equation of motion

$$m\frac{\mathrm{d}^2u(t)}{\mathrm{d}t^2} = mgh(t) - F_e(u(t)) - F_{\mathrm{ve}}(u(t)) - F_f(u(t)), \tag{86}$$

where m is the system oscillating mass and $h(t)$ is a step function. Under free vibration the response was obtained by numerically solving Eq. (86) using Newmark algorithm for $t = 5\,\mathrm{s}$ and time step of $\Delta t = 3.33 \times 10^{-4}\,\mathrm{s}$. The solid curve response shown in Fig. 49(a) is due to nonlinear elastic, viscoelastic and friction forces, while the dashed line displays the contribution of the linear elastic force. The maximum undamped natural frequency was found to be 955 Hz. Fig. 49(b) shows a zoomed segment of the force displacement diagram. It was reported that the mass oscillates strongly, with the maximum total force as the first turning point exceeds twice the static weight of the mass, then the mass exhibits a rapid decreasing amplitude oscillations. The mass was observed to move toward the focal point (indicated by the symbol $\odot$ in Fig. 49(b)) at the nonlinear elastic force–displacement curve, given by $F_e(u_0) = mg$.

Under harmonic excitation of the rigid mass mounted on the vibration isolator, the response was decomposed into $u = -(u_0 + \Delta u)$, where $\Delta u(t) = \Delta u_d \sin(\omega_d t)$, Δu_d is the dynamic compression displacement and ω_d is its frequency. The FFT force–frequency content is shown in Fig. 50. It is seen that the linearized model does not reveal the even-order harmonics due to the point of symmetry of the hysteretic force–displacement. Furthermore, the magnitude of the even-order harmonics for the fully nonlinear model decreases rapidly. Note that friction forces are characterized by a point of symmetry and thus contain only odd-order harmonics while the nonlinear elastic forces lack that symmetry and thus contain all higher-order harmonics.

7.5. Smart material isolator elements

Several attempts have been made for using smart materials, which allow stiffness and/or damping to vary during operation. Time-varying damping elements include magnetohydrorheological fluids [459], electro-rheological fluids [460,461], and piezoelectrics [462,463]. These dampers have the ability to change their damping characteristics by application of an electric field for electrorheological fluids or by applying a magnetic field for magnetohydrorheological fluids. Field strength can be increased to the point where the chains solidify resulting in a high yield stress and an increase in damping for magnetohydrorheological or electrorheological dampers. Removal of the field results in the fluid returning to its original state. Changes in state occur within milliseconds [464,465]. When electrorheological fluids are stressed electrically they demonstrate a controllable, massive change in effective viscosity. Sproston and Stanway [461] showed that continuous control of viscosity could be achieved through the applied electric field. They also demonstrated the work of these fluids on the development of an automotive engine mount. When piezoelectrics are combined with a resistor, they create damping analogous to viscoelastic damping. The piezoelectric combined with the resistor electrically creates a resistance capacitance shunt network, since the piezoelectric acts like a capacitor [462].

Examples of variable stiffness elements are shape (or smart) memory alloys [466], magnetohydrorheological elastomers and piezoelectrics. Stable phases of shape memory alloys include a low-temperature phase referred to as *martensite* and a high-temperature phase known as *austenite*. Shape memory alloys are metal alloys that recover otherwise permanent strain when heated. Shape memory alloys have two properties, the shape memory effect and the pseudo-elasticity effect. The shape memory effect occurs when shape memory alloys in martensitic state is deformed by a load and then heated to austenitic form where it recovers its original shape. The pseudo-elasticity effect occurs when a load is applied to shape memory alloys in austenitic state, which under proper conditions can induce a phase change to martensitic form. When the load is released, the material is transformed back to austenitic form and recovers its original shape [466]. Models describing both shape memory and pseudo-elasticity effects in shape memory alloys have been reviewed by Saadat et al. [467].

The pseudo-elasticity effect of shape memory alloys was proposed for use in place of soft nonlinear springs for passive isolation of large loads. While a soft spring is desirable for low-frequency resonant isolation, yet a stiff spring is needed to avoid large displacements. Thus the use of a soft spring degrades high frequency isolation. Instead one might consider the use of shape memory alloys to remove such trade-off as considered by Lagoudas et al. [468] and Khan and Lagoudas [469]. Magnetohydrorheological elastomers are made of rubber mixed with micron-sized magnetizable particles. The elastomer is cured in a magnetic field causing the magnetic particles to align in chains and remain aligned after the magnetic field is removed. Ginder et al. [470] reported that the application of a magnetic field changes the stiffness of the elastomer. The stiffness of piezoelectrics can be varied by connecting them to a capacitive shunt circuit [463]. Davis [471] examined and modeled the magnetohydro-rheological elastomer phenomena. Ginder et al. [472] showed that with increasing input acceleration amplitude attributed to strain-softening behavior of the elastomer the spring exhibited variable stiffness nonlinearity.

In view of the variation of the structure parameters of shape memory alloys the equation of motion may be written in the form [473]

$$\tilde{m}\frac{\mathrm{d}^2x}{\mathrm{d}t^2}+\left(\frac{\mathrm{d}\tilde{m}}{\mathrm{d}t}+\tilde{C}\right)\frac{\mathrm{d}x}{\mathrm{d}t}+\tilde{k}x+\left(\frac{1}{2}\frac{\partial\tilde{c}}{\partial(\mathrm{d}x/\mathrm{d}t)}\frac{\mathrm{d}x}{\mathrm{d}t}-\frac{\partial\tilde{k}}{\partial\dot{x}}x\right)=F(t). \tag{87}$$

This equation can be written in the form

$$\ddot{x}+f(x,\dot{x},t)\dot{x}+g(x,\dot{x},t)=e(t). \tag{88}$$

If f and g are functions of position only, then Eq. (88) is known as Lienard's equation [474]. Research activities dealing with this equation have been devoted to study the existence and uniqueness of solutions for both autonomous and non-autonomous versions of Eq. (88). Conditions for existence and number of limit cycle oscillations have been obtained when both f and g are functions of position [475–478].

The effect of nonlinear hysteretic damping of a magnetohydrorheological damper on the response of suspension systems was studied using the equivalent linearization and averaging method by Shen et al. [479]. The results of the two approaches were found in good agreement. The agreement was found to be preserved as long as the nonlinearity of the damper used is small enough. In another study, Narimani and Golnaraghi [480] considered the nonlinearities of a vibration isolator to improve the performance of linear mounts. Both nonlinear damping and stiffness rates were found to have interacting effects on the dynamic behavior of the mount. It was found that the effect of nonlinear stiffness rate on frequency response is opposite to that of the nonlinear damping rate [481,482]. The load-leveling suspension system of vehicles can make the sprung mass to have different acceleration and relative displacement transmissibilities by applying different values of magnetorheological dampers. This provides improvement in vibration isolation for both low-frequency excitation and high-frequency excitation. Shen et al. [483] found the load-leveling suspension system resulted in an increase of the frequency range of control in comparison to traditional suspension systems.

7.6. Isolation of aerospace structures

Vibration isolation of aerospace structures is essential for space launch vehicles including space telescopes and microgravity effects on liquids, combustion, and material management. Most of research activities of

vibration control in aerospace applications rely on active control means rather than passive means. Vibration isolations with constant stiffness elements and damping elements such as viscoelastic materials, viscous fluids, magnetic and passive piezoelectrics have been extensively used in aerospace applications [484,485]. Yiu and Regelbrugge [486] proposed the shape memory alloy isolators for vibration suppression in space applications. It was shown that the shape memory alloy isolators enable inexpensive components to be designed with improved performance for space applications.

It is essential to prevent damage to the payload of launch space vehicles by isolating structural and acoustical vibrations. Cobb et al. [487] described the design and performance of a vibration isolation and suppression system, which can be used to isolate a precision payload from spacecraft borne disturbances. The passive isolation was provided using a flight proven D-strut design. Winthrop and Cobb [473] mentioned that in small launch vehicles, the sound level can exceed 130 dB and can cause payload damage. High levels of axial vibrations of spacecraft structures due to resonant excitations from the motors of the solid-fueled booster were found to cover several frequency bands. Vibrations have long been a source of problems for space systems, with acoustic and aerodynamic excitations causing failures during launch and periodic disturbances degrading performance on-orbit. Whole-space vibration isolation systems known as single-axis SoftRide systems have been developed for the first and second orbital/suborbital Program (OSP) launches and for the Taurus/MTI launch [488–492]. The structures on either side of the isolation system, namely the launch vehicle and the spacecraft, are both very rich in dynamics. Dynamic launch loads from some launch vehicles, particularly solid boosters, may be drastically attenuated through the use of an axial SoftRide isolation system. The use of viscoelastic material causes both the stiffness and the damping to be frequency dependent. The isolation system was made up of a series of identical isolator elements. Typical results revealed 85% attenuation for the worst-case resonant burn condition and 59% attenuation for a combination of static plus worst case resonant burn condition in the axial spacecraft center of mass location.

An extension of the single-axis SoftRide system is the multi-axis system, which inserts flexibility and damping in three orthogonal axes between the launch vehicle and the satellite [492]. This multi-axis whole-space vibration isolator resulted in mitigating dynamic launch loads. Additionally, these isolation systems provided extreme reductions to shock and structure-borne acoustic loads. The performance of six-axis vibration isolation systems was assessed by O'Brien et al. [493]. In particular, space-borne interferometers require isolation of the reaction wheel disturbances in order to stabilize the precision optical elements to the required levels. Dual-chamber pneumatic springs are widely used in the vibration isolation systems for precision instruments such as optical devices or nano-scale equipment owing to their superior stiffness and damping characteristics. The experimental results measured by Kim and Lee [494] for a dual-chamber pneumatic spring exhibited significantly amplitude-dependent nonlinear behavior. They proposed nonlinear complex stiffness model, which reflects dependency on both frequency and excitation amplitude.

The advantage of nonlinear isolators over the linear ones makes them very attractive for implementation for missile structures isolation from shock loading [495]. Park and Fowler [496] proposed the zero-spring-rate mechanism as a suspension device for supporting a given range of payload weight of the Space Station Freedom. The Hubble Space Telescope requires the safe transportation of electronic Orbital Replacement Units on the Space Transportation System. It was imperative to provide isolation from the Space Transportation System launch random vibration, while maintaining fundamental modes above the transient load environment. Denoyer et al. [497] and Jedrich and Pendleton [498] addressed two isolation systems for electronic black-box transportation orbit. The first system utilized a refined open/closed cell foam design to provide the required damping and corner frequency, while the second used a viscoelastic material design.

Key issues related to passive vibro-acoustic isolation for container-type structures were discussed by Griffin et al. [499]. The key noise reduction principle was the passive application of a characteristic impedance mismatch in conjunction with a vibration isolation suspension system to limit structural transmission. The characteristic impedance mismatch was created by imposing a near vacuum condition between partitions of a container structure.

The vibration isolation and suppression system was designed to isolate a precision payload from spacecraft borne disturbances using passive isolation in combination with voice coil actuators [500,501]. Passive isolation technology has been accepted by Satellite designers for space applications [502–505]. Passive D-strut systems

were originally developed for satellite reaction wheels and the reaction wheel assemblies in the Hubble Space Telescope [502]. Space flight experiments demonstrated that smart structures provided high-performance on-orbit isolation to precision spacecraft payloads [506]. Hadden et al. [507] described a vibration isolation system for airborne payloads from aircraft disturbances. The system was in the form of six pneumatic struts configured as a hexapod or Stewart Platform, which makes up the primary portion of the isolation system. Each isolator has a capacity for large energy storage and possesses a near linear viscosity over a broad temperature range. Isolation estimate followed damage failure in aerospace structures was reported by Zimmerman and Lyde [508] and Roemer et al. [509].

Satellite structures are normally constructed from very lightweight alloy materials and operate in environments where there is almost no damping because the lack of atmospheric damping and desire minimize payload. These structures carry sensitive instruments in very precise alignments, which make them very susceptible to unwanted structural vibrations. It was imperative to build passive vibration isolation into these structures [510]. Keane and Bright [511] described an experimental investigation on a revised design of a two-dimensional lattice structure. It was shown that significant noise isolation characteristics could be achieved into a regular structure by modifying it in a controlled way without using damping material or active control means.

7.7. Isolation of automotive systems

There is a growing interest in automotive industry to isolate the power-train system, engine, and engine cooling system through proper design of rubber and hydraulic mounting systems. Hydraulic engine mounts exhibit nonlinearities due to internal fluid flow characteristics, compliances of elastomeric fluid chambers, decoupler switching mechanisms, and vacuum formation [512,513]. Colgate et al. [513] studied the frequency response characteristics of a highly nonlinear hydraulic engine mount. They considered the nonlinearity due to an amplitude-limited floating piston (the 'decoupler'), which enables the response to large amplitude road-induced excitations. Tiwari et al. [514] modeled and simulated different configurations of the mount in an attempt to quantify these nonlinearities from the steady-state behavior at different frequencies and amplitudes of displacement excitation. Golnaraghi and Jazar [515,516] found that the behavior of the nonlinear hydraulic mount at resonance is associated with the jump phenomenon. The nonlinear resonance results in high-amplitude steady state or unstable behavior at high frequencies and is not predicted by the linear model. The basic design considerations and optimization for engine mounting were discussed in Refs. [517–524]. The modern engine mounting systems have to isolate the driver and passengers from both noise and vibration generated by the engine.

Christopherson et al. [525] described the nonlinearities in the lumped parameter modeling by the geometric and constitutive relationship-induced nonlinearity, including hysteretic behavior. They showed that under certain conditions, the nonlinearities involved in the hydraulic engine mounts could result in a chaotic response. Ohadi and Maghsoodi [526] studied the influence of nonlinearities due inertia and decoupler resistances in turbulent region. They found that hydraulic mounts provide better isolation than rubber mounts only in the low-frequency region.

Shangguan and Lu [527] developed a fluid structure interaction finite element analysis model to examine the dynamic behavior of a hydraulic engine mount with an inertia track and a free decoupler. The results of the time histories of some variables in the model, such as the pressure in the upper chamber and the displacement of free decoupler under different excitations, demonstrated the mount working mechanism. Zhang and Shangguan [528] and Shangguan et al. [529] identified the nonlinear damping of the inertia track for a generic hydraulic engine mount using experimental investigations and ADINA simulation approach. The problem of parameter identification of hydraulic engine mounts was further examined by Kyprianou et al. [530] and Fan and Lu [531]. The working principles of hydraulic mechanisms and the relationship between the dynamic properties of three types of mounts were presented. It was found that the frequency-variant dynamic properties of the mounts with an inertia track or an orifice have excitation amplitude-invariant fixed points. A nonlinear lumped parameter model for a hydraulic mount with an inertia track was developed and analyzed to predict the fixed point of dynamic stiffness. The results showed that the fluid flow through an orifice could be replaced by a fluid flow through an equivalent length of inertia track.

He and Singh [532] identified and quantified discontinuous compliance nonlinearities of hydraulic engine mounts. These included asymmetric nonlinearities in transient step-up and step-down responses by using a quasi-linear mount model. They also developed an improved multistaged top chamber compliance model, which exhibited the existence of highly nonlinear region(s) during the step transitions as well as during the decaying transients. A mean displacement-dependent model was proposed for the bottom chamber compliance.

Viscoelastic materials such as rubber are widely utilized in vibration damping mounts [533–537]. The dynamic stiffness of an elastomeric mount is known to be greater at high frequencies than its value at low frequencies due to damping. This characteristic makes it difficult to design a mount system that satisfies the design requirements [538–540]. Examples of vibration damping mounts in automotive industry are engine, front end cooling system, and body-frame rubber mounts. Corcoran and Ticks [17] and Flower [18] replaced the rubber engine mounts by hydraulic engine mounts. Passive hydraulic mounts provide the ability to reduce the compromise between engine isolation and shake control when developing engine-mounting systems. They also can provide better performance than elastomeric mounts over a low-frequency range [417,541–545]. However, they cannot solve all inherent problems during vehicle operations.

Wei-Ge et al. [546] proposed the utilization of magnetorheological fluids in hydraulic engine mount for damping vehicle noise and vibration. Their experimental results showed that the dynamic characteristics of a magnetorheological mount, such as dynamic stiffness and loss angles, vary distinctly. Kelso et al. [547] presented experimental investigation for a prototype device utilizing magnetorheological fluid damper constituting a piston/dashpot configuration. During reciprocation, the fluid is circulated through the device with the generated pressure providing viscous damping. In addition, the damper is also intended to accommodate off-axis loading; i.e., rotation moments and lateral loads orthogonal to the axis of operation. With magnetorheological fluid, the seals can act as sources of nonlinear friction effects (stiction) and possess a shorter lifespan due to the abrasive nature of the ferrous particles suspended in the fluid. The goal of the work of Kelso et al. [547] was the development of a stiction-free magnetorheological isolator whose damping force can be predicted.

Vibration isolators made of rubber pads have a hysteretic nonlinearity. The combination of hydraulic device with rubber pads for introducing damping effect and by attaching a stopper to the rubber pads for limiting amplitude was proposed by Irino, Sato et al. [548,549]. They described the hysteretic nonlinearity using Preisach distribution function, which makes it possible to evaluate equivalent damping coefficient and stiffness in terms of excitation amplitude and frequency in equation of motion. The frequency response characteristics of a single-degree-of-freedom with a hydraulic rubber pads was evaluated in terms of equivalent damping coefficient and stiffness.

The development of engine mounting systems has mostly concentrated on improvement of frequency- and amplitude-dependent properties. The conventional elastomeric mounts do not meet all the requirements and can only offer a trade-off between static deflection and vibration isolation. Passive hydraulic mounts can provide a better performance than elastomeric mounts especially in the low-frequency range. Yu et al. [538–540] provided some views regarding the ideal engine mount system that should isolate vibration caused by engine disturbance in various speed ranges and prevent engine bounce from shock excitation. This implies that the dynamic stiffness and damping of the engine mount should be frequency and amplitude dependent. Therefore, the development of engine mounting systems has mostly concentrated on improvement of frequency and amplitude-dependent properties.

Dhaubhadel [550] considered Fluidlastic(R) engine mount and solved for the time-dependent Navier–Stokes equations governing laminar and turbulent flows using a penalty finite element method. The results were presented for a generic Fluidlastic(R) engine mount for Reynolds numbers ranging from 40 to 120,000. It was found that the flow resistance is very sensitive to the viscosity of the fluid, length and diameter of the inertia track, and frequency and amplitude of oscillation of the fluid chamber walls. The relationship between the pressure differential across the inertia track and the flow rate is nearly linear for low Reynolds number flows and nonlinear for high Reynolds number laminar and turbulent flows.

8. Conclusions

Recent advances in metallic and viscoelastic nonlinear vibration isolators have been presented and covered traditional and non-traditional systems. The main features of nonlinear isolators have been described. These

features include the shift of resonance frequency, jump phenomena, chaotic motion, and internal resonance. The measure of transmissibility of nonlinear isolators experiencing non-harmonic behavior requires special description in terms of the mean squares of response and excitation amplitudes.

Metallic nonlinear isolators include pendulum systems, Euler springs, and sliding beams. These isolators were designed primarily to isolate excitation signals such as gravitational waves at very low-frequency levels. Specific ultra-low-frequency isolators include the folded pendulum isolator, the X-pendulum isolator table, and the conical pendulum. Efforts for reducing the resonant frequency such as magnetic anti-spring, torsion-crank linkage, and geometric anti-spring have been outlined. The analyses of these isolators were based on approximate elastic and axial stiffness of the Euler column. So it was imperative to introduce the exact analysis of the *elastica* and axial stiffness, which can be utilized for accurate modeling of Euler spring vertical isolator. The Euler spring has been used for vertical vibration isolation at low frequencies. However, the Euler beam, known as the Gospodnetic–Frisch beam sliding on two supports without constraints was introduced and it revealed isolation superiority in the neighborhood of the resonant frequency. Its restoring force was found to vanish at a critical deflection similar to the roll restoring moment of ships near the angle of capsizing. This disadvantage can be avoided and eliminated by introducing damped bumpers. Accurate modeling of Euler spring or Gospodnetic–Frisch beam should be formulated based on the exact *elastica* and restoring force in terms of elliptic integrals. The influence of friction at the beam supports should be included and means to minimize wear should be developed. It is not expected that analytical approaches such as asymptotic techniques will provide accurate results. However, numerical simulations should be performed whether the excitation is deterministic or stochastic.

Protection of buildings, bridges, and liquid storage tanks against earthquakes has been achieved by different types of base-isolation systems such as passive friction dampers, rubber-lead bearings and friction-pendulum systems. Many studies considered the ground motion to be horizontal random stationary. However, most of earthquakes exhibit non-stationarity and realistic friction coefficient exhibit stochasticity with time. The influence of excitation non-stationarity and stochastic friction should be considered for future research.

Viscoelastic nonlinear isolators exhibit different mechanical characteristics due to the dependence of their stiffness and damping parameters on frequency and temperature. It was reported that as the excitation amplitude of the nonlinear viscoelastic isolator increases, the response amplitude decreases and the transmissibility is improved over that of the linear isolator for excitation frequency that exceeds a particular value governed by the temperature and excitation amplitude. For each type of elastomer material the designer should develop phenomenological modeling of the shear storage modulus and shear loss factor. These models can provide better and accurate analytical dynamical modeling of the elastomer isolator.

In order to enhance the performance of passive isolators, an overall nonlinear control design should be utilized as those proposed in references (see, e.g., Refs. [551–555]). Note that this article did not address the semi-active or active control of nonlinear isolators. The active/semi-active control means of vibration isolation have been introduced in vehicle suspension and base-isolation buildings. A hybrid seismic control system for building structures was considered in the literature (see, e.g., Ref. [551]), which combines a class of passive nonlinear base isolator with an active control system. The design of semi-active and active suspension systems has been pursued to attenuate the vibrations between the vehicle's sprung and unsprung masses [552]. However, this approach tends to be expensive (e.g., actuators, sensors, and computational burden) and power intensive (e.g., hydraulic or pneumatic sources).

Acknowledgment

This work has been supported by a grant from the ONR under Grant no. N00014-05-1-0040. Dr. Kelly Cooper is the Program Director.

References

[1] C.E. Crede, *Vibration and Shock Isolation*, Wiley, New York, 1951.
[2] J.C. Snowdon, *Vibration and Shock in Damped Mechanical Systems*, Wiley, New York, 1968.
[3] J.C. Snowdon, Vibration isolation use and characterization, *Journal of the Acoustical Society of America* 66 (1979) 1245–1279.

[4] E.I. Rivin, *Passive Vibration Isolation*, ASME Press, New York, 2001.
[5] J. Winterflood, D.G. Blair, B. Slagmolen, High performance vibration isolation using springs in Euler column buckling mode, *Physics Letters A* 300 (2002) 122–130.
[6] J. Winterflood, T.A. Barber, D.G. Blair, Using Euler buckling springs for vibration isolation, *Classical and Quantum Gravity* 19 (2002) 1639–1645.
[7] A.J.H. Goodwin, Vibration isolators, U.S. Patent No. 3,202,388, 1965.
[8] D.R. Halwes, Vibration suppression system, U.S. Patent No. 4,236,607, 1980.
[9] W.G. Flannelly, Dynamic anti-resonant vibration isolator, U.S. Patent No. 3,322,379, 1967.
[10] C. Yilmaz, N. Kikuchi, Analysis and design of passive band-stop filter-type vibration isolators for low-frequency applications, *Journal of Sound and Vibration* 291 (2006) 1004–1028.
[11] A.D. Rita, J.H. McGravey, R. Jones, Helicopter rotor isolation evaluation utilizing the dynamic anti-resonant vibration isolator, *Journal of the American Helicopter Society* 23 (1978) 22–29.
[12] D. Braun, Development of anti-resonance force isolators for helicopter vibration reduction, *Journal of the American Helicopter Society* 27 (1982) 37–44.
[13] D. Braun, Vibration isolator particularly of the anti-resonance force type, U.S. Patent No. 4,781,363, 1988.
[14] R.A. Desjardins, Vibration isolation system, U.S. Patent No. 4,140,028, 1979.
[15] R.A. Desjardins, W.E. Hooper, Anti-resonant rotor isolation for vibration reduction, *Journal of the American Helicopter Society* 25 (1980) 46–55.
[16] V.A. Ivovich, M.K. Savovich, Isolation of floor machines by lever-type inertia vibration corrector, *Proceedings of the Institution of Civil Engineers: Structures and Buildings* 146 (2001) 391–402.
[17] P.E. Corcoran, G.E. Ticks, Hydraulic engine mount characteristics, *Proceedings of the 1984 Society of Automotive Engineers International Congress and Exhibition, Advances in Elastomeric Applications*, Detroit, MI, USA, SAE Paper No. 840407, 1984, pp. 29–34.
[18] W.C. Flower, Understanding hydraulic mounts for improved vehicle noise, vibration and ride qualities, *Surface Vehicle Noise and Vibration Conference Proceedings*, Traverse City, MI, USA, SAE Paper No. 850975, 1985, pp. 123–132.
[19] C. Yilmaz, N. Kikushi, Analysis and design of passive low-pass filter-type vibration isolators considering stiffness and mass limitations, *Journal of Sound and Vibration* 293 (2006) 171–195.
[20] M.Z. Kolovsky, *Nonlinear Dynamics of Active and Passive Systems of Vibration Protection*, Springer, Berlin, 1999.
[21] G.S. Yuryev, *Vibration Isolation of Precision Instruments*, Russian Academy of Sciences, Siberian Branch, Institute of Nuclear Physics Press, Novosibirsk, Reprint, 1991, pp. 89–146 (in Russian).
[22] J.P. Den Hartog, Forced vibrations with constrained coulomb damping and viscous friction, Transactions of the ASME Advance Papers, New York, USA, 1931, pp. 107–115.
[23] J.E. Ruzicka, T.F. Derby, *Influence of Damping in Vibration Isolation*, The Shock and Vibration Information Center, Washington, DC, 1971.
[24] Y.K. Dange, S.R. Gore, Analysis of a nonlinear vibration isolator with the help of an analog computer, *Indian Journal of Technology* 16 (1978) 282–285.
[25] L. Jiang, D. Stredulinsky, J. Szabo, M.W. Chernuka, Numerical characterization of nonlinear stiffness properties of pre-stressed vibration isolation mounts, *Canadian Acoustics—Acoustique Canadienne* 30 (2002) 70–71.
[26] M.S. Hundal, P.S. Parnes, Response of a base excitation system with Coulomb and viscous friction, *Journal of Sound and Vibration* 64 (1979) 371–378.
[27] S.M. Metwalli, Optimum nonlinear suspension system, *ASME Design Engineering Technical Conference*, Vol. A4, Cincinnati, OH, USA, 1985, 6pp.
[28] T.A. Nayfeh, E. Emaci, A.F. Vakakis, Application of nonlinear localization to the optimization of a vibration isolation system, *American Institute of Aeronautics and Astronautics Journal* 35 (1997) 1378–1386.
[29] X. Yu, S.J. Zhu, S.Y. Liu, Nonlinear normal modes for multi-degree-of-freedom nonlinear vibration isolation system, *Proceedings of the ASME Dynamic Systems and Control Division (Publication) DSC, IMECE2006*, Chicago, IL, USA, 2006, 5pp.
[30] B. Ravindra, A.K. Mallik, Performance of nonlinear vibration isolators under harmonic excitation, *Journal of Sound and Vibration* 170 (1994) 325–337.
[31] G. Popov, S. Sankar, Modeling and analysis of nonlinear orifice type damping in vibration isolators, *Journal of Sound and Vibration* 183 (1995) 751–764.
[32] J.J. Lou, S.J. Zhu, L. He, X. Yu, Application of chaos method to line spectra reduction, *Journal of Sound and Vibration* 286 (2005) 645–652.
[33] Y.P. Xiong, J.T. Xing, W.G. Price, Interactive power flow characteristics of an integrated equipment—nonlinear isolator—traveling flexible ship excited by sea waves, *Journal of Sound and Vibration* 287 (2005) 245–276.
[34] A.M. Ulanov, G.V. Lazutkin, Description of an arbitrary multi-axial loading process for nonlinear vibration isolators, *Journal of Sound and Vibration* 203 (1997) 903–907.
[35] O. Qing, Z. Shi-Jian, S. Yin, A study of chaotic motion on nonlinear vibration-isolation system, *Proceedings of the 18th ASME Biennial Conference on Mechanical Vibration and Noise*, Pittsburgh, PA, USA, September 9–12, Vol. 6C, 2001, pp. 2785–2787.
[36] L. Kari, A nonlinear dynamic stiffness model of a vibration isolator at finite deformation, *Materials Science Forum* 440–441 (2003) 475–480.
[37] L. Kari, On the dynamic stiffness of preloaded vibration isolators in the audible frequency range: modeling and experiments, *Journal of Acoustical Society of America* 113 (2003) 1909–1921.

[38] R.J. Jiang, S.J. Zhu, Vibration isolation and chaotic vibration, *Proceedings of the ASME International Design Engineering Technical Conferences and Computers and Information in Engineering Conference—DETC2005, 18th Biennial Conference on Mechanical Vibration and Noise*, Chicago, IL, Vol. 5C, 2005, pp. 2375–2377.
[39] S. Liu, S. Zhu, X. Yu, J. Lou, Study on chaotic parameter range of nonlinear vibration isolation system, *Proceedings of the 2004 International Symposium on Safety Science and Technology*, Shanghai, China, Part B, Vol. 4, 2004, pp. 2064–2068.
[40] X. Yu, S. Zhu, J. Lou, Bifurcation analysis of nonlinear vibration isolation with hard stiffness by cell mapping, *Proceedings of the ASME Design Engineering Technical Conference on Mechanical Vibration and Noise*, Chicago, IL, USA, Vol. 5B, 2003, pp. 1615–1619.
[41] X. Yu, S.J. Zhu, S. Liu, X. Zeng, Study on performance of nonlinear vibration isolation under chaotic state, *Proceedings of the International Symposium on Safety Science and Technology*, Shanghai, China, Vol. 4, 2004, pp. 1417–1421.
[42] Z. Yi-Feng, T. Jin-Yuan, H. Xu-Hui, Response and transmissibility of strong nonlinear active isolation system, *Journal of Central South University (Science and Technology)* 36 (2005) 496–500.
[43] B. Ravindra, A.K. Mallik, Chaotic response of a harmonically excited mass on an isolator with nonlinear stiffness and damping characteristics, *Journal of Sound and Vibration* 182 (1995) 345–353.
[44] O.A. Pringle, L.M. Waganer, Experimental simulation of nonlinear vibration isolating systems with one and two degrees of freedom (forced nonlinear vibration of Duffing type experimentally simulated with models of isolating systems, obtaining response curves), *ASME Meeting 67Vibr-35*, Boston, MA, USA, March 29–31, 1967, 8pp.
[45] G.J. Efstathiades, C.J.H. Williams, Vibration isolation using nonlinear springs, *International Journal of Mechanical Science* 9 (1967) 27–44.
[46] G.J. Efstathiades, Subharmonic instability and coupled motions in nonlinear vibration isolating suspensions, *Journal of Sound and Vibration* 10 (1969) 81–102.
[47] S. Natsiavas, P. Tratskas, On vibration isolation of mechanical systems with nonlinear foundations, *Journal of Sound and Vibration* 194 (1996) 173–185.
[48] S. Yamamoto, Response analysis of base isolated structure with nonlinearity considering higher harmonic components, *Proceedings of the ASME Pressure Vessels and Piping Division PVP, Seismic Engineering*, Denver, CO, USA, Vol. 256 (Part 2), 1993, pp. 103–110.
[49] Y. Chen, S. Chen, Response and transmissibility of nonlinear isolating systems, *Journal of Vibration and Shock* 17 (1998) 18–22.
[50] R. Kawana, T. Tokoyoda, K. Sato, M. Yoshizawa, T. Sugiure, Passage through resonance in a three-degree-of-freedom vibration isolation system, *Proceedings of the ASME International Design Engineering Technical Conferences and Computers and Information in Engineering Conference—20th Biennial Conference on Mechanical Vibration and Noise*, Long Beach, CA, USA, Vol. 1C, 2005, pp. 1907–1915.
[51] P. Alabuzhev, A. Gritchin, L. Kim, G. Migirenko, V. Chon, P. Stepanov, *Vibration Protecting and Measuring Systems with Quasi-Zero Stiffness*, Hemisphere Publishing Co., Taylor & Francis Group, New York, 1989.
[52] V.P. Roslyakov, N.G. Nakhtigal, Choice of parameters of vibration protecting system with nonlinear characteristics, *Mechanization and Electrification of Agriculture* 10 (1975) 36–37.
[53] A.K. Zuyev, A.A. Nikitin, Vibration protecting mechanism for a riveting hammer, *Proceedings of Dynamics of Vibro-Impact Mechanical Systems*, NETI, Novosibirsk, 1973, pp. 50–52.
[54] P. Alabuzhev, A. Gritchin, P. Stepanov, V.F. Khon, Studies of vibro-protecting systems with stiffness correction, *Physico-Technical Problems of Exploitation of Mineral Resources* 3 (1977) 136–149.
[55] P.T. Stepanov, *Investigation of Vibro-impact Mechanical Systems*, NETI, Novosibirsk, 1979, pp. 67–71.
[56] I.I. Gerner, L.I. Kim, N.V. Mokin, Calculation of nonlinear corrector for vibration isolated suspension, *Proceedings of the Research for Railway Transportation, Nauchnii Institut Zheleznodoro-zhnogo Transporta (NIZhT)*, Novosibirsk No. 156, 1974, pp. 152–159.
[57] A.F. Yashin, L.I. Kim, I.S. Nikiforov, Nonlinear vibrations of systems with an arbitrary polynomial restoring force, *Proceedings of Mechanics of Deformed Bodies and Structural Calculations*, Novosibirsk, NIIZhT, 1975, pp. 136–143.
[58] V.N. Goverdovskiy, B.S. Gyzatullin, V.A. Petrov, Method of vibration isolation for the man-operator of transport-technological machine, Patent 2115570, Russia, 1998.
[59] C.M. Lee, V.N. Goverdovskiy, Alternative vibration protecting systems for men-operators of transport machines: modern level and prospects, *Journal of Sound and Vibration* 249 (2002) 635–647.
[60] C.M. Lee, V.N. Goverdovskiy, S.B. Samoilenko, Prediction of non-chaotic motion of the elastic system with small stiffness, *Journal of Sound and Vibration* 272 (2004) 643–655.
[61] R. Dufour, J. Der Hagopian, M. Pompei, C. Garnier, *Shock and Sine Response of Rigid Structures on Nonlinear Mounts*, Vol. 34, ASME Design Engineering Division, Structural Vibration and Acoustics, Miami, FL, USA, 1991 (pp. 171–176).
[62] M.W. Dobry, J. Brzezinski, Vibro-isolation of pneumatic hammer, *Revue Francaise de Mecanique* 3 (1993) 439–444 (in French).
[63] D.V. Balandin, N.N. Bolotnik, W.D. Piley, Limiting performance analysis of impact isolation systems for injury prevention, *Shock and Vibration Digest* 33 (2001) 453–472.
[64] C. Zhiqing, W.D. Pilkey, Application of wavelets to optimal shock and impact isolation, *Transactions of Nanjing University of Aeronautics and Astronautics* 18 (2001) 1–10.
[65] A.M. Veprik, A. Meromi, A. Leschecz, Novel technique of vibration control for split Sterling crycooler with linear compressor, *Proceedings of SPIE 11th Annual International Symposium on Aerospace/Defense Sensing, Simulation and Controls AeroSense, Orlando, FL, USA, Vol. 3061: Infrared Technology and Applications XXIII*, 1997, p. 640.
[66] V.I. Babitsky, *Theory of Vibro-Impact Systems with Applications*, Springer, Berlin, 1998.

[67] V.I. Babitsky, A.M. Veprik, Universal bumpered vibration isolator for severe environment, *Journal of Sound and Vibration* 218 (1998) 269–292.
[68] G.N. Jazar, A. Narmani, M.F. Golnaraghi, D.A. Swanson, Practical frequency and time optimal design of passive linear vibration isolation mounts, *Journal of Vehicle System Dynamics* 39 (2003) 437–466.
[69] G.N Jazar, R.M. Aagaah, M. Mahinfalah, G. Nazari, Comparison of exact and approximate frequency response of a piecewise linear vibration isolator, *Proceedings of the ASME International Design Engineering Technical Conferences and Computers and Information in Engineering Conference—DETC2005, 20th Biennial Conference on Mechanical Vibration and Noise*, Long Beach, CA, USA, Vol. 1A, 2005, pp. 107–115.
[70] A. Narimani, M.F. Golnaraghi, G.N. Jazar, Frequency response of a piecewise linear vibration isolator, *Journal of Vibration and Control* 10 (2004) 1775–1794.
[71] S. Patrick, G.N. Jazar, Frequency response analysis of piecewise nonlinear vibration isolator, *Proceedings of the ASME International Design Engineering Technical Conferences and Computers and Information in Engineering Conference—DETC2005, 20th Biennial Conference on Mechanical Vibration and Noise*, Long Beach, CA, USA, Vol. 1B, 2005, pp. 917–924.
[72] S. Patrick, G.N. Jazar, Stability analysis of a piecewise nonlinear vibration isolator, *Proceedings of the ASME Design Engineering Division*, Orlando, FL, USA, Vol. 118B(2), 2005, pp. 1115–1123.
[73] M. Mahinfala, M.R. Aagaah, G.N. Jazar, N. Mahmoudian, Frequency response of vibration isolators with saturating spring elements, *Proceedings of the ASME International Design Engineering Technical Conference and Computers and Information in Engineering Conference—DETC2005, V1C, 20th Biennial Conference on Mechanical Vibration and Noise*, Long Beach, CA, USA, 2005, pp. 1845–1854.
[74] S. Deshpande, S. Mehta, G.N. Jazar, Jump avoidance conditions for piecewise linear vibration isolator, *Proceedings of the ASME International Design Engineering Technical Conferences and Computers and Information in Engineering Conference—DETC2005, 20th Biennial Conference on Mechanical Vibration and Noise*, Long Beach, CA, USA, Vol. 1C, 2005, pp. 1955–1962.
[75] S. Deshpande, S. Mehta, G.N. Jazar, Sensitivity of jump avoidance condition of a piecewise linear vibration isolator to dynamical parameters, *Proceedings of the ASME International Design Engineering Technical Conferences and Computers and Information in Engineering Conference—DETC2005, 20th Biennial Conference on Mechanical Vibration and Noise*, Long Beach, CA, USA, Vol. 118(2), 2005, pp. 1108–1113.
[76] J. Orzechowski, M. Murphree, P. Haggerty, Use of nonlinear isolation mounts to reduce vehicle after shake, *Proceedings—National Conference on Noise Control Engineering*, Bellevue, Washington, USA, Vol. 1, 1996, pp. 503–508.
[77] A. Narimani, M.F. Golnaraghi, Parameter optimizing for piecewise linear isolator, *Proceedings of the ASME Applied Mechanics Division 2004*, Anaheim, CA, USA, 2004, Vol. 255, pp. 257–261.
[78] Y. Fujiwara, Y. Murotsu, Optimum design of vibration isolators for random excitations, *Bulletin of the Japan Society of Mechanical Engineers* 17 (1974) 68–72.
[79] C.L. Kirk, Nonlinear random vibration isolators, *Journal of Sound and Vibration* 124 (1988) 157–182.
[80] J. Miao, H. Liu, The analysis of nonlinear random vibration of vehicles, *ASME Biennial Conference on Mechanical Vibration and Noise*, Pittsburgh, PA, USA, Vol. 6C, 2001, pp. 2961–2962.
[81] A. Abramovici, W.E. Althouse, R.W.P. Drever, Y. Gursel, S. Kawamura, F.J. Raab, D. Shoemaker, L. Seivers, R.E. Spero, K.S. Thorne, R.E. Vogt, R. Weiss, S.E. Whitcomb, M.E. Zucker, LIGO: The laser Interferometer gravitational-wave observatory, *Science* 256 (1992) 325.
[82] C. Bradashia, R. Del Fabbro, A. Di Virgilio, A. Giazotto, H. Kautzky, V. Montelatici, D. Passuello, A. Brillet, O. Cregut, P. Hello, C.N. Man, P.T. Manh, A. Marraud, D. Shoemaker, J.Y. Vinet, F. Barone, L. Di Fiore, L. Milano, G. Russo, J.M. Aguirregabiria, H. Bel, J.P. Duruisseau, G. Le Denmat, Ph. Tourrence, M. Capozi, M. Longo, M. Lops, I. Pinto, G. Rotoli, T. Damour, S. Bonazzola, J.A. Marck, Y. Gourghoulon, L. Holloway, F. Fuligni, V. Iafolla, G. Natale, The VIRGO Project: a wide band antenna for gravitational wave detection, *Nuclear Instruments and Methods in Physical Research A* 289 (1990) 518–525.
[83] G. Losurdo, M. Bernardini, S. Braccini, C. Bradaschia, C. Casciano, V. Dattilo, R. De Salvo, A. Di Virgilio, F. Frasconi, A. Gaddi, A. Gennai, A. Giazotto, H.B. Pan, F. Paoletti, A. Pasqualetti, R. Passaquieti, D. Passuello, R. Taddei, Z. Zhang, G. Cella, E. Cuoco, E. D'Ambrosio, F. Fidecaro, S. Gaggero, P. La Penna, S. Mancini, R. Poggiani, A. Vicerè, M. Mazzoni, R. Stanga, L. Holloway, J. Winterflood, An inverted pendulum pre-isolator stage for the VIRGO suspension system, *Review of Scientific Instruments* 70 (1999) 2507–2515.
[84] D.G. Blair, L. Ju, H. Peng, Vibration isolation for gravitational wave detection, *Classical and Quantum Gravity* 10 (1993) 2407–2418.
[85] J. Winterflood, D.G. Blair, A long-period conical pendulum for vibration isolation, *Physics Letters A* 222 (1996) 141–147.
[86] R. DeSalvo, A. Gaddi, G. Gennaro, L. Holloway, G. Losurdo, J. Winterflood, A proposal for a pre-isolator stage for the VIRGO super-attenuator, VIRGO, NTS-096/034, 1996.
[87] M.A. Barton, T. Uchiyama, K. Kuroda, N. Kanda, H. Ishizuka, Two-dimensional X pendulum vibration isolation table, *Review of Scientific Instruments* 70 (1999) 2150–2154.
[88] D.L. Platus, Negative-stiffness-mechanism vibration isolation systems, *Proceedings of SPIE—The International Society for Optical Engineering, Vibration Control in Microelectronics, Optics, and Metrology*, San Jose, CA, USA, Vol. 1619, 1992, pp. 44–54.
[89] D.L. Platus, Negative-stiffness-mechanism vibration isolation systems, *Proceedings of the Optomechanical Engineering and Vibration Control Conference, SPIE—The International Society for Optical Engineering*, Denver, CO, USA, Vol. 3786, 1999, pp. 98–105.
[90] J.Z. Zhang, D. Li, M.J. Chen, S. Dong, An ultra-low frequency parallel connection nonlinear isolator for precision instruments, *Key Engineering Materials* 257–258 (2004) 231–236.
[91] J.Z. Zhang, D.D. Li, D. Shen, C.M. Jun, Study on Euler spring used in ultra-low frequency vertical vibration isolation system, *Journal of Mechanical Strength* 26 (2004) 237–241.

[92] J. Winterflood, High Performance Vibration Isolation for Gravitational Wave Detection, PhD Thesis, Department of Physics, University of Western Australia, Perth, 2001.
[93] C.Y. Lee, C. Zhoa, E.J. Chin, J. Jacob, D. Li, D.G. Blair, Control of pre-isolators for gravitational wave detection, *Classical Quantum Gravity* 21 (2004) S1015–S1022.
[94] P. Barriaga, M. Barton, D.G. Blair, A. Brooks, R. Burman, R. Burston, E.J. Chin, J. Chow, D. Coward, B. Cusack, G. de Vine, J. Degallaix, J.C. Dumas, M. Feat, S. Gras, M. Gray, M. Hamilton, D. Hosken, E. Howell, J.S. Jacob, L. Ju, T.L. Kelly, B.H. Lee, C.Y. Lee, K.T. Lee, A. Lun, D.E. McClelland, K. McKenzie, C. Mow-Lowrry, A. Moylan, D. Mudge, J. Munch, D. Rabeling, D. Reitze, A. Romann, S. Schediwy, S.M. Scott, A. Searle, B.S. Sheard, B.J.J. Slagmolen, P. Veitch, J. Winterflood, A. Woolley, Z. Yan, C. Zhao, Thechnology developments for ACIGA high power test facility for advanced interferometry, *Classical Quantum Gravity* 22 (2005) S199–S208.
[95] M. Pinoli, D.G. Blair, L. Ju, Tests on a low-frequency inverted pendulum system, *Measurement Science and Technology* 4 (1993) 995–999.
[96] P.R. Saulson, The inverted pendulum as a probe of anelasticity, *Review of Scientific Instruments* 65 (1994) 182–191.
[97] D.G. Blair, J.F. Liu, E.F. Moghaddam, L. Ju, Performance of an ultra low-frequency folded pendulum, *Physics Letters A* 193 (1994) 223–226.
[98] J. Liu, L. Ju, D.G. Blair, Vibration isolation performance of an ultra-low frequency folded pendulum resonator, *Physics Letters A* 228 (1997) 243–249.
[99] R. Stebbins, D. Newell, S. Richman, P. Bender, J. Faller, J. Mason, Low-frequency active vibration isolation system, *Proceedings of the SPIE—The International Society for Optical Engineering*, San Diego, CA, USA, Vol. 2264, 1994, pp. 27–37.
[100] J. Liu, J. Winterflood, D.G. Blair, Transfer function of an ultra-low frequency vibration isolation system, *Review of Scientific Instruments* 66 (1994) 3216–3218.
[101] J. Winterflood, Z.B. Zgou, D.G. Blair, Reducing low-frequency residual motion in vibration isolation to the nanometer level, in: S. Meshkov (Ed.), *Third Edoardo Amaldi Conference on Gravitational Waves*, Vol. 523, *American Institute of Physics Conference Proceedings*, 2000, Pasedena, CA, USA, pp. 325–331.
[102] J. Winterflood, Z.B. Zhou, L. Ju, D.G. Blair, Tilt suppression for ultra-low residual motion vibration isolation in gravitational wave detection, *Physics Letters A* 277 (2000) 143–155.
[103] J.M. Ko, Y.Q. Ni, Q.L. Tian, Hysteretic behavior and empirical modeling of a wire-cable vibration isolator, *International Journal of Analytical and Experimental Modal Analysis* 7 (1992) 111–127.
[104] C.W. Wong, Y.Q. Ni, J.M. Ko, Steady-state dynamic response of structures with nonlinear hysteretic isolators, *Modal Analysis: International Journal of Analytical and Experimental Modal Analysis* 8 (1993) 63–78.
[105] G.F. Demetriades, M.C. Constantinou, A.M. Reinhorn, Study of wire rope systems for seismic protection of equipment in buildings, *Engineering Structures* 15 (1993) 321–334.
[106] N. Kanda, M.A. Barton, K. Kuroda, Transfer function of a crossed wire pendulum isolation system, *Review of Scientific Instruments* 65 (1994) 3780–3783.
[107] M.A. Barton, K. Kuroda, Ultra-low frequency oscillator using a pendulum with crossed suspension wires, *Review of Scientific Instruments* 65 (1994) 3775–3779.
[108] M.A. Barton, N. Kanda, K. Kuroda, A low-frequency vibration isolation table using multiple crossed-wire suspensions, *Review of Scientific Instruments* 67 (1996) 3994–3999.
[109] J. Winterflood, G. Losurdo, D.G. Blair, Initial results from a long-period conical pendulum vibration isolator with application for gravitational wave detection, *Physics Letters A* 263 (1999) 9–14.
[110] J.S. Beggs, *Mechanism*, McGraw-Hill, New York, 1955.
[111] F. Garoi, J. Winterflood, L. Ju, J. Jacob, D.G. Blair, Passive vibration isolation using a Roberts linkage, *Review of Scientific Instruments* 74 (2003) 3487–3491.
[112] L. Euler, Methodus Inveniendi Lineas Curves Maximi Minimive Propriete Gaudentes, Additamentum I. De Curvis Elasticis, Lausanne and Geneva, 1774.
[113] A.E.H. Love, *A Treatise on the Mathematical Theory of Elasticity*, Dover Publications, New York, 1927.
[114] E.P. Popov, *Nonlinear Problems of Statics of Thin Bars*, Gostekhizdat, Leningrad, Moskva, 1948 (in Russian).
[115] S.P. Timoshenko, J.M. Gere, *Theory of Elastic Stability*, McGraw-Hill, New York, 1961.
[116] R. Frisch-Fay, *Flexible Bars*, Butterworths, London, 1962.
[117] H. Ziegler, *Principles of Structural Stability*, Blaisdell, 0chusetts, 1968.
[118] J.W. Hutchinson, W.T. Koiter, Post-buckling theory, *ASME Applied Mechanics Reviews* 23 (1970) 1353–1366.
[119] S.S. Antman, The theory of rods, in: C. Truedell, (Ed.), *Encyclopedia of Physics*, Vol. 2 (*Mechanics of Solids II*), Springer, Berlin, 1972.
[120] J.M.T. Thompson, G.W. Hunt, *A General Theory of Elastic Stability*, Wiley, London, 1973.
[121] S.J. Britvec, *The Stability of Elastic Systems*, Pergamon Press, New York, 1973.
[122] B. Budiansky, Theory of buckling and post-buckling behavior of elastic structures, *Advances in Applied Mechanics* 14 (1974) 1–65.
[123] C.L. Dym, *Stability Theory and its Applications to Structural Mechanics*, Noordhoff, Leyden, 1974.
[124] K. Huseyin, *Nonlinear Theory of Elastic Stability*, Noordhoff, Leyden, 1975.
[125] G.J. Simitses, *Elastic Stability of Structures*, Prentice-Hall, Englewood Cliffs, NJ, 1976.
[126] G. Wimpner, *Mechanics of Solids with Applications to Thin Bodies*, Sijthoff and Noordhoff, The Netherlands, 1981.
[127] M. Potier-Ferry, *Buckling and Post-buckling, Lecture Notes in Physics*, Springer, New York, 1987.
[128] X.P. Bažant, L. Cedolin, *Stability of Structures*, Oxford University Press, Oxford, 1991.

[129] R. Schmidt, D.A. Da Deppo, A survey of literature on large deflection of non-shallow arches, bibliography of finite deflections of straight and curved beams, rings, and shallow arches, *The Journal of the Industrial Mathematics Society* 21 (1971) 91–114.
[130] J.F. Wilson, J.M. Snyder, The *elastica* with end-loaded flip-over, *ASME Journal of Applied Mechanics* 55 (1988) 845–848.
[131] J.F. Wilson, U. Mahajan, The mechanics and positioning of highly flexible manipulator limbs, *Journal of Mechanism, Transmission, and Automation Design III* (1989) 232–235.
[132] B.K. Lee, S.J. Wilson, S.J. Oh, Elastica of cantilevered beams with variable cross sections, *International Journal of Nonlinear Mechanics* 28 (1993) 579–589.
[133] V.V. Bolotin, *The Dynamic Stability of Elastic Systems*, Holden-Day, San Francisco, 1964.
[134] V.V. Bolotin, *Random Vibration of Elastic Systems*, Martinus and Nijhoff Publishers, The Netherlands, 1984.
[135] A.H. Nayfeh, D.T. Mook, *Nonlinear Oscillations*, Wiley-Interscience, New York, 1979.
[136] R.A. Ibrahim, *Parametric Random Vibration*, Wiley, New York, 1985 (Second Edition by Dover Publications, New York, 2007).
[137] S. Woinowsky-Kreiger, The effect of an axial force on the vibration of hinged bars, *ASME Journal of Applied Mechanics* 17 (1950) 35–36.
[138] D. Burgreen, Free vibration of a pin-ended column with constant distance between pin ends, *ASME Journal of Applied Mechanics* 18 (1951) 135–139.
[139] W.Y. Tseng, J. Dugundji, Nonlinear vibrations of buckled beam under harmonic excitation, *ASME Journal of Applied Mechanics* 38 (1971) 467–476.
[140] G.B. Min, J.G. Eisley, Nonlinear vibration of buckled beams, *Journal of Sound and Vibration* 71 (1980) 333–346.
[141] S. Boustra, B. Geijselaers, On the resonance frequencies of micro-bridges, *Proceedings of the International Conference on Solid-State Sensors and Actuators*, San Francisco, CA, USA, 1991, pp. 538–542.
[142] A.H. Nayfeh, W. Kreider, T.J. Anderson, Investigation of the natural frequency and mode shapes of buckled beams, *American Institute of Aeronautics and Astronautics Journal* 33 (1995) 1121–1124.
[143] W. Lestari, S. Hanagud, Nonlinear vibration of buckled beams: some exact solutions, *International Journal of Solids and Structures* 38 (2001) 4741–4757.
[144] D. Addessi, W. Lacarbonara, A. Paolone, On the linear normal modes of planar pre-stressed curved beams, *Journal of Sound and Vibration* 284 (2005) 1075–1097.
[145] S.S. Antman, Bifurcation problems for nonlinearly elastic structures, in: P.H. Rabinowitz (Ed.), *Applications of Bifurcation Theory*, Academic Press, New York, 1977.
[146] M. Pignataro, A. Di Carlo, On nonlinear beam models from the point of view of computational post-buckling analysis, *International Journal of Solids and Structures* 18 (1982) 327–347.
[147] H.W. Haslach, Post-buckling behavior of columns with nonlinear constitutive equations, *International Journal of Nonlinear Mechanics* 20 (1985) 51–67.
[148] C.Y. Wang, Post-buckling of a clamped–simply supported elastica, *International Journal of Nonlinear Mechanics* 32 (1997) 1115–1122.
[149] J.S. Jensen, Buckling of an elastic beam with added high-frequency excitation, *International Journal of Nonlinear Mechanics* 35 (2000) 217–227.
[150] M.A. Vaz, D.F.C. Silva, Post-buckling analysis of slender elastic rods subjected to terminal forces, *International Journal of Nonlinear Mechanics* 38 (2003) 483–492.
[151] M.A. Vaz, G.H.W. Mascaro, Post-buckling analysis of slender elastic vertical rods subjected to terminal forces and self-weight, *International Journal of Nonlinear Mechanics* 40 (2005) 1049–1056.
[152] M. Życzkowski, Post-buckling analysis of non-prismatic columns under general behavior of loading, *International Journal of Nonlinear Mechanics* 30 (2005) 445–463.
[153] H. Yabuno, K. Tsumoto, Experimental investigation of a buckled beam under high-frequency excitation, *Archive of Applied Mechanics* 77 (2007) 339–351.
[154] V.N. Chelomei, On the possibility of increasing the stability of elastic systems by using vibration, *Doklady Akademii Nauk SSSR* 110 (1956) 345–347 (in Russian).
[155] V.N. Chelomei, Mechanical paradoxes caused by vibrations, *Soviet Physics Doklady* 28 (1983) 387–390.
[156] J. Winterflood, T.A. Barber, D.G. Blair, Mathematical analysis of an Euler spring vibration isolator, *Physics Letters A* 300 (2002) 131–139.
[157] A.N. Kounadis, J.G. Mallis, Elastica type buckling analysis of bars from nonlinearly elastic material, *International Journal of Nonlinear Mechanics* 22 (1987) 99–107.
[158] A.B. Sotiropoulou, D.E. Panayotounakos, Exact parametric analytic solutions of the elastica ODEs for bars including effects of the transverse deformation, *International Journal of Nonlinear Mechanics* 39 (2004) 1555–1570.
[159] D.G. Blair, F.J. van Kann, A.L. Fairhall, Behavior of a vibration isolator suitable for use in cryogenic or vacuum environments, *Measurement Science and Technology* 2 (1991) 846–850.
[160] L. Ju, D.G. Blair, Low resonant frequency cantilever spring isolator for gravitational wave detectors, *Review of Scientific Instruments* 65 (1994) 3482–3488.
[161] M.V. Plissi, C.I. Torrie, M.E. Husman, N.A. Robertson, K.A. Strain, H. Ward, H. Lück, J. Hough, GEO 600 triple pendulum suspension system: Seismic isolation and control, *Review of Scientific Instruments* 71 (2000) 2539–2545.
[162] G. Ballardin, L. Bracci, S. Braccini, C. Bradaschia, C. Casciano, G. Calamai, R. Cavalieri, R. Cecchi, G. Cella, E. Cuoco, E. D'Ambrosio, V. Dattilo, A. Di Virgilio, L. Fabbroni, F. Fidecaro, F. Frasconi, A. Gaddi, A. Gennai, A. Giazotto, G. Losurdo, L. Holloway, P. La Penna, F. Lelli, E. Majorana, M. Mazzoni, F. Paoletti, M. Pasotti, A. Pasqualetti, R. Passaquieti, D. Passuello,

R. Poggiani, P. Puppo, F. Rafaelli, P. Rapagnani, F. Ricci, R. Ruggi, R. Stanga, R. Taddei, F. Vetrano, A. Vicerè, Z. Zhang, Measurement of the VIGRO super-attenuator performance for seismic noise suppression, *Review of Scientific Instruments* 72 (2001) 3643–3652.

[163] R. Takahashi, F. Kuwahara, E. Majorana, M.A. Barton, T. Uchiyama, K. Kuroda, A. Araya, K. Arai, A. Takamori, M. Ando, K. Tsubono, M. Fukushima, Y. Saito, Vacuum-compatible vibration isolation stack for an interferometric gravitational wave detector TAMA300, *Review of Scientific Instrument* 73 (2002) 2428–2433.

[164] R. Takahashi, K. Arai, and the TAMA Collaboration, Improvement of the vibration isolation system for TAMA300, *Classical and Quantum Gravity* 19 (2002) 1599–1604.

[165] L. Ju, D.G. Blair, H. Peng, F. van Kann, High dynamic range measurements of an all metal isolator using a sapphire transducer, *Measurement Science and Technology* 3 (1992) 463–470.

[166] M. Beccaria, M. Bernardini, E. Bougleux, S. Braccini, C. Bradaschia, C. Casciano, G. Cella, E. Cuoco, E. D'Ambrosio, G. De Carolis, R. Del Fabbro, R. De Salvo, A. Di Virgilio, I. Ferrante, F. Fidecaro, R. Flaminio, A. Gaddi, A. Gennai, G. Gennaro, A. Giazotto, L. Holoway, P. La Penna, G. Losurdo, S. Malik, S. Mancini, J. Nicolas, F. Palla, H.B. Pan, F. Paoletti, A. Pasqualetti, D. Passuello, R. Poggiani, P. Popolizio, F. Rafaelli, A. Vicere, F. Waharte, Z. Zhang, Extending the VIRGO gravitational wave detection band down to a few Hz: metal blade springs and magnetic anti-springs, *Nuclear Instruments and Methods in Physics Research A* 394 (1997) 397–408.

[167] L. Ju, D.G. Blair, J. Winterflood, Long-term length stability and search for excess noise in multi-stage cantilever spring vibration isolators, *Physics Letters A* 266 (2000) 219–227.

[168] J. Winterflood, D.G. Blair, A long-period vertical vibration isolator for gravitational wave detection, *Physics Letters A* 243 (1998) 1–6.

[169] T. Mizuno, Proposal of a vibration isolation system using zero-power magnetic suspension, *Proceedings of Asia-Pacific Vibration Conference*, Seoul, Korea, Vol. 2, 2001, pp. 423–427.

[170] T. Mizuno, Vibration isolation using zero-power magnetic suspension, *Proceedings of the 15th World Congress of the International Federation of Automatic Control (IFAC)*, Barcelona, Spain, 2002, p. 955.

[171] T. Mizuno, R. Yshitomi, Vibration isolation system using zero-power magnetic suspension, *Transactions of Japan Society of Mechanical Engineers, Series C* 68 (673) (2002) 2599–2604 (First Report, Principles and basic experiments) (in Japanese).

[172] T. Mizuno, T. Toumiya, M. Takasaki, Vibration isolation system using negative stiffness, *Japan Society of Mechanical Engineers International Journal, Series C* 46 (2003) 807–812.

[173] A. Bertolini, G. Cella, R. DeSalvo, V. Sannibale, Seismic noise filters, vertical resonant frequency reduction with geometric anti-springs: a feasibility study, *Nuclear Instruments and Methods in Physics Research A* 435 (1999) 475–483.

[174] A. Bertolini, G. Cella, W. Chenyang, R. DeSalvo, J. Kovalik, S. Márka, V. Sannibale, A. Takamori, H. Tariq, N. Viboud, Recent progress on the R&D program of seismic attenuation system (SAS) proposed for the advanced gravitational wave detector, LIGO II, *Nuclear Instruments and Methods in Physics Research A* 461 (2001) 300–303.

[175] G. Cella, R. DeSalvo, V. Sannibale, H. Tariq, N. Viboud, A. Takamori, Seismic attenuation performance of the first prototype of a geometric anti-spring filter, *Nuclear Instruments and Methods in Physics Research A* 487 (2002) 652–660.

[176] C. Wang, H. Tariq, R. DeSalvo, Y. Iida, A. Marka, Y. Nishi, V. Sannibale, A. Takamori, Constant force actuator for gravitational wave detector's seismic attenuation systems, *Nuclear Instruments and Methods in Physics Research A* 489 (2002) 563–569.

[177] G. Cella, V. Sannibale, R. DeSalvo, S. Márka, A. Takamori, Monolithic geometric anti-spring blades, *Nuclear Instruments and Methods in Physics Research A* 540 (2005) 502–519.

[178] R. DeSalvo, Sz. Márka, K. Numata, V. Sannibale, A. Takamori, H. Tariq, E.J. Ugas, T. Yoda, Y. Aso, A. Bertolini, Study of quality factor and hysteresis associated with the state-of-the-art passive seismic isolation system for Gravitational Wave Interferometric Detectors, *Nuclear Instruments and Methods in Physics Research A* 538 (2005) 526–537.

[179] T.E. Shoup, Shock and vibration isolation using a nonlinear elastic suspension, *American Institute of Aeronautics and Astronautics (AIAA) Journal* 9 (1971) 1643–1645.

[180] T.E. Shoup, G.E. Simmonds, An adjustable spring rate suspension system, *American Institute of Aeronautics and Astronautics (AIAA) Journal* 15 (1977) 865–866.

[181] E.J. Chin, K.T. Lee, J. Winterflood, J. Jacob, D.G. Blair, L. Ju, Techniques for reducing the resonant frequency of Euler spring vibration isolators, *Classical and Quantum Gravity* 31 (2004) S959–S963.

[182] E.J. Chin, K.T. Lee, J. Winterflood, L. Ju, D.G. Blair, Low frequency vertical geometric anti-spring vibration isolators, *Physics Letters A* 336 (2005) 97–105.

[183] J.C. Dumas, K.T. Lee, J. Winterflood, L. Ju, D.G. Blair, J. Jacob, Testing of a multi-stage low-frequency isolator using Euler spring and self-damped pendulum, *Classical Quantum Gravity* 21 (2004) S965–S971.

[184] L.N. Virgin, R.B. Davis, Vibration isolation using buckled structures, *Journal of Sound and Structures* 260 (2003) 965–973.

[185] R.H. Plaut, J.E. Sidbury, L.N. Virgin, Analysis of buckled and pre-bent fixed-end columns used as vibration isolators, *Journal of Sound and Vibration* 283 (2005) 1216–1228.

[186] R.H. Plaut, L.A. Alloway, L.N. Virgin, Nonlinear oscillations of a buckled mechanism used as a vibration isolator, in: G. Rega, F. Vestroni, (Eds.), *Proceedings of the IUTAM Symposium on Chaotic Dynamics and Control of Systems and Processes in Mechanics*, Springer, The Netherlands, 2005, pp. 241–250.

[187] D. Gospodnetic, Deflection curve of a simply supported beam, *ASME Journal of Applied Mechanics* 26 (1959) 675–676.

[188] D. Kisliakov, Dynamic analysis of a multiple-supported pressure pipeline subjected to both axial and vertical seismic excitation components, *Proceedings of the Third International Conference on Seismology and Earthquake Engineering*, Iran, Vol. II, 1999, pp. 881–898.

[189] D. Kisliakov, Axial earthquake-induced vibrations of a pressure pipeline on frictional support columns, *Proceedings of the Anniversary Scientific Conference on 50 years Faculty of Hydraulic Engineering at UACEG*, Sofia, Vol. III, 1999.
[190] R. Somnay, R.A. Ibrahim, R.C. Banasik, Nonlinear dynamics of a sliding beam on two supports and its efficacy as a non-traditional isolator, *Journal of Vibration and Control* 12 (2006) 685–712.
[191] J.B. Roberts, A stochastic theory for nonlinear ship rolling in irregular seas, *Journal of Ship Research* 26 (1982) 229–238.
[192] N.K. Moshchuk, R.A. Ibrahim, R.Z. Khasminskii, P. Chow, Asymptotic expansion of ship capsizing in random sea waves, part I: first-order approximation, *International Journal of Nonlinear Mechanics* 30 (1995) 727–740.
[193] R.A. Ibrahim, R.J. Somnay, Nonlinear dynamic analysis of an elastic beam isolator sliding on frictional supports, *Journal of Sound and Vibration* 308 (2007) 735–757.
[194] J.M. Kelly, A seismic base isolation: review and bibliography, *Soil Dynamics and Earthquake Engineering* 5 (1986) 202–216.
[195] J.M. Kelly, *Earthquake-Resistant Design with Rubber*, second ed., Springer, Berlin, 1997.
[196] N. Mostaghel, J. Tanbakuchi, Response of sliding structures to earthquake support motion, *Earthquake Engineering and Structural Dynamics* 11 (1983) 729–748.
[197] V.A. Zayas, S.S. Low, S.A. Mahin, The FPS earthquake resisting system experimental report, Technical Report UCB/EERC-87/01, Earthquake Engineering Research Center, University of California, Berkeley, CA, 1987.
[198] S. Kawamura, K. Kitazawa, M. Hisano, I. Nagashima, Study of a sliding-type base-isolation system: System composition and element properties, *Proceedings of the Ninth World Conference on Earthquake Engineering*, Tokyo–Kyoto, Vol. V, 1988, pp. 735–740.
[199] I.G. Buckle, R.L. Mayes, Seismic isolation: history, application and performance—a world overview, *Earthquake Spectra* 6 (1990) 161–202.
[200] Y.B. Yang, T.Y. Lee, I.C. Tsai, Response of multi-degree-of-freedom structures with sliding supports, *Earthquake Engineering and Structural Dynamics* 19 (1990) 739–752.
[201] G. Juhn, G.D. Manolis, M.C. Constantinou, Stochastic response of secondary systems in base-isolated structures, *Probabilistic Engineering Mechanics* 7 (1992) 91–102.
[202] T. Lin, C. Hone, Base isolation by free rolling rods under basement, *Earthquake Engineering and Structural Dynamics* 22 (1993) 261–273.
[203] R.S. Jangid, Seismic response of structures isolated by free rolling rods, *European Earthquake Engineering* 3 (1995) 3–11.
[204] R.S. Jangid, Stochastic seismic response of structures isolated by rolling rods, *Engineering Structures* 22 (2000) 937–946.
[205] R.S. Jangid, Y.B. Londhe, Effectiveness of elliptical rolling rods for base-isolation, *ASCE Journal of Structural Engineering* 124 (1998) 469–472.
[206] R.I. Skinnner, J.M. Kelly, A.J. Heine, Hysteresis dampers for earthquake-resistant structures, *Earthquake Engineering & Structural Dynamics* 3 (1975) 287–296.
[207] A.S. Pall, C. Marsh, Response of friction damped braced frames, *ASCE Journal of the Structural Design* 108 ST9 (1982) 1313–1323.
[208] N.R. Vaidya, Base isolation in the design and construction of power plant structures, *Proceedings of the ASCE Conference on Recent Advances in Structural Dynamics*, Seattle, WA, USA, 1986, pp. 1–15.
[209] A. Filiatrault, S. Cherry, Seismic design spectra for friction damped structures, *ASCE Journal of Structural Engineering* 116 (1990) 1334–1355.
[210] A.S. Whittaker, V.V. Bertero, C.L. Thompson, L.J. Alonso, Seismic testing of steel plate energy dissipation devices, *Earthquake Spectra* 7 (1991) 563–604.
[211] J.H. Yu, H.W. Liu, Mechanical behavior of base isolators and dynamical response of isolated buildings, *Computational Mechanics*, Balkema, Rotterdam, 1991, pp. 287–293.
[212] M.C. Constantinou, M.D. Symans, Experimental and analytical investigation of seismic response of structures with supplemental fluid viscous dampers, Report NCEER-92-0032, National Center for Earthquake Engineering Research, State University of New York, NY, 1992.
[213] R.I. Skinner, H.W. Robinson, H.C. McVerry, *An Introduction to Seismic Isolation*, Wiley, Chichester, England, 1993.
[214] K. Kasai, Y. Fu, A. Watanabe, Passive control systems for seismic damage mitigation, *ASCE Journal of Structural Engineering* 124 (1998) 501–512.
[215] F. Naeim, J.M. Kelly, *Design of Seismic Isolated Structures: From Theory to Practice*, Wiley, New York, 1999.
[216] S.K. Deb, Seismic base isolation—an overview, *Current Science* 87 (2004) 1426–1430.
[217] R.E. Klein, C. Cusano, J. Stukel, Investigation of a method to stabilize wind induced oscillation in large structures, in: *ASME Winter Annual Meeting*, 72-WA/AUT-H, New York, USA, 1992.
[218] B. Delfino, G.B. Denegri, P. Pinceti, Dynamic impact of wind generation on an isolated power system, *Proceedings of the IEEE Melecon'85: Mediterranean Electrochemical Conference,* Vol. 4: *Solar Energy*, Madrid, Spain, 1985, pp. 213–217.
[219] J.E. Luco, H.L. Wong, Control of the seismic response of adjacent elastic structures, *Proceedings of the Fifth World Conference on Structural Control TA2-21-30*, Los Angeles, USA, 1994.
[220] J.E. Luco, C.P. De Barros, Optimal damping between two adjacent elastic structures, *Earthquake Engineering and Structural Dynamics* 27 (1998) 649–659.
[221] Z. Zhang, Y.L. Xu, Dynamic characteristics and seismic response of adjacent buildings linked by discrete dampers, *Earthquake Engineering & Structural Dynamics* 28 (1999) 1163–1185.
[222] Z. Yang, Y.L. Xu, X.L. Lu, Experimental seismic study of adjacent buildings with fluid dampers, *ASCE Journal of Structural Engineering* 129 (1999) 197–205.
[223] Y.L. Xu, Q. He, J.M. Ko, Dynamic response of dynamic-connected adjacent buildings under earthquake excitation, *Engineering Structures* 21 (1999) 135–148.

[224] Y. Kobori, T. Yamada, Y. Takenake, Y. Maeda, Effect of dynamic tuned connector on reduction of seismic response-application to adjacent office buildings, *Proceedings of the Ninth World Conference on Earthquake Engineering*, Tokyo–Kyoto, Japan, Vol. V, 1988, pp. 773–778.
[225] M. Takeda, Y. Ohkawa, T. Komura, Y. Akutsi, T. Hirotani, Probabilistic evaluation of seismic isolation effect with respect to sitting of a fusion reactor facility, *Proceedings of the ASME Pressure Vessels and Piping Division PVP, Seismic, Shock, and Vibration Isolation*, Honolulu, HI, USA, Vol. 319, 1995, pp. 317–322.
[226] R. Gueraud, J.P. Moel-Leroux, M. Livolant, A.P. Michalopoulos, Seismic isolation using sliding elastomer bearing pads, *Journal of Nuclear Engineering Design* 84 (1985) 363–377.
[227] N. Mostaghel, M. Khodaverdian, Response of structures supported on resilient-friction base isolator (R-FBI), *Earthquake Engineering and Structural Dynamics* 15 (1987) 379–390.
[228] L. Su, G. Ahmadi, I.G.A. Tadjbakhsh, A comparative study of base isolation systems, *ASCE Journal of Engineering Mechanics Division* 115 (1990) 1976–1992.
[229] A.G. Hernried, K.M. Lei, Parametric studies on the response of equipment in resilient-friction base isolated structures subjected to ground motion, *Engineering Structures* 15 (1993) 349–357.
[230] R.S. Jangid, T.K. Datta, Performance of base isolation systems for asymmetric building subject to random excitation, *Engineering Structures* 17 (1995) 443–454.
[231] R.S. Jangid, Optimum damping in a nonlinear base isolation system, *Journal of Sound and Vibration* 189 (1996) 477–487.
[232] M. Kikuchi, I.D. Aiken, Analytical hysteresis model for elastomeric seismic isolation bearings, *Earthquake Engineering & Structural Dynamics* 26 (1997) 215–231.
[233] T.T. Soong, State-of-the-art review: active control in civil engineering, *Engineering Structures* 10 (1988) 74–84.
[234] K. Fujita, T. Kimura, Y. Ohe, Vibration characteristics and seismic responses of mechanical structures with hysteresis elements, *ASME Journal of Pressure Vessel Technology* 126 (2004) 98–104.
[235] M. Kurihara, K. Nashimoto, M. Shigeta, Y. Tachi, Study on response during large deformation in a seismic isolation system of nuclear island buildings, *Japan Society of Mechanical Engineers International Journal, Vibration, Control Engineering, Engineering for Industry* 33 (1990) 404–411.
[236] H.M.R. Suy, R.H.B. Fey, F.M.B. Galanti, H. Nimeijer, Nonlinear dynamic analysis of a structure with a friction-based seismic base isolation system, *Nonlinear Dynamics* 50 (2007) 523–538.
[237] R. Villaverde, Roof isolation system to reduce the seismic response of buildings: a preliminary assessment, *Earthquake Spectra* 14 (1998) 521–532.
[238] R. Villaverde, G. Mosqueda, A seismic roof isolation system: analytic and shake table studies, *Earthquake Engineering and Structural Dynamics* 28 (1999) 217–234.
[239] A.X. Guo, Y.L. Xu, B. Wu, Seismic reliability analysis of hysteretic structure with viscoelastic dampers, *Engineering Structures* 24 (2002) 373–383.
[240] C. Alhan, H. Gavin, Reliability of base isolation for the protection of critical equipment from earthquake hazards, *Engineering Structures* 27 (2005) 1435–1449.
[241] R.A. Ibrahim, Friction-induced vibration, chatter, squeal, and chaos, part I: mechanics of contact and friction, and part II: dynamics and modeling, *ASME Applied Mechanics Review* 47 (1994) (209–226, 227–243).
[242] R.A. Ibrahim, C.L. Pettit, uncertainties and dynamic problems of bolted joints and other fasteners, *Journal of Sound and Vibration* 279 (2005) 857–936.
[243] Y.Q. Ni., J.M. Ko, C.W. Wong, Identification of nonlinear hysteretic isolators from periodic vibration tests, *Journal of Sound and Vibration* 217 (1997) 737–756.
[244] A. Pirrotta, R.A. Ibrahim, Experimental investigation of friction-base isolation, *Probabilistic Engineering Mechanics* 12 (1997) 125–136.
[245] S. Nagarajaiah, A.M. Reinhorn, M.C. Constantinou, Nonlinear dynamic analysis of three-dimensional base isolated structures (3D-BASIS), Report No. NCEER-89-0019, National Center for Earthquake Engineering Research, State University of New York, Buffalo, NY, USA, 1989.
[246] S. Nagarajaiah, A.M. Reinhorn, M.C. Constantinou, Nonlinear dynamic analysis of 3-D-base-isolated structures, *ASCE Journal of Engineering Structures* 117 (1990) 2035–2054.
[247] S. Nagarajaiah, A.M. Reinhorn, M.C. Constantinou, 3D-BASIS: Nonlinear dynamic of three-dimensional base isolated structures: part II, Report No. NCEER-91-0005, National Center for Earthquake Engineering Research, State University of New York, Buffalo, NY, USA, 1991.
[248] G.B. Warburton, *Reduction of Vibrations: The Third Mallet– Milne Lecture*, Wiley, New York, 1992.
[249] R.S. Jangid, T.K. Datta, Seismic behavior of base isolated buildings—a state-of-the-art review, *Journal of Structures and Buildings* 110 (1995) 186–203.
[250] S.L. Dimova, K. Meskouris, W.B. Krätzig, Numerical technique for dynamic analysis of structures with friction devices, *Earthquake Engineering and Structural Dynamics* 24 (1995) 881–891.
[251] M.C. Constantinou, A. Papageorgiou, A stochastic response of practical sliding isolation system, *Probabilistic Engineering Mechanics* 5 (1990) 27–34.
[252] L. Su, G. Ahmadi, Response of frictional base isolation systems to horizontal–vertical random earthquake excitations, *Probabilistic Engineering Mechanics* 3 (1990) 12–21.
[253] F.G. Fan, G. Ahmadi, Random response analysis of frictional base isolation system, *ASCE Journal of Engineering Mechanics Division* 116 (1990) 1881–1901.

[254] F.G. Fan, G. Ahmadi, Multi-storey base-isolated buildings under a harmonic ground motion—part II: a comparison of various systems, *Nuclear Engineering and Design* 123 (1990) 14–26.
[255] M. De Angelis, V. Ciampu, Effectiveness of dissipative connections on improving earthquake response of adjacent buildings, in: G. Duma (Ed.), *Proceedings of the 10th European Conference on Earthquake Engineering*, Balkema, Rotterdam, 1995, pp. 1891–1896.
[256] M.D. Pandey, Stochastic response of structures with passive seismic control, *Canadian Journal of Civil Engineers* 22 (1995) 970–980.
[257] I. Caliò, M. Marletta, F. Vinciprova, Seismic response of multi-storey buildings base-isolated by friction devices with restoring properties, *Computers and Structures* 81 (2003) 2589–2599.
[258] W.K. Hong, H.C. Kim, Performance of a multi-storey structure with a resilient-friction base isolation system, *Computers and Structures* 82 (2004) 2271–2283.
[259] C.A. Kircher, B. Lashkari, R. Mayes, T. Kelly, *Evaluation of Nonlinear Response in Seismically Isolated Buildings*, ASME Pressure Vessels and Piping Division Publication 147, 1988, pp. 71–81.
[260] B.M. Shahrooz, J.P. Moehle, Seismic response and design setback buildings, *ASCE Journal of Structural Engineering* 16 (1990) 1423–1439.
[261] C.L. Ng, Y.L. Xu, Seismic response control of a building complex utilizing passive friction damper: experimental investigation, *Earthquake Engineering and Structural Dynamics* 35 (2006) 657–677.
[262] Y. Chen, G. Ahmadi, Wind effects on base-isolated structure, *ASCE Journal of Engineering Mechanics* 118 (1992) 1708–1727.
[263] R.S. Jangid, Seismic response of asymmetric base isolated structure, *Computers and Structures* 60 (1996) 261–267.
[264] Y. Chen, G. Ahmadi, Stochastic earthquake response of secondary systems in base-isolated structures, *Earthquake Engineering and Structural Dynamics* 21 (1992) 1039–1057.
[265] R.S. Jangid, Optimum frictional elements in sliding isolation systems, *Computers and Structures* 76 (2000) 651–661.
[266] S.L. Dimova, Seismic protection of frame structures by friction devices with restrictors, *Proceedings of the 11th European Conference on Earthquake Engineering (ECEE)*, Belkema, Rotterdam, 1998 (on CD).
[267] K. Hirata, T. Somaki, Fragility estimation of an isolated FBR structure considering the ultimate state of rubber bearings, *Nuclear Engineering Design* 147 (1994) 183–196.
[268] S.L. Dimova, K. Hirata, Simplified seismic fragility analysis of structures with two types of friction devices, *Earthquake Engineering & Structural Dynamics* 29 (2000) 1153–1175.
[269] S.L. Dimova, K. Hirata, Simplified method of fragility analysis of structures with non-traditional seismic protection, *Proceedings of the 12th World Conference on Earthquake Engineering (WCEE)*, New Zealand, Paper No. 0550, 2000.
[270] S.L. Dimova, A. Elenas, Seismic intensity parameters for fragility analysis of structures with energy dissipating devices, *Structural Safety* 24 (2002) 1–28.
[271] T.F. FitzGerald, T. Anagnos, M. Goodson, T. Zsutty, Slotted bolted connections in a seismic design for concentrically braced connections, *Earthquake Spectra* 5 (1989) 383–391.
[272] S.L. Dimova, L. Tzenov, Analysis of a system of special seismic protection to real strong ground motion, *Proceedings of the Ninth European Conference on Earthquake Engineering (ECEE)*, Moscow, Vol. 7-B, 1990, pp. 50–56.
[273] C.E. Grigorian, T.S. Yang, E.P. Popov, Slotted bolted connections for energy dissipation, *Earthquake Spectra* 9 (1993) 491–504.
[274] I. Tadjbakhsh, B.C. Lin, Displacement-proportional friction (DPF) in base isolation, *Earthquake Engineering and Structural Dynamics* 15 (1987) 799–813.
[275] M.Q. Feng, M. Shinozuka, Friction controllable bearings for sliding base isolation systems, National Institute of Standards and Technology (NIST) Special Publication, Gaithersburg, MD, USA, Vol. 843, 1992, pp. 189–198.
[276] M.Q. Feng, M. Shinozuka, S. Fujii, Friction controllable sliding isolation system, *ASCE Journal of Engineering Mechanics* 119 (1993) 1845–1964.
[277] D.J. Dowdell, S. Cherry, Structural control using semi-active friction dampers, *Proceedings of the First World Conference on Structural Control*, Los Angeles, CA, USA, Vol. FA1, 1994, pp. 59–68.
[278] C. Alhan, H. Gavin, A parametric study of linear and nonlinear passively damped seismic isolation systems for buildings, *Engineering Structures* 26 (2004) 485–497.
[279] A. Filiatrault, S. Cherry, Comparative performance of friction damped systems and base isolation systems for earthquake retrofit and a seismic design, *Earthquake Engineering and Structural Dynamics* 16 (1988) 389–416.
[280] U.E. Dorka, G.A. Conversano, Seismic retrofit of Allstate Building, *Report of the IABSE Symposium*, San Francisco, CA, 1995, pp. 145–150.
[281] H.J. Pradlwarter, G.I. Schueller, U. Dorka, Reliability of MDOF-systems with hysteretic devices, *Engineering Structures* 20 (1998) 685–691.
[282] H.W. Shenton, E.S. Holloway, Effect of stiffness variability on the response of isolated structures, *Earthquake Engineering and Structural Dynamics* 29 (2000) 19–36.
[283] D.H. Turkington, A.J. Carr, N. Cooke, P.J. Moss, Design methods for bridges on lead rubber bearings, *ASCE Journal of Structural Engineering* 115 (1989) 3017–3030.
[284] A. Greiner, Seismic protection of bridges by the viscoelastic technique, *Proceedings of the Third World Congress on Joints and Bearings*, Toronto, Canada, 1991, pp. 1205–1223.
[285] G. Bondonet, A. Filiatrault, Frictional response of PTFE sliding bearings at high frequencies, *ASCE Journal of Bridge Engineering* 2 (1997) 139–148.
[286] M.T.A. Chaudhary, Evaluation of Seismic Performance of Base Isolation of Bridges Based on Earthquake Records, PhD Dissertation, University of Tokyo, Department of Civil Engineering, Japan, 1999.

[287] M.T.A. Chaudhary, M. Abe, Y. Fujino, J. Yoshida, System identification of two base-isolated bridges using seismic records, *Journal of Structural Engineering* 126 (2000) 1187–1195.
[288] M.T.A. Chaudhary, M. Abe, Y. Fujino, Performance evaluation of base-isolated Yama-age bridge with high damping rubber bearings using recorded seismic data, *Engineering Structures* 23 (2001) 902–910.
[289] R.S. Jangid, Seismic response of isolated bridges, *ASCE Journal of Bridge Engineering* 9 (2004) 156–166.
[290] R.S. Jangid, Equivalent linear stochastic seismic response of isolated bridges, *Journal of Sound and Vibration* 309 (2008) 805–822.
[291] R. Boroschek, M. Moroni, M. Sarrazin, Dynamic characteristics of a long span seismic isolated bridge, *Engineering Structures* 25 (2003) 1479–1490.
[292] V.M. Daza, M. Moroni, J.M. Roesset, M. Sarrazin, Seismic behavior of a bridge with base isolation, *Proceedings of the Fourth Seismic Conference and Workshop on Bridges and Highways*, University of Illinois at Urbana-Champaign, USA, 2004.
[293] W. Dai, M.O. Moroni, J.M. Roesset, M. Sarrazin, Effect of isolation pads and their stiffness on the dynamic characteristics of bridges, *Engineering Structures* 28 (2006) 1298–1306.
[294] E. Delis, C. Tokas, M. Madani, K. Thompson, Analytical studies for seismic isolation in highway bridges, *Proceedings of Structures Congress*, Portland, OR, USA, Vol. 2, 1997, pp.1471–1478.
[295] D.J. Dowdell, S. Cherry, Optimal seismic response control of friction damped structures, in: G. Duma (Ed.), *Proceedings of the 10th European Conference on Earthquake Engineering (ECEE)*, Balkema, Rotterdam, 1995, pp. 2051–2056.
[296] R. Antonucci, R. Giacchetti, G. Di Matteo, Design parameters optimization for R.C. structures incorporating energy dissipation bracings, *Proceedings of the EERC–CURE Symposium in Honor of V.V. Bertro*, Vol. EERC-97/05, University of California, Berkeley, 1997, pp. 211–215.
[297] R.M. Mutobe, T.R. Cooper, Nonlinear analysis of a large bridge with isolation bearings, *Computers and Structures* 72 (1999) 279–292.
[298] I. Savage, J.C. Eddy, G.I. Orsolini, Seismic analysis and base isolation retrofit design of a steel truss vertical lift bridge, *Computers and Structures* 72 (1999) 317–327.
[299] T.J. Ingham, Analysis of the Million Dollar Bridge for seismic retrofit, *Computers and Structures* 81 (2003) 673–679.
[300] M. Shinozuka, M.Q. Feng, J.M. Kim, F. Nagashima, H.K. Kim, Mitigation of seismic pounding effect on bridges using dynamic restrainers, *Proceedings of the SPIE—The International Society for Optical Engineering, Smart Structures and Materials: Damping and Isolation*, Newport Beach, CA, USA, Vol. 3989, 2000, pp. 377–387.
[301] J.S. Hwang, L.H. Sheng, Equivalent elastic seismic analysis of base-isolated bridges with lead–rubber bearings, *Engineering Structures* 16 (1994) 201–209.
[302] J.S. Hwang, Evaluation of equivalent linear analysis methods of bridge isolation, *ASCE Journal of Structural Engineering* 122 (1996) 972–976.
[303] J.S. Hwang, J.M. Chiou, An equivalent linear model of lead–rubber seismic isolation bearings, *Engineering Structures* 18 (1996) 528–536.
[304] C.J. Younis, J.G. Tadjbakhsh, Response of sliding rigid structure to base excitation, *ASCE Journal of Engineering Mechanics* 110 (1984) 417–432.
[305] R.S. Jangid, J.M. Kelly, Torsional displacements in base-isolated buildings, *Earthquake Spectra* 16 (2000) 443–454.
[306] V.A. Matsagar, R.S. Jangid, Influence of isolator characteristics on the response of base-isolated structures, *Engineering Structures* 26 (2004) 1735–1749.
[307] R.L. Mayes, Seismic isolation of bridges in the USA, *Proceedings of the Third US–Japan Workshop on Earthquake Protective Systems for Bridges, Berkeley, CA, Report NCEER-94-0009*, National Center for Earthquake Engineering Research, State University of New York, Buffalo, NY, 1994.
[308] T.T. Soong, M.C. Constantinou (Eds.), *Passive and Active Structural Vibration Control in Civil Engineering*, Verlag, New York, 1994.
[309] M.C. Constantinou, A. Kartoum, A.M. Reinhorn, P. Bradford, Experimental and theoretical study of a sliding isolation system for bridges, Technical Report MCEER-91-0027, State University of New York at Buffalo, 1991.
[310] R. Medeot, The evolution of seismic devices for bridges in Italy', *Third World Congress on Joint Sealing and Bearing Systems for Concrete Structures*, Vol. 2, Toronto, Canada, 1991, pp. 1295–1320.
[311] P. Tsopelas, M.C. Constantinou, NCEER—Taisei Corporation research program on sliding seismic isolation systems for bridges—experimental and analytical study of a system consisting of lubricated PTFE sliding bearing and mild steel dampers, Report NCEER-94-0022, National Center for Earthquake Engineering Research, State University of New York, Buffalo, NY, 1994.
[312] P. Tsopelas, M.C. Constantinou, Study of elasto-plastic bridge seismic isolation systems, *ASCE Journal of Structural Engineering* 123 (1997) 489–498.
[313] P. Tsopelas, M.C. Constantinou, Y.S. Kim, S. Okamoto, Experimental study of FPS system in bridge seismic isolation, *Earthquake Engineering and Structural Dynamics* 25 (1996) 65–78.
[314] K. Kawashima, S. Unjoh, Menshin design of highway bridges in Japan, *Proceedings of the Third US–Japan Workshop on Earthquake Protective Systems for Bridges*, Berkeley, CA, Report NCEER-94-0009, National Center for Earthquake Engineering Research, State University of New York, Buffalo, NY, 1994.
[315] P. Tsopelas, S. Okamoto, M.C. Constantinou, D. Ozaki, S. Fujii, NCEER-Taisei Corporation research program on sliding seismic isolation systems for bridges—experimental and analytical study of a system consisting of sliding bearings, rubber restoring force devices and fluid dampers, Report NCEER-94-0002, National Center for Earthquake Engineering Research, State University of New York, Buffalo, NY, 1994.
[316] G. Warn, Performance Estimates in Seismically Isolated Bridge Structures, MS Thesis, University at Buffalo, NY, 2003.

[317] G.P. Warn, A.S. Whittaker, Performance estimates in seismically isolated bridge structures, *Engineering Structures* 26 (2004) 1261–1278.
[318] M.T.A. Chaudhary, M. Abe, Y. Fujino, Role of structural details in altering the expected seismic response of base-isolated bridges, *Mechanical Systems and Signal Processing* 16 (2002) 413–428.
[319] M.K. Kim, Y.M. Lim, S.Y. Cho, K.H. Cho, K.W. Lee, Seismic analysis of base-isolated liquid storage tanks using the BE–FE–BE coupling technique, *Soil Dynamics and Earthquake Engineering* 22 (2002) 1151–1158.
[320] R.A. Ibrahim, *Liquid Sloshing Dynamics: Theory and Applications*, Cambridge University Press, Cambridge, 2005.
[321] M.S. Chalhoub, J.M. Kelly, Shake table test of cylindrical water tanks in base-isolated structure, *ASCE Journal of Engineering Mechanics* 116 (1990) 1451–1472.
[322] M.S. Chalhoub, J.M. Kelly, Theoretical and experimental studies of cylindrical water tanks in base isolated structures, Earthquake Engineering Research Center, Technical Report No. EERC 88-07, University of California, Berkeley, CA, 1988.
[323] T.E. Kelly, R.L. Mayes, Seismic isolation of storage tanks, in: C.A. Kircher, A.K. Chopra (Eds.), *ASCE Proceedings Sessions to Seismic Engineering at Structures Congress '89*, New York, USA, 1989, pp. 408–417.
[324] F.E. Tajiran, Seismic isolation of critical components and tanks, *Proceedings of the ATC-17-1 Seminar on Seismic Isolation, Passive Energy Dissipation, and Active Control*, San Francisco, CA., USA, Vol. 1, 1993, pp. 233–244.
[325] V.A. Zayas, D.S. Low, Application of seismic isolation to industrial tanks, *ASME/JSME Proceedings of Pressure Vessels and Piping Conference*, Hawaii, USA, PVP-Vol. 319, 1995, pp. 273–286.
[326] K.H. Cho, M.K. Kim, Y.M. Lim, S.Y. Cho, Seismic response of base-isolated liquid storage tanks considering fluid–structure–soil interaction in time domain, *Soil Dynamics and Earthquake Engineering* 24 (2004) 839–852.
[327] P.B. Rao, R.S. Jangid, Performance of sliding systems under near-fault motions, *Nuclear Engineering and Design* 203 (2001) 259–272.
[328] M.K. Shrimali, Seismic Response of Isolated Liquid Storage Tanks, PhD Thesis, Indian Institute of Technology, Bombay, India, 2003.
[329] M.K. Shrimali, R.S. Jangid, Nonlinear seismic response of base-isolated liquid storage tanks to bi-directional excitation, *Nuclear Engineering and Design* 217 (2002) 1–20.
[330] M.K. Shrimali, R.S. Jangid, Seismic response of liquid storage tanks isolated by sliding bearings, *Engineering Structures* 24 (2002) 909–921.
[331] M.K. Shrimali, R.S. Jangid, A comparative study of performance of various isolation systems for liquid storage tanks, *International Journal of Structural Stability and Dynamics* 2 (2002) 573–591.
[332] M.K. Shrimali, R. Jangid, Dynamic analysis of liquid storage tanks with sliding systems, *Advances in Structural Engineering* 6 (2003) 145–158.
[333] M.K. Shrimali, R.S. Jangid, The seismic response of elevated liquid storage tanks isolated by lead–rubber bearings, *Bulletin of the New Zealand Society for Earthquake Engineering* 36 (2003) 141–164.
[334] M.K. Shrimali, R.S. Jangid, Seismic analysis of base-isolated liquid storage tanks, *Journal of Sound and Vibration* 275 (2004) 59–75.
[335] M.B. Jadhav, R.S. Jangid, Response of base-isolated liquid storage tanks, *Shock and Vibration* 11 (2004) 33–45.
[336] M.B. Jadhav, R.S. Jangid, Response of base-isolated liquid storage tanks to near-fault motions, *Structural Engineering and Mechanics* 23 (2006) 615–634.
[337] N.S. Kim, D.G. Lee, Pseudo-dynamic test for evaluation of seismic performance of base-isolated liquid storage tanks, *Engineering Structures* 17 (1995) 198–208.
[338] L. Bo, T. Jia-Xiang, Vibration studies of base-isolated liquid storage tanks, *Computers and Structures* 52 (1994) 1051–1059.
[339] P.K. Malhotra, Method for seismic base isolation of liquid-storage tanks, *ASCE Journal of Structural Engineering* 123 (1997) 113–116.
[340] P.K. Malhotra, New method for seismic isolation of liquid-storage tanks, *Earthquake Engineering and Structural Dynamics* 26 (1997) 839–847.
[341] H.M. Koh, J.K. Kim, K.S. Park, D.H. Ha, Stochastic analysis of base-isolated pool structure considering fluid–structure interaction effects, *Journal of Korean Society of Civil Engineers* 14 (1994) 463–472.
[342] H.M. Koh, J.K. Kim, K.S. Park, S.J. Kim, Recent research on seismic isolation considering fluid–structure interaction effects in Korea, *Shock and Vibration Isolation, ASME Pressure Vessels and Piping*, Montreal, Canada, Vol. PVP341, 1996, pp. 47–54.
[343] H.M. Koh, K.S. Park, J. Song, Optimal seismic design method for base-isolated pool structure by minimizing life cycle cost, *Proceedings of the 15th International Conference on Structural Mechanics in Reactor Technology*, Vol. X, Seoul, South Korea, 15–20 August, 1999, pp. 427–434.
[344] J.H. Park, Analysis of the Dynamic Behavior of Isolated and Non-Isolated Rectangular Liquid Storage Structures, PhD Thesis, Seoul National University, South Korea, 1997.
[345] J.H. Park, H.M. Koh, J.K. Kim, Seismic isolation of pool-type tanks for the storage of nuclear spent fuel assemblies, *Nuclear Engineering and Design* 199 (2000) 143–154.
[346] K.S. Park, H.M. Koh, J. Song, Cost-effectiveness analysis of seismically isolated pool structures for the storage of nuclear spent-fuel assemblies, *Nuclear Engineering and Design* 231 (2004) 259–270.
[347] C.S. Tsai, C.S. Chen, B.J. Chen, T.C. Chiang, *Seismic Behavior of Oil-storage Tank Equipped with Friction Pendulum System*, ASME Pressure Vessels and Piping Division, New York, USA, Vol. 402, 2000, pp. 107–111.
[348] Y.P. Wang, M.C. Teng, K.W. Chung, Seismic isolation of rigid cylindrical tanks using friction-pendulum bearings, *Earthquake Engineering and Structural Dynamics* 30 (2001) 1083–1099.

[349] J. Eibl, K.H. Hehn, D. Schwartz, Performance tests of high damping steel-laminated seismic isolation bearings for LNG storage tanks, *Proceedings of the Second International Conference on Earthquake Resistant Construction and Design*, Berlin, Germany, Vol. 2, June 15–17, 1994, p. 963.
[350] T. Baumann, J. Boehler, Seismic design of base-isolated LNG-storage-tanks, *Structural Engineering International: Journal of the International Association for Bridge and Structural Engineering (IABSE)* 11 (2001) 139–144.
[351] T. Baumann, M. Lieb, J. Boehler, Sensitivity of seismic response with regard to the computational modeling of the nonlinear characteristics of isolators, *Proceedings of the ASME Pressure Vessels and Piping Division, Seismic, Shock, and Vibration Isolation*, San Diego, CA, USA, Vol. 379, 1998, pp. 9–17.
[352] M. Fornl, Shaking table tests on a spherical tank mock-up provided with seismic isolation and flexing piping connections, *Proceedings of the ASME Pressure Vessels and Piping Conference*, Denver, CO, USA, Vol. 8, July 17–21, 2005, pp. 123–129.
[353] N. Mastan-Zada, G. Yazici, Dynamic behavior of seismically isolated cylindrical offshore storage tanks, *Proceedings of the 24th International Conference on Offshore Mechanics and Arctic Engineering (OMAE)*, Halkidiki, Greece, 2005, pp. 573–577.
[354] J.G. Sun, Z.Q. Yuan, J.F. Hao, Experimental research on rubber base isolation tank, *Journal of Harbin Institute of Technology* 37 (2005) 806–809 (in Chinese).
[355] V.A. Zayas, S.S. Low, S.A. Mahin, L. Bozzo, Feasibility and performance studies on improving the earthquake resistance of new existing buildings using the friction-pendulum system, Report No. UCB/EERC 89-09, Earthquake Engineering and Research Center, College of Engineering, University of California, Berkeley, CA, 1989, 308pp.
[356] V.A. Zayas, S.S. Low, S.A. Mahin, A simple pendulum technique for achieving seismic isolation, *Earthquake Spectra* 6 (1990) 317–333.
[357] M.C. Constantinou, P. Tsopelas, Y.S. Kim, S. Okamoto, NCEER—Taisei Corporation program on sliding seismic isolation systems for bridges—experimental and analytical study of friction-pendulum system (FPS) Report NCEER-93-0020, National Center for Earthquake Engineering Research, State University of New York, NY, 1993.
[358] A.S. Mokha, M.C. Constantinou, A.M. Reinhorn, Experimental study and analytical prediction of earthquake response of a sliding isolation system with spherical surface, Technical Report NCEER-90-0020, State University of New York at Buffalo, 1990.
[359] G. Mosqueda, A.S. Whittaker, G.L. Fenves, Characterization and modeling of friction-pendulum bearings subjected to multiple components of excitation, *ASCE Journal of Structural Engineering* 130 (2004) 433–442.
[360] K.L. Ryan, A.K. Chopra, Estimating the seismic displacement of friction-pendulum isolator based on nonlinear response history analysis, *Earthquake Engineering and Structural Dynamics* 33 (2004) 359–373.
[361] M.C. Constantinou, J. Caccese, H.G. Harris, Frictional characteristics of teflon–steel interface under dynamic conditions, *Earthquake Engineering and Structural Dynamics* 15 (1987) 751–759.
[362] M.C. Constantinou, R. Mokha, A.M. Reinhorn, Teflon bearings in base isolation, II: modeling, *ASCE Journal of Structural Engineering* 116 (1990) 455–474.
[363] A.S. Mokha, M.C. Constantinou, A.M. Reinhorn, Teflon bearings in base-isolation, I: testing, *ASCE Journal of Structural Engineering* 116 (1990) 438–454.
[364] A.S. Mokha, M.C. Constantinou, A.M. Reinhorn, Teflon bearings in base-isolation, II: modeling, *ASCE Journal of Structural Engineering* 116 (1990) 455–474.
[365] A.S. Mokha, M.C. Constantinou, A.M. Reinhorn, Experimental study of friction-pendulum isolation system, *ASCE Journal of Structural Engineering* 117 (1991) 1201–1217.
[366] A.S. Mokha, M.C. Constantinou, A.M. Reinhorn, Verification of friction model of teflon bearings under triaxial load, *ASCE Journal of Structural Engineering* 119 (1993) 240–261.
[367] R.S. Jangid, J.M. Kelly, Base isolation for near-fault motions, *Earthquake Engineering and Structural Dynamics* 30 (2001) 692–707.
[368] C.S. Tsai, T.C. Chiang, B.J. Chen, Finite element formulations and theoretical study for variable curvature friction pendulum system, *Engineering Structures* 25 (2003) 1719–1730.
[369] C.S. Tsai, Y.C. Lin, W.S. Chen, Shaking table tests of a building isolated with trench friction pendulum system, *Proceedings of the Pressure Vessels and Piping Division Conference, PVP2006-ICPVT-11-93253*, Vancouver, Canada, July 23–27, 2006, 5pp.
[370] C.S. Tsai, Y.C. Lin, W.S. Chen, Seismic behavior of high-tech facility isolated with trench friction pendulum system, *Proceedings of the Pressure Vessels and Piping Division Conference, PVP2006-ICPVT-11-93474*, Vancouver, Canada, July 23–27, 2006, 5pp.
[371] E. Abrahamson, S. Mitchell, Seismic response modification device elements for bridge structures development and verification, *Computers and Structures* 81 (2003) 463–467.
[372] K.L. Ryan, A.K. Chopra, Estimation of seismic demands on isolators based on nonlinear analysis, *ASCE Journal of Structural Engineering* 130 (2004) 392–402.
[373] R.S. Jangid, Optimum friction pendulum system for near-fault motions, *Engineering Structures* 27 (2005) 349–359.
[374] N. Amin, A.S. Mokha, Base isolation gets its day in court, *ASCE Civil Engineering* 65 (1995) 44–47.
[375] S. Fujita, Y. Morikawa, I. Shimoda, S. Nagata, H. Shimosaka, Isolation system for equipment using friction-pendulum bearings (First Report, Shaking table tests and response analysis on isolated equipment), *Nippon Kikai Gakkai Ronbunshu, C Hen/Transactions of the Japan Society of Mechanical Engineers, Part C* 59 (1993) 11–16.
[376] S. Fujita, H. Yamamoto, N. Kitagawa, H. Kurabayashi, Research and development of the friction-pendulum isolation device with poly-curvature (investigation of isolation performance on shake test and response analysis using vending machine model), *Transactions of the Japan Society of Mechanical Engineers, Part C* 69 (2003) 1990–1996.
[377] C.S. Tsai, Seismic behavior of buildings with FPS isolators, *ASCE Proceedings of the Second Congress on Computing in Civil Engineering*, Atlanta, GA, USA, 1995, Vol. 2, pp. 1203–1211.

[378] C.S. Tsai, Finite element formulation for friction-pendulum seismic isolation bearings, *International Journal for Numerical Methods in Engineering* 40 (1997) 29–49.
[379] Y.P. Wang, L.L. Chung, W.H. Liao, Seismic response analysis of bridges isolated with friction pendulum behavior, *Earthquake Engineering and Structural Dynamics* 27 (1998) 1069–1093.
[380] Y.P. Wang, W.H. Liao, C.L. Lee, A state-space approach for dynamic analysis of sliding structures, *Engineering Structures* 23 (2001) 790–801.
[381] Y.S. Kim, C.B. Yun, Seismic response characteristics of bridges using double concave friction pendulum bearings with tri-linear behavior, *Engineering Structures* 29 (2007) 3082–3093.
[382] S. Okamura, S. Fujito, Study on motion analysis of friction pendulum isolation systems during earthquakes: fourth report, the stochastic examination of the isolation performance by Monte Carlo simulation, *Nippon Kikai Gakkai Ronbunshu, Transactions of the Japan Society of Mechanical Engineers, Part C* 69 (2003) 1983–1989 (in Japanese).
[383] S. Okamura, S. Fujito, M. Ikenaga, Motion analysis of pendulum-type isolation system during earthquakes: dynamic test and response analysis on a three storey steel frame model supported by four friction-pendulum bearings, *ASME Journal of Pressure Vessel Technology* 126 (2004) 34–45.
[384] S. Ates, A.A. Dumanoglu, A. Bayraktar, Stochastic response of seismically isolated highway bridges with friction-pendulum systems to spatially varying earthquake ground motions, *Engineering Structures* 27 (2005) 1843–1858.
[385] S. Ates, A. Bayraktar, A.A. Dumanoglu, The effect of spatially varying earthquake ground motions on the stochastic response of bridges isolated with friction-pendulum systems, *Soil Dynamics and Earthquake Engineering* 26 (2006) 31–44.
[386] A.A. Papageorgio, M.C. Constantinou, Response of sliding structures with restoring force to stochastic excitation, *Probabilistic Engineering Mechanics* 5 (1990) 19–26.
[387] R.S. Jangid, P. Banerji, Effect of isolation damping on stochastic response of structures with nonlinear base isolators, *Earthquake Spectra* 14 (1998) 95–114.
[388] M. Dicleli, M.Y. Mansour, Seismic retrofitting of highway bridges in Illinois using friction-pendulum seismic isolation bearing and modeling procedure, *Engineering Structures* 25 (2003) 1139–1156.
[389] P.C. Roussis, M.C. Constantinou, Experimental and analytical studies of structures seismically isolated with an uplift-restraint isolation system, University of Buffalo, New York, Multidisciplinary Center for Earthquake Engineering Research, Technical Report No. MCEER-05-0001, 2005, 160pp.
[390] P.C. Roussis, M.C. Constantinou, Uplift-restraining friction-pendulum seismic isolation system, *Earthquake Engineering and Structural Dynamics* 35 (2006) 577–593.
[391] P.C. Roussis, M.C. Constantinou, Experimental an analytical studies of structures seismically isolated with an uplift-restraining friction-pendulum system, *Earthquake Engineering and Structural Dynamics* 35 (2006) 595–611.
[392] M. Pranesh, R. Sinha, VFPI: An isolation device for aseimic design, *Earthquake Engineering and Structural Dynamics* 29 (2000) 603–627.
[393] M. Pranesh, R. Sinha, Aseimic design of tall structures using variable frequency pendulum isolator, *Proceedings of the 12th World Conference on Earthquake Engineering*, Auckland, New Zealand, Paper No. 284, 2000.
[394] M. Pranesh, R. Sinha, Earthquake resistant design of structures using VFPI, *ASCE Journal of Structural Engineering* 128 (2002) 870–880.
[395] P. Murnal, R. Sinha, Aseismic design of structure-equipment systems using variable frequency pendulum isolator, *Nuclear Engineering and Design* 231 (2004) 129–139.
[396] J.D. Ferry, *Viscoelastic Properties of Polymers*, Wiley, New York, 1980.
[397] J.J. Aklonis, W.J. MacKnight, *Introduction to Polymer Viscoelasticity*, second ed., Wiley, New York, 1983.
[398] A.N. Gent, *Engineering with Rubber*, Oxford University Press, New York, 1992.
[399] B.J. Lazan, *Damping of Materials and Members in Structural Mechanics*, Pergamon Press, New York, 1968.
[400] G.B. McKenna, S.L. Simon, Time dependent volume and enthalpy responses in polymers, *American Society of Testing and Materials* 1357 (2000) 18–46.
[401] D.I.G. Jones, Temperature–frequency dependence of dynamic properties of damping materials, *Journal of Sound and Vibration* 33 (1973) 451–470.
[402] A. Schallamach, D.B. Sellen, H.W. Greensmith, Dynamic behavior of rubber during moderate extensions, *British Journal of Applied Physics* 16 (1965) 241–249.
[403] J.A.C. Harwood, A. Schallamach, Dynamic behavior of natural rubber during large extensions, *Journal of Applied Polymer Science* 2 (1967) 1835–1845.
[404] H. McCallion, D.M. Davies, Behavior of rubber in compression under dynamic conditions, *Proceedings of the Institute of Mechanical Engineers (London)* 169 (1955) 1124–1134.
[405] W.S. Mitchell, Physical properties of rubber, *Vibration and Acoustics Measurements Handbook*, Spartan Books, New York, 1972, pp. 181–203 (Chapter 7).
[406] F.J. Lockett, *Nonlinear Viscoelastic Solids*, Academic Press, New York, 1972.
[407] R.M. Christensen, *Theory of Viscoelasticity*, Academic Press, New York, 1971.
[408] I.D. Skrypnyk, J.L. Spoormaker, P. Kandachar, A constitutive model for long-term behavior of polymer, *American Society of Testing and Materials* 1357 (2000) 71–82.
[409] I.D. Skrypnyk, J.L. Spoormaker, W. Smit, Implementation of constitutive model in FEA for nonlinear behavior of plastics, *American Society of Testing and Materials* 1357 (2000) 83–97.
[410] J.E. Mark, B. Erman, F.R. Eirich, *Science and Technology of Rubber*, Academic Press Inc., London, 1994.

[411] R.A. Schapery, D.A. Cantey, Thermo-mechanical response studies of solid propellants subjected to cyclic and random loading, *American Institute of Aeronautics and Astronautics (AIAA) Journal* 4 (1966) 255–264.
[412] R.A. Schapery, On characterization of nonlinear viscoelastic materials, *Journal of Polymers Engineering Science* 9 (1969) 295–310.
[413] H.J. Golden, T.W. Strganac, R.A. Schapery, An approach to characterize nonlinear viscoelastic material behavior using dynamic mechanical tests and analysis, *ASME Journal of Applied Mechanics* 66 (2001) 872–878.
[414] X. Gong, Z. Xie, Z. Luo, M. Zhao, The characteristics of a nonlinear damper for vibration isolation, *Journal of Vibration Engineering* 14 (2001) 334–338 (in Chinese).
[415] X. Gong, Y. Tang, J. Jing, Experimental investigations on dynamic performance of vibration isolator made of reinforced foam plastics, *Acta Materiae Compositae Sinica* 20 (2003) 135–141 (in Chinese).
[416] M.G. Sharma, Dynamic behavior of rubber, *Vibration and Acoustics Measurements Handbook*, Spartan Books, New York, 1972, pp. 205–261 (Chapter 8).
[417] G. Kim, R. Singh, Resonance, isolation and shock control of automotive nonlinear hydraulic engine mounts, *ASME Dynamic Systems and Control Division DSC, Anaheim, California* 44 (1992) 165–180.
[418] G.D. Jones, *Handbook of Viscoelastic Vibration Damping*, Wiley, New York, 2001.
[419] N.K. Lee, M.S. Lee, H.Y. Kim, J.J. Kim, Design of engine mount using finite element method and optimization technique, *Proceedings of the 1998 Society of Automotive Engineers International Congress & Exposition*, Detroit, MI, USA, Paper No. 980379, 1998.
[420] K.N. Morman, Jr., B.G. Kao, J.C. Nagragaal, Finite element analysis of viscoelastic elastomeric structures vibrating about nonlinear statically stressed configurations, *Proceedings of the 1981 Society of Automotive Engineers International Congress & Exposition*, Detroit, MI, USA, Paper No. 811309, 1981.
[421] I.L. Ver, Measurement of dynamic stiffness and loss factor of elastic mounts as a function of frequency and static loads, *Noise Control Engineering* 3 (1974) 37–42.
[422] J. Harris, A. Stevenson, On the role of nonlinearity in the dynamic behavior of rubber components, *Rubber Chemistry and Technology* 59 (1986) 740–764.
[423] K. Gjika, R. Dufour, G. Ferraris, Transient response of structures on viscoelastic or elastoplastic mounts: prediction and experiment, *Journal of Sound and Vibration* 198 (1996) 361–378.
[424] P. Culbertstone, H. Yang, J. Peng, M. Huang, S. Kang, Use of body mount stiffness and damping in CAE crash modeling, Society of Automotive Engineers Paper No. 2000-01-0120, 2000.
[425] N.W. Tschoegl, *The Phenomenological Theory of Linear Viscoelastic Behavior*, Springer, Berlin, 1989.
[426] C.R. Lin, Y.D. Lee, Effects of viscoelasticity on rubber vibration isolator design, *Journal of Applied Physics* 83 (1998) 8027–8035.
[427] C.R. Lin, Y.D. Lee, Strain-dependent dynamic properties of filled rubber network systems, *Macromolecular Theory and Simulations* 5 (1996) 1075–1104.
[428] C.R. Lin, Y.D. Lee, Strain-dependent dynamic properties of filled rubber network systems, 2: the physical meaning of parameters in the L–N–B model and their applications, *Macromolecular Theory and Simulations* 6 (1997) 339–350.
[429] A. Coniglio, Cluster structure near the percolation threshold, *Journal of Physics A: Mathematical and General* 15 (1982) 3829–3844.
[430] A. Aharony, Y. Gefen, Y. Kantor, Magnetic correlations of fractals, *Journal of Statistical Physics* 36 (1984) 795–805.
[431] P.K. Mallick, Design and development of composite elliptic springs for automotive suspension, *Proceedings of the 40th Annual Conference on Reinforced Plastic/Composites Institute*, The Society of the Plastics Industry, January 28–February 1, 1985, Atlanta, GA, Session 14. cp.
[432] P.K. Mallick, Static mechanical performance of composite elliptic springs, *ASME Journal of Engineering Material Technology* 109 (1987) 22–26.
[433] G.D. Scowen, D. Hughes, The sulcated spring, *International Seminar, Autotech 85 Congress, The Institution of Mechanical Engineers, Autotech '85—International Automotive Technology Exhibition and Congress*, Springtime, Birmingham, UK, 1985, 26pp.
[434] G.D. Scowen, Transport application for fiber reinforced composites, *Proceedings of the Institution of Mechanical Engineers C* 49/86 (1986) 245–255.
[435] C.K. So, P.C. Tse, T.C. Lai, K.M. Young, Static mechanical behavior of composite cylindrical springs, *Composite Science and Technology* 40 (1991) 251–263.
[436] P.C. Tse, T.C. Lai, C.K. So, C.M. Cheng, Large deflection of elastic composite circular springs under uniaxial compression, *International Journal of Nonlinear Mechanics* 29 (1994) 781–798.
[437] P.C. Tse, S.R. Reid, K.J. Lau, W.H. Wong, Large deflections of composite circular springs with extended flat contact surfaces, *Composite Structures* 63 (2004) 253–260.
[438] P.C. Tse, T.C. Lai, C.K. So, A note on large deflection of elastic composite circular springs under tension and in push–pull configuration, *Composite Structures* 40 (1998) 223–230.
[439] P.C. Tse, C.T. Lung, Large deflections of elastic composite circular springs under uniaxial tension, *International Journal of Nonlinear Mechanics* 35 (2000) 293–307.
[440] ASTM D-945-92 (Reapproved 2001), Standard test methods for rubber properties in compression or shear (Mechanical Oscillograph), American Society of Testing and Materials, 2001.
[441] K. Shaska, R.A. Ibrahim, R.F. Gibson, Influence of excitation amplitude on the characteristics of nonlinear butyl rubber isolators, *Nonlinear Dynamics* 47 (2007) 83–104.
[442] H.Y. Kim, W.J. Bang, J.S. Kim, Large deformation FEA of automotive rubber components by using ABAQUS, *ABAQUS User's Conference Procedure*, Newport, USA, 1992, pp. 255–269.

[443] P.J. Machioce, A.D. Nashif, T.M. Lewis, Direct measurement of the dynamic material properties of polymers for low frequency, *Proceedings of Damping '91*, San Diego, California, 13–15 February 1991, Vol. 2, pp. EBA 1–EBA 17.
[444] T. Murayama, *Dynamic Mechanical Analysis of Polymeric Material*, Elsevier Scientific Publishing Company, New York, 1978.
[445] S.S. Sattinger, Direct method for measuring the dynamic shear properties of damping polymers, *American Chemical Society Symposium Series* 424 (1990) 79–91.
[446] P.T. Weissman, R.P. Chartoff, Extrapolation viscoelastic data in the temperature–frequency domain, *American Chemical Society Symposium Series* 424 (1990) 111–131.
[447] M.F. Tedesco, Investigation of elastomeric vibration isolators, Air Force Institute of Technology, Wright-Patterson Air Force Base Ohio School of Engineering, Report: GA/MC/73-6, 1973, 73pp.
[448] N. Chandra Shekhar, H. Hatwal, A.K. Mallik, Performance of nonlinear isolators and absorbers to shock excitation, *Journal of Sound and Vibration* 217 (1999) 293–307.
[449] N. Chandra Shekhar, H. Hatwal, A.K. Mallik, Response of nonlinear dissipative shock isolators, *Journal of Sound and Vibration* 214 (1999) 589–603.
[450] C.M. Richards, R. Singh, Identification of nonlinear properties of rubber isolators using experimental and analytical methods, *Proceedings of the 1998 National Conference on Noise Control Engineering*, Ypsilanti, MI, USA, Part 1 (of 3), 1998, pp. 391–396.
[451] C.M. Richards, R. Singh, Feasibility of identifying nonlinear vibratory systems consisting of unknown polynomial forms, *Journal of Sound and Vibration* 220 (1999) 413–450.
[452] C.M. Richards, R. Singh, Characterization of rubber isolator nonlinearities in the context of single- and multi-degree-of-freedom experimental systems, *Journal of Sound and Vibration* 247 (2001) 834–907.
[453] A.K. Mallik, V. Kher, M. Puri, H. Hatwal, On the modeling of nonlinear elastomeric vibration isolators, *Journal of Sound and Vibration* 219 (1999) 239–253.
[454] C.A.J. Biejers, A. De Boer, Numerical modeling of rubber vibration isolators, *Proceedings of the 10th International Congress on Sound and Vibration*, Stockholm, Sweden, 2003, pp. 805–812.
[455] L. Kari, The nonlinear temperature dependent stiffness of pre-compressed rubber cylinders, *Kautschuk Gummi Kunststoffe* 55 (2002) 76–81.
[456] J. Padovan, J.T. Sawicki, Nonlinear vibrations of fractionally damped systems, *Nonlinear Dynamics* 16 (1998) 321–336.
[457] M. Sjöberg, L. Kari, Nonlinear behavior of a rubber isolator system using fractional derivatives, *Vehicle System Dynamics* 37 (2002) 217–236.
[458] M. Sjöberg, L. Kari, Nonlinear isolator dynamics at finite deformations: An effective hyperelastic, fractional derivative, generalized friction model, *Nonlinear Dynamics* 33 (2003) 323–336.
[459] Lord Corporation, Rheonetic MR technology from Lord Corporation in Cadillac suspension takes prestigious award from popular Science Magazine 〈http://www.rheonetic.com〉, 2002.
[460] R. Stanway, J. Sproston, A. El-Wahed, Applications of electrorheological fluids in vibration control: a survey, *Smart Materials and Structures* 5 (1996) 464–482.
[461] J.L. Sproston, R. Stanway, An electro-rheological automotive engine mount: aspects of identification and control, *Proceedings of the 11th International Association of Science and Technology for Development (IASTED) International Conference, Modeling, Identification and Control*, Innsbruck, Austria, 1992, pp. 275–276.
[462] N. Hagood, A. Von Flotow, Damping of structural vibrations with piezoelectric materials and passive electrical networks, *Journal of Sound and Vibration* 146 (1991) 243–268.
[463] G. Lesieutre, Vibration damping and control using shunted piezoelectric materials, *Shock and Vibration Digest* 30 (1998) 187–196.
[464] M. Jolly, J. Carison, B. Munoz, A model of the behavior of magnetoreheological materials, *Smart Materials and Structures* 5 (1996) 607–614.
[465] B. Spencer, S. Dyke, M. Sain, J. Carlson, Phenomenological model of a magnetorheological damper, *ASCE Journal of Engineering Mechanics* 123 (1997) 230–238.
[466] K. Otsuka, C. Wayman, *Shape Memory Materials*, Cambridge University Press, Cambridge, 1998.
[467] S. Saadat, J. Salichs, M. Noori, Z. Hou, H. Davoodi, Y. Bar-On, Y. Suzuki, A. Masuda, An overview of vibration and seismic applications of NiTi shape memory alloy, *Smart Materials and Structures* 11 (2002) 218–229.
[468] D. Lagoudas, J. Mayes, M. Khan, Simplified shape memory alloy (SMA) material model for vibration isolation, *Proceedings of the International Society for Optical Engineering (SPIE) Conference on Smart Structures and Materials Modeling, Signal Processing, and Control in Smart Structures*, Newport Beach, CA, USA, Vol. 4326, 2001, pp. 452–461.
[469] M. Khan, D. Lagoudas, Modeling of shape memory alloy pseudoelastic spring elements using Preisach model for passive vibration isolation, *Proceedings of the International Society for Optical Engineering (SPIE), Conference on Smart Structures and Materials Modeling, Signal Processing, and Control in Smart Structures*, San Diego, CA, USA, Vol. 4693, 2002, pp. 336–347.
[470] J. Ginder, M. Nichols, L. Elie, J. Tardiff, Magnetorheological elastomers: properties and applications, *Proceedings of the International Society for Optical Engineering (SPIE) Conference on Smart Structures and Materials, Smart Materials Technologies*, Newport Beach, CA, USA, Vol. 3675, 1999, pp. 131–138.
[471] L. Davis, Model of magnetorheological elastomers, *Journal of Applied Physics* 85 (1999) 3348–3351.
[472] J. Ginder, W. Schlotter, M. Nichols, Magnetorheological elastomers in tunable vibration absorbers, *Proceedings of the International Society for Optical Engineering (SPIE) Conference on Smart Structures and Materials, Damping and Isolation*, Newport Beach, CA, USA, Vol. 4331, 2001, pp. 103–110.

[473] M.F. Winthrop, R.G. Cobb, Survey of state-of-the-art vibration isolation research and technology for space applications, *Proceedings of the SPIE—The International Society for Optical Engineering: Smart Structures and Materials (Damping and Isolation)*, San Diego, CA, USA, Vol. 5052, 2003, pp. 13–26.
[474] M. Hazewinkel, *Encyclopaedia of Mathematics, An Updated and Annotated Translation of the Soviet Mathematical Encyclopaedia*, Kluwer Academic Press, The Netherlands, 1988.
[475] H. Giacomini, S. Neukirch, On the number of limit cycles of the Lienard equation, *Chaotic Dynamics* (1997) (eprint arXiv:chao-dyn/9705006).
[476] H. Giacomini, S. Neukirch, Improving a method for the study of limit cycles of the Lienard equation, *Chaotic Dynamics* (1997) (eprint arXiv:chao-dyn/9709036).
[477] K. Odani, On the limit cycle of the Lienard equation, *Archivum Mathematicum* 36 (2000) 25–31.
[478] J.L. Lopez, R. Lopez-Ruiz, The limit cycles of Lienard equations in the strongly nonlinear regime, *Nonlinear Sciences* 11 (2001) 745–756.
[479] Y. Shen, M.F. Golnaraghi, G.R. Heppler, Analytical and experimental study of the response of a suspension system with a magnetorheological damper, *Journal of Intelligent Material Systems and Structures* 16 (2005) 135–147.
[480] A. Narimani, M.F. Golnaraghi, Isolation application of controlled and uncontrolled magnetorheological dampers for random base excitation, *ASME Dynamic Systems and Control Division (Publication) DSC*, Orlando, Florida, Vol. 74 DSC, No. 2 (Part B), 2005, pp. 1789–1797.
[481] A. Narimani, M.F. Golnaraghi, Nonlinear isolator optimization using RMS cost function, *Proceedings of the ASME International Mechanical Engineering Congress and Exposition*, Design Engineering Division, Anaheim, California, 2004, Vol. 117, pp. 893–899.
[482] G.N. Jazar, R. Hounim, A. Narimani, M.F. Golnaraghi, Frequency response and jump avoidance in a nonlinear passive engine mount, *Journal of Vibration and Control* 12 (2006) 1205–1237.
[483] Y. Shen, N. Eslaminasab, B. Schubert, A. Narimani, M.F. Golnaraghi, Load-leveling suspension system with a magnetorheological damper, *Vehicle System Dynamics* 45 (2007) 297–312.
[484] L. Davis, B. Workman, C.C Chu, E. Anderson, Design of D-strut and its application results in the JPL, MIT, and LARC test beds, *Proceedings of the 33rd American Institute of Aeronautics and Astronautics Structural Dynamics Meeting*, Dallas, TX, USA, 1992, p. 1524.
[485] C. Johnson, Design of passive damping systems, *A Special Combined Issue of the Journal of Mechanical Design and the Journal of Vibration and Acoustics (ASME 50th Anniversary of the Design Engineering Division)* 117 (1995) 171–176.
[486] Y.C. Yiu, M.E. Regelbrugge, M. E., Shape-memory alloy isolators for vibration suppression in space applications, *Collection of Technical Papers—AIAA/ASME/ASCE/AHS/ASC Structures, Structural Dynamics & Materials Conference*, New Orleans, LA, USA, Vol. 5, 1995, pp. 3390–3398.
[487] R.G. Cobb, J.M. Sullivan, A. Das, P.L. Davis, T.T. Hyde, T. Davis, Z.H. Rahman, J.T. Spanos, Vibration isolation and suppression system for precision payloads in space, *Smart Materials and Structures* 8 (1999) 798–812.
[488] E.K. Hall, J.T. Mueller, Coupled vibration isolation/suppression systems for space applications of structural design, *Proceedings of the International Society for Optical Engineering (SPIE) Conference on Smart Structures and Materials: Smart Structures and Integrated Systems*, San Diego, CA, USA, Vol. 2443, 1995, pp. 136–144.
[489] G.G. Karahalis, G.S. Agnes, Preliminary analysis of hybrid launch isolation for spacecraft, *Proceedings of the International Society for Optical Engineering (SPIE) Conference on Smart Structures and Materials: Industrial and Commercial Applications of Smart Structures Technologies*, Newport Beach, CA, USA, Vol. 3674, 1999, pp. 360–370.
[490] P.S. Wilke, C.D. Johnson, P.J. Grosserode, D. Siciulli, Whole-spacecraft vibration isolation on small launch vehicles, *Proceedings of the International Society for Optical Engineering (SPIE) Conference on Smart Structures and Materials: Damping and Isolation*, Newport Beach, CA, USA, Vol. 3989, 2000, pp. 440–451.
[491] P.S. Wilke, C.D. Johnson, P.J. Grosserode, D. Siciulli, Whole-spacecraft vibration isolation for broadband attenuation, *Proceedings of the IEEE Aerospace Conference*, Big Sky, MT, USA, Vol. 4, 2000, pp. 315–321.
[492] C.G. Johnson, P.S. Wilke, K.R. Darling, Multi-axis whole-spacecraft vibration isolation for small launch vehicles, *Proceedings of the International Society for Optical Engineering (SPIE) Conference on Smart Structures and Materials: Damping and Isolation*, Newport Beach, CA, USA, Vol. 4331, 2001, pp. 153–161.
[493] J.F. O'Brien, R. Goullioud, G.W. Neat, Micro-precision interferometer: evaluation of new disturbance isolation solutions, *Proceedings of the International Society for Optical Engineering (SPIE) Conference on Smart Structures and Materials: Passive Damping and Isolation*, San Diego, CA, USA, Vol. 3327, 1998, pp. 387–398.
[494] K.J. Kim, J.H. Lee, Modeling of nonlinear complex stiffness of dual-chamber pneumatic spring for precision vibration isolations, *Journal of Sound and Vibration* 301 (2007) 909–926.
[495] Y.C. Fung, M.V. Barton, Performance of nonlinear systems subjected to ground shock, *Aerospace Engineering* 21 (1962) 46–57.
[496] H. Park, J.R. Fowler, Dynamic isolation test and analysis of a zero-spring-rate mechanism, *Proceedings of the 13th Aerospace Testing Seminar*, 8–10 October, Manhattan Beach, CA, USA, 1991, pp. 321–326.
[497] Denoyer, K. K., Griffin, S. F., Das, A., Passive vibroacoustic isolation for reusable launch vehicle payload containers, *Collection of Technical Papers Proceedings of the AIAA/ASME/ASCE/AHS/ASC Structures, Structural Dynamics & Materials Conference*, Long Beach, CA, USA, Vol. 3, 1998, pp. 2248–2256.
[498] N.M. Jedrich, S.C. Pendleton, Isolation systems for electronic black-box transportation to orbit, *Proceedings of the International Society for Optical Engineering (SPIE) Conference on Smart Structures and Materials: Passive Damping and Isolation*, San Diego, CA, USA, Vol. 3327, 1998, pp. 423–430.

[499] S.F. Griffin, K.K. Denoyer, A. Das, Passive vibroacoustic isolation for payload containers, *Journal of Intelligent Material Systems and Structures* 10 (1999) 83–87.
[500] T.T. Hyde, E.H. Anderson, Actuator with built-in viscous damping for isolation and structural control, *American Institute of Aeronautics and Astronautics (AIAA) Journal* 33 (1996) 129–135.
[501] L.P. Davis, D.R. Carter, T.T. Hyde, Second generation hybrid D-strut, *Proceedings of the SPIE: The International Society of Optical Engineering: Smart Structures and Materials Conference*, San Diego, CA, USA, Vol. 2445, 1995, pp. 161–175.
[502] J.F. Wilson, L.P. Davis, Viscous damped space structure for reduced jitter, *Proceedings of the 58th Shock and Vibration Symposium*, Huntsville, AL, USA, Vol. 1, 1987, pp. 233–243.
[503] D. Cunningham, L.P. Davis, A multiaxis passive isolation system for magnetic bearing reaction wheel, *Proceedings of the 16th Advances in the Astronautical Sciences (AAS) Rocky Mountain Guidance and Control Conference*, Keystone, CO, USA, Vol. 81, 1993, p. 454.
[504] L.P. Davis, D. Cunningham, J. Harrel, Advanced 1.5 Hz passive viscous isolation system, *Proceedings of the 35th AIAA/ASME/ASCE/AHS/ASC Structures, Dynamics, and Materials Conference*, Hilton Head, SC, USA, Part 5 (of 5), 1994, pp. 2655–2665.
[505] T. Davis, L.P. Davis, High performance passive viscous isolator element for active/passive (hybrid) isolation, *Proceedings of the International Society for Optical Engineering (SPIE) Conference on Smart Structures and Materials: Smart Structures and Materials Conference*, San Diego, CA, USA, Vol. 2720, 1996, pp. 281–292.
[506] L.A. Sullivan, R.S. Erwin, K.K. Denoyer, Experiences with smart structures for on-orbit vibration isolation, *Proceedings of the International Society for Optical Engineering (SPIE) Conference on Smart Structures and Materials: Industrial and Commercial Applications of Smart Structures Technologies*, Newport Beach, CA, USA, Vol. 3991, 2000, pp. 122–130.
[507] S. Hadden, T. Davis, P. Buchele, J. Boyd, T. Hintz, Heavy load vibration isolation system for airborne payloads, *Proceedings of the International Society for Optical Engineering (SPIE) Conference on Smart Structures and Materials: Industrial and Commercial Applications of Smart Structures Technologies*, Newport Beach, CA, USA, Vol. 4332, 2001, pp. 171–182.
[508] D.C. Zimmerman, T.L. Lyde, Sensor failure detection and isolation in flexible structures using system realization redundancy, *Journal of Guidance, Control, and Dynamics* 16 (1993) 490–497.
[509] M.J. Roemer, J. Ge, A. Leberson, G.P Tandon, R.Y. Kim, Autonomous impact damage detection and isolation prediction and isolation for aerospace structures, *Proceedings of the 2005 IEEE Aerospace Conference*, 5–12 March 2005, Big Sky, MT, USA, IEEE Cat. No. 05th8788, 2005, pp. 3592–3600.
[510] A.J. Keane, Passive vibration isolation control via unusual geometries: the application of genetic algorithm optimization to structural design, *Journal of Sound and Vibration* 185 (1995) 441–453.
[511] A.J. Keane, A.P. Bright, Passive vibration control via unusual geometries: experiments on model aerospace structures, *Journal of Sound and Vibration* 190 (1996) 713–719.
[512] G. Kim, R. Singh, Nonlinear analysis of automotive hydraulic engine mount, *ASME Journal of Dynamic Systems, Measurement and Control* 115 (1993) 482–487.
[513] J.E. Colgate, C.T. Chang, Y.C. Chiou, W.K. Liu, L.M. keer, Modeling of a hydraulic engine mount focusing on response to sinusoidal and composite excitations, *Journal of Sound and Vibration* 184 (1995) 503–528.
[514] M. Tiwari, H. Adiguna, R. Singh, Experimental characterization of a nonlinear hydraulic engine mount, *Noise Control Engineering Journal* 51 (2003) 36–49.
[515] M.F. Golnaraghi, G.N. Jazar, Development and analysis of a simplified nonlinear model of a hydraulic engine mount, *Journal of Vibration and Control* 7 (2001) 495–526.
[516] M.F. Golnaraghi, G.N. Jazar, Nonlinear modeling, experimental verification, and theoretical analysis of a hydraulic engine mount, *Journal of Vibration and Control* 8 (2002) 87–116.
[517] F.F. Timpner, Design considerations for engine mounting, *Proceedings of the 1965 International Society of Automotive Engineering Congress and Exhibition*, Detroit, MI, USA, (SAE) Paper Series 650093 (Papers, 966B), 1965, 5pp.
[518] S.R. Racca, How to select power-train isolators for good performance and long service life? *Proceedings of the 1982 International Off-Highway Meeting & Exposition (SAE)*, Milwaukee, WI, USA, Society of Automotive Engineers, SAE Paper Series 821095, 1982.
[519] J.E. Bernard, J.M. Starkey, Engine mount optimization, *Proceedings of the 1983 International Society of Automotive Engineers Congress and Exhibition*, Detroit, Michigan, USA, SAE Transactions 92:11, 1-1, Technical Paper Series 830257, 1983.
[520] P.E. Geck, R.D. Patton, Front wheel drive engine mount optimization, *Proceedings of the 1984 International Society of Automotive Engineers Congress and Exhibition, Fifth International Conference on Vehicular Structural Mechanics*, Detroit, Michigan, USA, Technical Paper Series 840736, 1984.
[521] D.M. Ford, An analysis and application of a decoupled engine mount systems for idle isolation, *Proceedings of the Society of Automotive Engineers*, Traverse City, MI, USA, Technical Paper Series 850976, 1985, pp. 133–142.
[522] C.E. Spiekermann, C.J. Radcleffe, E.D. Goodman, Optimal design and simulation of vibrational isolation systems, *ASME Journal of Mechanisms, Transmissions and Automotive Design* 107 (1985) 271–276.
[523] M. Muller, U. Weltin, C. Freudenberg, D. Law, M.M. Roberts, T.W. Siebler, Engine mounts and NVH, *Automotive Engineering (Warrendale, Pennsylvania)* 102 (1994) 19–23.
[524] R.M. Brach, Automotive power-plant isolation strategies, *Proceedings of 1997 Society of Automotive Engineers Congress and Exhibition*, Detroit, MI, USA, Technical Paper Series 971942, 1997.
[525] J. Christopherson, G.N. Jazar, M. Mahinfalah, Chaotic behavior of hydraulic engine mount, *Proceedings of the ASME 2006 International Mechanical Engineering Congress and Exposition*, Chicago, IL, USA, ASME Design Engineering Division (Publication) DE, *Proceedings of IMECE2006—Design Engineering*, 8pp.

[526] A.R. Ohadi, G. Maghsoodi, Simulation of engine vibration on nonlinear hydraulic engine mounts, *ASME Journal of Vibration and Acoustics* 129 (2007) 417–424.
[527] W. Shangguan, Z. Lu, Nonlinear modeling of hydraulic engine mounts of a car powertrain with computational fluid structure interaction finite element analysis models, *Chinese Journal of Mechanical Engineering* 40 (2004) 80–86 (in Chinese).
[528] Y.Q. Zhang, W.B. Shangguan, A novel approach for lower frequency performance design of hydraulic engine mounts, *Computers and Structures* 84 (2006) 572–584.
[529] W.B. Shangguan, Z.S. Song, Y.Q. Yun, K.H. Jiang, C. Xu, Experimental study and simulation analysis of hydraulic engine mounts with multiple inertia tracks, *Zhendong Gongcheng Xuebao/Journal of Vibration Engineering* 18 (2005) 318–323 (in Chinese).
[530] A. Kyprianou, J. Giacomin, K. Worden, M. Heidrich, J. Bocking, Differential evolution based identification of automotive hydraulic engine mount model parameters, *Proceedings of the Institution of Mechanical Engineers, Part D: Journal of Automobile Engineering* 214 (2000) 249–264.
[531] R. Fan, Z. Lu, Fixed points on the nonlinear dynamic properties of hydraulic engine mounts and parameter identification method: experiment and theory, *Journal of Sound and Vibration* 305 (2007) 703–727.
[532] S. He, R. Singh, Discontinuous compliance nonlinearities in the hydraulic engine mount, *Journal of Sound and Vibration* 307 (2007) 545–563.
[533] R.V. Schmitt, C.J. Leingang, Design of elastomeric vibration isolation mounting systems for internal combustion engine, *Proceedings of the 1976 Society Automotive Engineers Congress and Exhibition*, Detroit, MI, SAE Reprints, 1976, Paper No. 760431.
[534] J.H. Bucksbee, The use of bonded elastomers for energy and motion control in construction, *Rubber World* 196 (1987) 38–45.
[535] K. Misaji, H. Kato, K. Shibata, Vibration characteristics of rubber vibration isolators of vehicles (analysis of nonlinear vibration response), *Transactions of Japan Society of Mechanical Engineers, Part C* 60 (1994) 3274–3280 (in Japanese).
[536] K. Misaji, S. Hirose, K. Shibata, Vibration analysis of rubber vibration isolators of vehicle using the restoring force model of power function type (analysis of nonlinear vibration using frequency characteristics determined by the hysteresis loop, *Japan Society of Mechanical Engineers International Journal, Series C* 38 (1995) 679–685.
[537] S. Hirose, H. Jinbo, K. Misaji, K. Shibati, Vibration characteristics of rubber vibration isolators of vehicles (analysis of nonlinear vibration response for multiple-degree-of-freedom system), *Transactions of Japan Society of Mechanical Engineers, Part C* 63 (1997) 3367–3373 (in Japanese).
[538] Y. Yu, N.G. Naganathan, R. Dukkipati, Review of automotive vehicle engine mounting systems, *International Journal of Vehicle Design* 24 (2000) 299–319.
[539] Y. Yu, N.G. Naganathan, R. Dukkipati, Literature review of automotive vehicle engine mounting systems, *Mechanism and Theory of Machine* 36 (2001) 123–142.
[540] Y. Yu, S.M. Peelamedu, N.G. Naganathan, R. Dukkipati, Automotive vehicle engine mounting systems: a survey, *ASME Journal of Dynamic Systems, Measurement and Control* 123 (2001) 186–194.
[541] R.A. Muzechuk, Hydraulic mounts: Improved engine isolation, *Proceedings of the Advances in Elastomeric Applications Symposium held at the SAE International Congress & Exposition*, Detroit, MI, USA, SAE Special Publications, 1984, pp. 61–70.
[542] G. Kim, R. Singh, A study of passive and adaptive hydraulic engine mount systems with emphasis on nonlinear characteristics, *Journal of Sound and Vibration* 179 (1995) 427–453.
[543] A.K.W. Ahmed, M.M. Haque, S. Rakheja, Nonlinear analysis of automotive hydraulic mounts for isolation of vibration and shock, *International Journal of Vehicle Design* 22 (1999) 116–128.
[544] M.S. Patil, M.K. Hada, S.Y. Bhave, S.G. Joshi, Vibration isolation and transmissibility characteristics of passive sequential damper, *Defense Science Journal* 54 (2004) 39–51.
[545] G.N. Jazar, J. Christpherson, Development of a new design hydraulic engine mount, *Proceedings of the ASME 2005 International Mechanical Engineering Congress and Exposition*, Orlando, Florida, USA, Design Engineering Division, DE, Vol. 118B, 2005, pp. 1125–1132 (ASME Paper Number: IMECHE2005-81860).
[546] Y. Wei-Ge, L. Shu-Yan, L. Jun-Jie, X. Yong-Qiang, Passive magnetorheological fluid filled hydraulic engine mount, *Journal of Beijing Institute of Technology* 9 (2000) 434–438.
[547] S.P. Kelso, K.K. Denoyer, R.M. Blankinship, K. Potter, J.E. Lindler, Experimental validation of a novel stictionless magnetorheological fluid isolator, *Proceedings of the SPIE: The International Society of Optical Engineering* 5052 (2003) 186–197.
[548] N. Irino, H. Sato, H. Osumi, H. Osumi, K. Watanabe, S. Kumakawa, Vibration analysis of mechanical system with hysteretic nonlinearity (first report, Description of hysteretic nonlinearity of restoring force by Preisach distribution function), *Nippon Kikai Gakkai Ronbunshu, C Hen/Transactions of the Japan Society of Mechanical Engineers, Part C* 69 (2003) 2556–2563.
[549] N. Irino, H. Sato, H. Osumi, K. Watanabe, S. Kumakawa, T. Katayama, Vibration analysis of mechanical systems with hysteretic nonlinearity (end report: Vibration analysis based on measured property of actual rubber pads), *Transactions of Japan Society of Mechanical Engineers, Part C* 70 (2004) 3070–3077 (in Japanese).
[550] M.N. Dhaubhadel, Oscillating flows in fluid tuned isolators, *ASME Winter Annual Meeting, Fluids Engineering Division, Advances in Finite Element Analysis in Fluid Dynamics*, Anaheim, CA, USA, FED, Vol. 137, 1992, pp. 27–30.
[551] A.H. Barbat, J. Rodellar, E.P. Ryan, N. Molinares, Active control of nonlinear base-isolated buildings, *ASCE Journal of Engineering Mechanics* 121 (1995) 676–685.
[552] J. Wagner, X. Liu, Nonlinear modeling and control of automotive vibration isolation systems, *Proceedings of the American Control Conference (ACC)*, IEEE Cat. No. 00CH36334, Chicago, IL, 2000, Vol 1, pp. 564–568.

[553] M. Heertjes, N. van de Wouw, Nonlinear dynamics and control of a pneumatic vibration isolator, *ASME Journal of Vibration and Acoustics* 128 (2006) 439–448.
[554] T.Y. Lee, K. Kawashima, Effectiveness of seismic displacement response control for nonlinear isolated bridge, *Structural Engineering/Earthquake Engineering* 23 (2006) 1s–15s.
[555] T.Y. Lee, K. Kawashima, Semiactive control of nonlinear isolated bridges with time delay, *ASCE Journal of Structural Engineering* 133 (2007) 235–241.